Improving an optimal estimation algorithm for surface and atmospheric parameter retrieval using passive microwave data in the Arctic

Vom Fachbereich für Physik und Elektrotechnik
der Universität Bremen

zur Erlangung des akademischen Grades eines
Doktors der Naturwissenschaften (Dr. rer. nat.)
vorgelegte Dissertation

von
MSc.
Raul Cristian Scarlat

Verteidigung der Dissertation
23. August 2018

1. Gutachter: Dr. Gunnar Spreen
2. Gutachter: Dr. Leif Toudal Pedersen

this page intentionally left blank

Abstract

In this study we present improvements on an integrated retrieval method for atmospheric and surface parameters in the Arctic. The instrument used is the Advanced Microwave Scanning Radiometer - Earth Observing System (EOS) (AMSR-E) radiometer on board NASA's Aqua satellite. The core of the method is a forward model which can ingest bulk data for seven geophysical parameters to reproduce the brightness temperatures observed by a passive microwave radiometer. The method inverts the forward model and produces ensembles of the seven parameters: wind speed, integrated water vapor, liquid water path, sea and ice temperature, sea ice concentration and multi-year ice fraction. The method is constrained using numerical weather prediction data in order to retrieve a set of geophysical parameters that best fit the measurements. An iterative method minimizes the cost function and finds the optimal ensemble of the seven parameters that best match the observed brightness temperatures.

Benchmark comparison data sets are used for testing method sensitivities and improvements as well as the consistency of the final retrieval set-up. It is found that the data source for the background covariance matrix should be representative for the spatial and temporal domain of the retrieval. The method is robust against the initialization conditions which can influence the number of iterations but not the solution. The brightness temperature covariance matrix that constrains the method to the observations has to include the measurement errors as well as the modeling errors to avoid biasing the retrieved parameters.

A number of improvements have been developed which include a correction to the empirical sea ice surface emissivities, a treatment of the sea ice surface temperature that takes into account the channel specific penetration depth and the use of pixel wise collocated reanalysis data as background source instead of one static set of mean values. All of these have led to a better agreement between the retrieval and atmospheric model data as well as validated sea ice concentrations. Over open water, for all atmospheric parameters, the retrieval improves on the background knwoledge and produces a better agreement with the different satellite retrievals used as benchmarks. The correlations are increased for wind speed from 0.6 to 0.8, for water vapor from 0.8 to 0.9, for liquid water path from 0.2 to 0.8 and for sea surface temperature from 0.6 to 0.8. Over sea ice, the retrieved water vapor has a moderately high agreement of 0.7 with the benchmark. This is caused in part by the temporal collocation between the retrieval and the benchmark and by the reduced impact of the low water vapor values on the brightness temperatures measured over sea ice. The sea ice concentration comparison results in a correlation of 0.99 with the benchmark. The retrieved sea ice concentrations are free of weather effects as the atmospheric influences have been retrieved as separate parameters.

An information content analysis of different combinations of the 12 radiometer channels shows that discarding the 6.9 GHz channels in order to increase the spatial resolution of the output from 56 km to 38 km reduces the information content for surface parameters by 28% over open water and by 16% over sea ice. By including the 89 GHz channels in the retrieval, the method benefits from higher sensitivity to liquid water and water vapor especially over sea ice where the other AMSR-E channels are dominated by the surface signal. This has resulted in an increase by 10% over open water and by 25% over sea ice in the information content for the atmospheric parameters.

Contents

1 Introduction

The Arctic sea ice and its seasonal variability heavily influence the heat balance between the atmosphere and the ocean. The Arctic is affected more than any other region by global warming and its evolution is a sensitive indicator for global climate change. Therefore a detailed monitoring of the Arctic climate is urgently required.

Satellite monitoring efforts have shown that sea ice extent has been in decline throughout all months of the year since 1979. This trend has been accelerating since the early 1990s. Sea ice thickness also shows a decline since 2001 that appears throughout the whole Arctic [Serreze et al., 2007].

The latest IPCC report concludes that under current predictions the Arctic will warm at a faster pace than the global mean [Pachauri et al., 2014]. Current models however have been shown to under predict the Arctic sea ice decline. In [Stroeve et al., 2007] the 2007 historic ice extent minima is estimated to have appeared 30 years ahead of the CMIP3 (World Climate Research Programme Coupled Model Intercomparison Project Phase 3) ensemble mean model forecast. This sea ice decline underestimation is attributed to an underestimation in the magnitude of anthropogenic forcing. In a following paper [Stroeve et al., 2012], the more advanced CMIP5 models are shown to better represent the historical ice conditions. The authors conclude that improved parameterizations in the sea ice components of the CMIP5 models have lead to the improvement. The model prediction skill can be greatly improved by increasing the amount and quality of observations and initial conditions [Msadek et al., 2014]. This means that there is a need for more and better observational data about the Arctic environment, describing the state of the ocean, the sea ice and the atmosphere.

Because of the hostile conditions in the Arctic, field measurements of these parame-

ters are scarce. Remote sensing satellites on polar orbits have very good coverage of the Arctic. Especially suited to this monitoring task are passive microwave radiometers such as AMSR-E, Special Sensor Microwave Imager (SSM/I) or Advanced Microwave Scanning Radiometer 2 (AMSR2) which measure the microwave emissions of the surface and the atmosphere. These instruments have a number of advantages over sensors that use different techniques and different portions of the electromagnetic (EM) spectrum. Microwave radiation is affected little by non-precipitating clouds, allowing the sensor to "see" through cloud cover. Because of the large footprint, these sensors offer daily coverage of the Arctic. As opposed to visible spectrum sensors, passive microwave radiometers are not effected by the polar night and offer year-round measurements.

A special characteristic of the Arctic sea ice covered regions at microwave imaging frequencies is the high emissivity of sea ice and snow that contribute more to the microwave signal than the often dry atmosphere [Selbach, 2003]. The satellite observed signal contains contributions from both surface and atmosphere so that retrievals of atmospheric parameters require some information about the surface emissivity. Over open ocean reliable models exist that can accurately represent the surface contribution to the microwave signal [English and Hewison, 1998, Wentz and Meissner, 2000]. Over sea ice, however, there is no operational surface emissivity model, but there are empirical measurements which provide an estimate for the sea ice contribution throughout the year and by ice type [Mathews, 2007].

Single parameter retrieval methods based on passive microwave satellite measurements have been developed for sea ice concentration retrieval e.g., Comiso et al. [1997], Svendsen et al. [1987], Spreen et al. [2008], Shokr et al. [2008], Markus and Cavalieri [2000] as well as integrated water vapor content [Melsheimer and Heygster, 2008, Scarlat et al., 2018]. In such algorithms the contribution of the retrieved parameter is the signal of interest while the contributions from all the other geophysical parameters that also influence the microwave emission are seen as noise that needs to be filtered out or compensated for by using other channels of the radiometer or through a priori data.

The basic idea of integrated retrieval is to find a set of geophysical parameters which, if applied to a forward model, simultaneously yield a best possible approximation of the observed brightness temperatures for all radiometer channels. Over open ocean, such integrated retrieval exists and has been applied for more than a decade e.g. Wentz and Meissner [2000]. However, over sea ice, an integrated retrieval is much more difficult. The main challenge is the high and highly variable surface emissivity which dominates the microwave signal. Although sea ice forward models exist [Wiesmann and Mätzler, 1999], their use in integrated retrieval has been limited because the number of required geophysical parameters is high and their values are generally unknown, so that until now only little effort has been undertaken for integrated retrieval of surface and atmospheric parameters over sea ice [Pedersen, 1994, Kongoli et al., 2011] compared to the established

retrieval methods over open ocean. In order to take advantage of the multispectral capabilities of imaging radiometers, in Melsheimer et al. [2008] an integrated retrieval method is proposed that can retrieve the seven geophysical parameters: wind speed (WSP), total water vapor (TWV), liquid water path (LWP), sea surface temperature (SST), ice surface temperature (IST), sea ice concentration (SIC) and multi-year ice fraction (MYIF). An optimal estimation (OE) technique is used to invert the forward model and extract the ensemble of seven parameters that optimally match the observed brightness temperatures. A priori information from climatological and meteorological sources is used to constrain the method to the natural variability of each parameter.

This study was started from the method prototype as described in Melsheimer et al. [2008] with three main aims for development:

(i) Explore the optimal estimation method's (OEM) sensitivities to the a priori constraints. The OE theory and literature on implementation give guidelines and examples on how to choose the a priori data. Given the unique combination of sensor, forward model and necessary simplifying assumptions for the OE integrated retrieval over sea ice, concrete examples had to be tested in order to find the best set-up for constraining the method.

(ii) Identifying and improving deficiencies in the OEM. Parameterizations and approximations are required in any retrieval system. Their influence on the retrieval and possible improvements need to be investigated. In order to avoid the discrepancies that occur between the different channel footprints covering slightly different regions of the Earth surface, we used the AMSR-E Level 2A product [Ashcroft and Wentz, 2000], where all channels have been interpolated to represent the same footprint on the surface. Sea ice surface emissivities, surface temperature treatment, the background data source and input channel combinations have been tested and improved from the prototype.

(iii) Test the method against benchmark data. Because validation data is scarce for some of the parameters retrieved in the OEM, comparative tests against proven retrieval products are needed in order to establish the reliability of the OEM output.

The final goal of developing the OEM is to obtain an operational retrieval method for providing more and self-consistent data about the Arctic surface and atmospheric parameters based on existing instrumental archives of passive microwave brightness temperatures.

For testing purposes it is important to isolate the contribution of the sea ice cover from that of the other parameters. To this end the Round Robin Data Package (RRDP) has been used extensively, a data set containing AMSR-E level 2A brightness temperatures as well as collocated ERA-Interim data for the retrieval parameters of the OEM. It is split into two subsets representing cases of 100% sea ice cover and open water [Pedersen and

Saldo, 2012]. In addition, for each pixel in these datasets atmospheric parameter data from the Arctic System Reanalysis (ASR) model [Bromwich et al., 2001] have been collocated.

In order to observe the retrieval version behavior throughout the seasonal cycle of freeze-up and melt, a separate, larger testing dataset was prepared including one full day of data every ten days for the year 2006 for a total of 18 winter and 18 summer season day. It covers the entire Arctic north of 60° N from January 11^{th} 2006 to January 6^{th} 2007. ASR was used for evaluating the retrieved atmospheric parameters for both the RRDP and the 2006 datasets. In order to evaluate the sea ice retrieval in the 2006 dataset we used the ASI sea ice retrieval [Spreen et al., 2008]. We compared the OEM results with those from Melsheimer and Heygster [2008] which is a microwave sounder based method that is especially accurate for the low atmospheric water vapor values encountered in the Arctic. A set of preliminary results for the OEM testing has been published in Scarlat et al. [2017].

The thesis is structured as follows:

Chapter 2 provides the theoretical basis for passive microwave retrieval as well as relevant background information about the Arctic environment which this method aims to monitor.

Chapter 3 describes the data sources used, starting from a description of the AMSR-E instrument, the resampled brightness temperatures product, the comparison datasets created for this study, atmospheric and surface parameter retrieval products used in evaluating OEM output as well as the sources for the a priori data.

Chapter 4 presents the a posteriori OEM used to solve the inverse problem as well as details about the forward model that needs to be inverted.

In Chapter 5 the tests for sensitivity to the a priori elements are shown and it concludes with a recommended setup for the OEM which is used for subsequent comparative tests with other retrieval products.

Chapter 6 details the results of comparing the improved OEM with different retrieval products used as benchmarks. Because there is no one single product that covers all of the retrieved parameters from the OEM, different benchmarks are used for different parameters. The Remote Sensing Systems (RSS) Ocean product [Wentz et al., 2014] was used for evaluating the WSP, TWV, LWP and SST retrieval over open ocean scenes only. The ASI algorithm is used for SIC output comparison, and the AMSU-B TWV [Melsheimer and Heygster, 2008] retrieval over sea ice.

Chapter 7 explores possibilities for using different AMSR-E channel combinations. Depending on possible applications for the OE retrieval, different input channel combinations can improve the sensitivity to atmospheric parameters, surface parameters or increase the retrieval resolution.

The conclusions are presented in Chapter 8 together with suggestions for the future development of the method.

2 | Physical background

This study is focused on satellite remote sensing in the Arctic region using passive microwave measurements. The regions of interest here are the sea ice covered Arctic Basin and the adjacent open ocean regions. This chapter introduces the theory elements of microwave remote sensing which are relevant to this study. General principles of radiation measurements and passive microwave applications are introduced in Section 2.1. The effect of the atmosphere on satellite measurements are discussed in Section 2.2. The distinct microwave signatures of open ocean and sea ice and the geophysical parameters that influence them are covered in Section 2.3 and Section 2.4 respectively. The content in this chapter closely follows Ulaby et al. [2014] which offers a comprehensive overview of passive and active microwave remote sensing theory.

2.1 Microwave remote sensing

2.1.1 Thermal radiation

The blackbody is the idealized model that helps in understanding how real world objects emit thermal radiation. A blackbody is defined as a material that absorbs all incident radiation. The conservation of energy states that in thermal equilibrium all absorbed energy has to be emitted. The radiation emitted by a blackbody with an absolute temperature T is given by the Planck radiation law

$$I(f) = \frac{2hf^3}{c^2}\left(\frac{1}{e^{hf/kT}-1}\right), \tag{2.1}$$

where f is the radiation frequency, h is Planck's constant, c is the speed of light in vacuum

and k is Boltzmann's constant. The spectral brightness intensity represents by definition the power (W) emitted by a blackbody surface of area equal to 1 m^2, through a solid angle of 1 sr and over a frequency bandwidth of 1 Hz.

Brightness intensity can be represented by a curve which increases with frequency up to a maximum value after which it decreases. The maximum of the intensity curve and the corresponding frequency increase with temperature T. For frequencies well below the maximum frequency ($hf/kt << 1$), the curve of Planck's law can be approximated by a linearized expression which is known as the Rayleigh-Jeans law:

$$I(f) = \frac{2f^2kT}{c^2}. \tag{2.2}$$

In the microwave frequency domain (1 GHz - 300 GHz) and for temperatures sufficiently higher than the cosmic background (2.73 K) the Rayleigh-Jeans approximation is valid. The gray body brightness intensity will be equal to that of a blackbody of a lower temperature. This blackbody equivalent temperature is called the brightness temperature:

$$T_b = \frac{Ic^2}{2kf^2}. \tag{2.3}$$

As a material characteristic of the gray body, emissivity is defined as the ratio between its brightness intensity to that of a blackbody of the same temperature:

$$e = \frac{I}{I_{bb}} = \frac{T_b}{T}, \tag{2.4}$$

where I_{bb} is the equivalent blackbody brightness intensity. As I is smaller or equal to I_{bb} the emissivity is always smaller or equal to 1, and the brightness temperature of a gray body is at most equal to its physical temperature. By using the material characteristic emissivity and its brightness temperature we can fully characterize the body's thermal emission.

Radiometry is concerned with the measurements of electromagnetic (EM) radiation. When applied to Earth observation systems, radiometers will observe the sum of emission contributions from all objects inside the antenna field of view. The simplest case for a scene measured by a downward looking radiometer involves a contribution from the surface emission, a contribution from the atmospheric upward emission and a reflected component that was emitted by the atmosphere and scattered in the direction of the radiometer antenna by the surface. Besides emission, there are also absorption and scattering terms that are associated with the atmospheric composition. These terms play an important role in relating the thermal measurements registered at the radiometer with the physical and chemical properties of the observed surface and atmosphere. During a radiometric measurement the antenna receives incoming thermal radiation which is described by two quantities. A brightness temperature angular distribution $T_A(\theta, \phi)d\Omega$ describes the energy

incident upon the antenna, while the antenna temperature

$$T_A = \frac{\iint T_B(\theta,\phi)F(\theta,\phi)d\Omega}{\iint F(\theta,\phi)d\Omega}. \tag{2.5}$$

represents the power that a perfect antenna delivers to the radiometer receiver. $F(\theta,\phi)$ represents the antenna radiation pattern and $d\Omega$ is the differential solid angle along direction (θ,ϕ). This perfect antenna is a simplification that assumes no absorption of energy in the antenna body itself.
The antenna temperature for a lossless antenna will be equal to the integrated value of the brightness temperature distribution weighted by the antenna radiation pattern.

Each antenna will have a particular radiation pattern. In an ideal case this pattern can be represented by a narrow beam with no side lobes, such that the radiation received by the antenna comes only from the target scene. In reality there will be contributions from the antenna side lobes and back lobes which are added to the power received from the antenna main beam. The difference between the main lobe solid angle

$$\Omega_m = \iint_{mainlobe} F(\theta,\phi)d\Omega, \tag{2.6}$$

which represents the target area of the antenna and the pattern solid angle

$$\Omega_p = \iint_{4\pi} F(\theta,\phi)d\Omega, \tag{2.7}$$

which represents all directions the antenna receives power from, including side and back lobes, are represented by the domain of integration for the antenna pattern.
The ratio of the two solid angles gives the antenna beam efficiency

$$\eta_b = \frac{\Omega_m}{\Omega_p}. \tag{2.8}$$

The ideal case where the antenna only receives power through its main lobe and does not have any side lobe contributions will have a beam efficiency of 1.

Influences from outside the antenna main lobe are one source of noise for radiometer measurements. Through the design of the antenna, engineers can maximize the antenna beam efficiency. Another source of noise in the measurements comes from the power absorption and emission that takes place in the antenna material itself. Thus the radiation efficiency of a receiver antenna is given by the ratio of power delivered to the receiver to the total power incident on the antenna. A radiometric measurement is represented by the brightness temperature of the target scene observed inside the antenna main lobe and the accuracy of this measurement is influenced by both the radiation efficiency, as a material property and the beam efficiency as a design property of the antenna.

2.1.2 Radiative Transfer Theory

Radiometric measurement accuracy is influenced by the technical characteristics of the radiometer but also by the varying conditions inside the observation scene.

As it travels from its source of emission to the radiometer receiver, radiation can pass through different materials. The nature of the materials will influence the radiation in different ways. When radiation encounters an interface between two different materials, a part of the radiation energy will be reflected back inside the initial medium and the rest will be refracted and transmitted through. The material property that determines the fraction of incident radiation that is reflected at the interface is reflectivity. For a plane boundary between two materials, and an incidence angle θ_1 the reflectivity is the square of the magnitude of the Fresnel reflection coefficient

$$\Gamma^h(\theta_1) = \left| \frac{\sqrt{\epsilon_1}cos\theta_1 - \sqrt{\epsilon_2}cos\theta_2}{\sqrt{\epsilon_1}cos\theta_1 + \sqrt{\epsilon_2}cos\theta_2} \right|^2, \tag{2.9}$$

$$\Gamma^v(\theta_1) = \left| \frac{\sqrt{\epsilon_1}cos\theta_2 - \sqrt{\epsilon_2}cos\theta_1}{\sqrt{\epsilon_1}cos\theta_2 + \sqrt{\epsilon_2}cos\theta_1} \right|^2. \tag{2.10}$$

ϵ_1 and ϵ_2 represent the complex relative dielectric constants for materials 1 and 2, respectively and θ_2 is the angle for the outgoing radiation represented as polarized EM waves. The polarization state in vertical or horizontal plane will be discussed later in this section. Here h and v denote the horizontal and respectively vertical polarization reflection coefficients. The relationship between the incidence angle θ_1 and the outgoing angle θ_2 is given by Snell's law

$$\sqrt{\epsilon_1}sin\theta_1 = \sqrt{\epsilon_2}sin\theta_2. \tag{2.11}$$

For a down-looking satellite radiometer, which is the case most relevant for this study, the brightness temperature incident on the receiver antenna is composed of different contributions from the surface and the atmosphere. The terrain will emit radiation in accordance to its specific emissivity and will give a surface component T_{SE} of the total brightness temperature signal. The atmosphere will also emit radiation in all directions in accordance with its constituent gases and their emission spectra. The atmospheric emission component that propagates towards the satellite radiometer is called the upward brightness temperature T_{UP}. There is a downward component of the atmospheric emission that is scattered by the surface and reflected in the direction of the radiometer noted by T_{SS}. As the surface emitted and surface scattered components pass through the atmosphere, part of the energy they carry is attenuated through scattering and absorption. The factor that describes the amount of energy that is transmitted through the atmosphere is called the atmospheric transmissivity Υ_a, so that the brightness temperature that reaches the radiometer antenna is given as

$$T_B = T_{UP} + \Upsilon_a(T_{SE} + T_{SS}). \tag{2.12}$$

One other characteristic of EM waves is their polarization state. The wave polarization refers to the alignment of the electric field vector of the EM wave. If the electric field vector is varying randomly without any discernible alignment then it is called unpolarized. If the vector oscillates in the EM wave incidence plane then the wave is called vertically polarized, and if it is oscillating in the plane perpendicular to the incidence plane then the wave is horizontally polarized. As a general rule a flat surface with respect to the radiation wavelength will have a polarized or partially polarized emission, while surface or volume scattering processes will lead to a depolarized EM wave. By measuring both polarization components of an EM wave, more information can be gathered about the state of the emitting surface as well as the medium that the wave traverses.

Equation 2.12 can be rewritten to represent the polarized components:

$$T_B^p = T_{UP} + \Upsilon_a(T_{SE}^p + T_{SS}^p). \tag{2.13}$$

Here the superscript p represents the polarization state (horizontal h or vertical v). In order to retrieve information about the geophysical state of the surface the other three components (T_{SS}^p, T_{UP} and Υ_a) have to be factored out of equation (2.13). This means that some knowledge of the atmospheric state is required in order to gain knowledge about the surface and vice versa.

Depending on the technical capabilities of the radiometer the vertical and horizontal polarization components can be measured simultaneously.

2.2 The atmosphere

Atmospheric constituents can be found in gaseous, liquid or solid state and they can prove to be completely opaque to microwave transmission, partially transparent or fully transparent depending on the frequency range. This behaviour is based on the absorption and emission spectra of each chemical component of the atmosphere, their abundance in the atmospheric column and, in the case of liquid or solid particles, their size relative to the radiation wavelength. Depending on the goal of the radiometric observations, different frequency channels can be used. For measuring atmospheric constituents the observation channel frequencies have to be close to the frequency ranges where these constituents exhibit strong interactions with the thermal radiation in the form of absorption and emission or scattering. The most important absorption ranges occur around 22.235 GHz and 183.31 GHz for water vapor and 50-70 GHz and 118.75 GHz for oxygen. If the purpose of the measurements is to gain knowledge on the surface state, so called atmospheric window frequency ranges have to be used where the lowest atmospheric attenuation is present.

These windows occur between 1-15 GHz, around the 35 GHz value and between 85 and 90 GHz. The absorption behaviour over a wide microwave frequency range for the most important atmospheric constituents is shown in Figure 2.1.

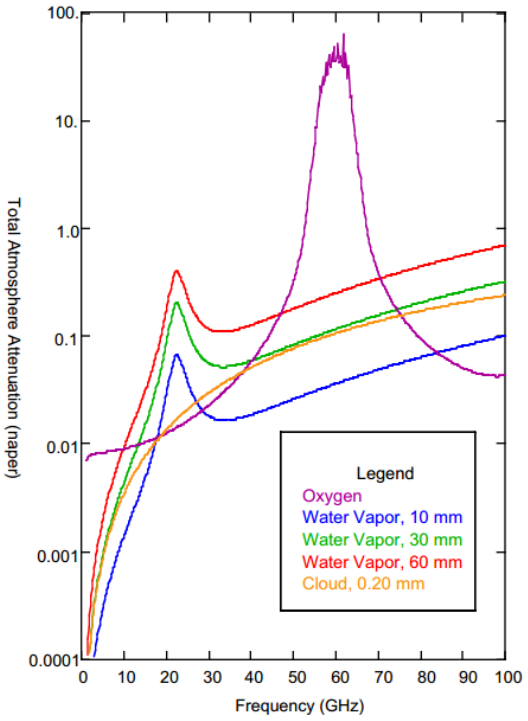

Figure 2.1: Atmospheric absorption in the microwave spectrum. Three water vapor absorption lines are shown for different total water vapor values. The cloud liquid water content of 0.2 mm represents a heavy non-precipitating cloud. From Wentz and Meissner [2000].

2.2.1 Interaction with gases

Oxygen represents 21% of air volume. Of interest in the microwave domain is that oxygen has the most significant absorption frequency range centred around 50 to 70 GHz. 37 absorption lines are spread here which blend together because of pressure broadening, forming one continuous absorption band at the air pressures typical for the lower part of the atmosphere. An additional absorption line is present at 118.75 GHz. An important feature of oxygen is that it has a homogeneous horizontal distribution in the atmosphere and it is stable in its concentration so that the absorption spectrum can be considered constant for any given downward looking microwave radiometer observation while mantaining a dependence on temperature however.

The other significant atmospheric absorber in the microwave range is water vapor. It has two rotational absorption lines at 22.235 GHz and 183.31 GHz. Water vapor has,

unlike oxygen, a heterogeneous horizontal and vertical distribution, is highly variable in time and important for the global weather and climate. In order to quantify the total mass of atmospheric water vapor in the atmosphere, the total integrated precipitable water vapor quantity is defined. This represents the water vapor mass contained in a vertical column with a base area of 1 cm^2 and is given by

$$M_V = \int_0^\infty \rho_V(z)dz, \qquad [\mathrm{g\,cm^{-2}}] \quad (2.14)$$

with $\rho_v(z)$ representing the water vapor density at altitude z. If this mass of water vapor would be condensed to liquid inside the vertical column then the height of the liquid would be equal to

$$h_V = \frac{M_V}{\rho_L}, \qquad [\mathrm{cm}] \quad (2.15)$$

where ρ_L is the liquid water density.

In the case of cloud liquid water we have a similar quantity defined as the liquid water path. For a cloud vertical thickness H (km) and assuming uniform water content m_V ($\mathrm{g/m^3}$) within the cloud volume the liquid water path is given by

$$h_L = \frac{m_V}{\rho_L} H. \qquad [\mathrm{cm}] \quad (2.16)$$

Oxygen, water vapor and cloud liquid water represent the biggest contributors to the atmospheric attenuation. Together these three atmospheric constituents define the total atmospheric opacity τ which quantifies the fraction of the microwave radiation that is absorbed or scattered as it passes through the atmosphere.

$$\tau = \tau_{O_2} + k_V h_V + k_L h_L, \quad (2.17)$$

where τ_{O_2} is the zenith opacity attributed to absorption by oxygen, k_V and k_L are the temperature dependent coefficients for water vapor and liquid water respectively which quantify the total absorption and scattering by water molecules and particles in the atmosphere.

Besides oxygen and water vapor there are other atmospheric constituents that can contribute to atmospheric attenuation. These include ozone O_3, SO_2, NO_2 and N_2O as the most significant. However for the purpose of nadir measurements these gases are found in concentrations so low that their contribution to atmospheric absorption is negligible. For applications of atmospheric limb sounding they are more important, but these are not considered here.

2.2.2 Interaction with hydrometeors

Besides absorption by atmospheric gases, upwelling thermal radiation can be attenuated also through interaction with hydrometeors. These particles both absorb and, depending on their dimensions, can scatter microwave radiation.

The relationship between the power incident on a particle and the fraction that is absorbed by the particle the absorption cross section is defined as

$$Q_a = \frac{P_a}{S_i} m^2, \tag{2.18}$$

with P_a representing the absorbed power and S_i the incident power density. The absorption cross section relates to the physical cross section of the particle through the absorption efficiency factor

$$\xi_a = \frac{Q_a}{\pi r^2}, \tag{2.19}$$

where r is the particle radius.

The corresponding parameters that characterize the amount of radiation scattered by the particle are the scattering cross section

$$Q_s = \frac{P_s}{S_i} m^2, \tag{2.20}$$

and the scattering efficiency factor

$$\xi_s = \frac{Q_s}{\pi r^2}. \tag{2.21}$$

Both absorption and scattering attenuate the upwelling microwave radiation. The attenuation (or extinction) cross section and the respective efficiency represent the sums of the individual absorption and scattering parameters:

$$Q_e = Q_a + Q_s, \tag{2.22}$$

$$\xi_e = xi_a + xi_s. \tag{2.23}$$

The Mie theory provides the general solution for scattering and absorption of EM waves by a dielectric sphere with radius r if the size parameter

$$\chi = \frac{2\pi r}{\lambda}. \tag{2.24}$$

is in the order of 1. The solution is given in terms of a normalized particle circumference χ that varies with wavelength and the relative index of refraction n which is a material constant.

These solutions are in terms of infinite series and include calculation of extinction, scattering, and absorption efficiencies. In more general terms, the Mie solution for absorption and scattering by spherical particles is used for conditions when the particle size is almost equal to the wavelength of the incident radiation.

In cases where the radiation wavelength is a lot larger than the diameter of the particles, an approximation of the Mie solution can be used, the Rayleigh approximation. For most computational purposes, the Rayleigh approximation achieves reasonable accuracies if $|n\chi < 0.5|$.

Besides the radiation wavelength and the size of the particle one more parameter influences the scattering and absorption characteristics of non gaseous atmospheric constituents. The particle's complex dielectric constant (or complex refraction index) determines how much of the incident energy is attenuated as the EM wave interacts with the particle.

For droplets of pure water in the atmosphere the complex dielectric constant depends on the radiation frequency and on the water temperature. A pure water droplet will exhibit large absorption and scattering effects in the frequency range 1-50 GHz, with a peak of the complex dielectric components depending on temperature.

Ice particles behave differently from water. The real part of the complex dielectric constant in the microwave frequency domain is smaller. It is also independent on frequency between 10 GHz and 300 GHz and weakly dependent on the particle temperature. The imaginary part of the dielectric constant (the dielectric loss factor) depends on both frequency and temperature but its magnitude is so small that ice is shown to be a weak absorber at microwave frequencies when compared to water. Another unique atmospheric constituent especially relevant to the polar regions is snow. Snowflakes can have complex shapes that differ from the simple spherical model. The shape has only a weak influence on the scattering and absorption efficiency [Atlas, 1964] so that snowflakes can be treated as spherical particles of an equivalent mass using the Rayleigh approximation, as long as the Rayleigh criterion is met. For evaluating the complex dielectric constant of a snowflake, it can be treated as a mixture of air and ice with a highly variable density.

2.3 Open ocean

The microwave emission of the ocean surface depends on the dielectric constant of sea water and on the surface roughness. The dielectric constant in turn depends on salinity, temperature and frequency.

At the window frequencies, the surface emission is the main source for microwave radiation that is received by a downward looking radiometer. If the ocean surface is calm and flat, it can be associated with a specular surface emitting upwards. Below the surface, the microwave emission of water is randomly polarized and the process of transmission across the interface determines what fraction of the upwelling power is transmitted for

each polarization. For this scenario with a calm ocean surface the brightness temperature seen by a downward looking radiometer will be

$$T_B^p(\theta_1) = [1 - \Gamma_a^p(\theta_1)]T, \tag{2.25}$$

where θ_1 is the angle of the outgoing radiation, Γ_a is the Fresnel reflectivity for incidence in air, T is the physical temperature of the emitting layer and p represents the polarization state, vertical or horizontal.

The corresponding specular emissivity of the flat ocean surface is then

$$e^p(\theta_1) = \frac{T_B^p(\theta_1)}{T}. \tag{2.26}$$

In the absence of wind the temperature of the uppermost layer of the ocean and the ocean salinity, determine the upwelling surface brightness temperature. The salinity sensitivity Q_S^p for an observed p-polarized brightness temperature T_B^p will be

$$Q_S^p = \frac{\partial T_B^p}{\partial S}, \tag{2.27}$$

for S being the sea surface salinity. The brightness temperature T_B^p has a non-linear dependence on salinity and the salinity sensitivity Q_S^p strongly depends on the sea surface temperature and the frequency. For microwave frequencies above 2 GHz the influence of salinity on the brightness temperature decreases rapidly to the point where it can be neglected.

The surface roughness becomes important when the wind disturbs the calm ocean so that the surface can no longer be considered specular. If the irregularities that appear on the surface reach the size of the wavelength of the emitted radiation, then the power incident on the surface from below will be transmitted into different directions. Observed from above, the emerging microwave emission is composed of contributions that have crossed the ocean-atmosphere interface under various angles. The ocean waves will also have a prevailing direction of propagation on the sea surface which is triggered by the wind direction, and the brightness temperature of the surface will depend on the prevailing wind direction relative to the antenna beam direction. Another important impact of wind action on the ocean surface appears at the higher wind speeds when foam is formed. The presence of foam patches presents a further alteration of the ocean surface emissivity in the microwave range. The emissivity of the wind roughened, partially foam-covered ocean surface is

$$e^p(\theta, u, C_f) = (1 - C_f)e_{rw}^p(\theta, u) + C_f e_f(\theta), \tag{2.28}$$

where p is the polarization state, θ is the antenna azimuth angle relative to the wind direction, u is the wind speed, C_f represents the fraction of ocean surface covered by foam, e_{rw} is the emissivity for the wind roughened sea surface and e_f is the emissivity of the

foam covered surface.

2.4 Sea ice

Sea ice is formed from freezing ocean water. In a first stage small ice crystals are nucleated in the seawater and grow to form randomly oriented needle like structures called frazil ice. The ice crystals then grow laterally forming a more consistent layer of flat patches on the sea surface called grease ice as it resembles an oil slick on the ocean surface. The last stage of ice growth entails vertical growth in which the ice layer thickens and is consolidated. Throughout the freezing process salt dissolved in the seawater is rejected from the emerging ice structure. This process mainly takes place at the ice-water interface with the resulting brine being drained in the water. As the geometry of the ice structure becomes more complex, some of the brine is trapped in the gaps between the ice discs and becomes fully enclosed as the ice layer thickens. These are called brine pockets which can remain isolated or form channels that drain into the seawater below or even up to the ice surface based on the internal pressure. This desalination process is driven by temperature variations and continues throughout the life cycle of the ice layer. The process of ice thickness growth occurs mostly thermodynamically in winter as the air temperature is colder than that of seawater but it can also occur mechanically as a result of ice floes colliding as they float on the ocean. Turbulent atmospheric and ocean conditions will favour the latter, as broken ice debris piles up along the edges of larger ice floes, rafting and ridging will lead to regions of thicker ice.

One factor that can work against the vertical ice growth is snow cover. As snow deposits on the sea ice it acts as a thermal insulator between the cold atmosphere and the ice layer, causing a reduction in the heat flux through the ice from the warmer water below. Solar radiation is reflected more efficiently by the higher albedo of dry snow. While the wetness of the snow will have an impact, in general the thermal conductivity of the snow layer is one order of magnitude lower than that of sea ice. The age of the snow layer will also influence its insulating effectiveness as older snow tends to be more compacted, with lower air content and as such a poorer insulator than fresh fallen snow.

As the ice floes float on the ocean, wind and ocean currents are the primary forces that drive their mobility. The ensuing interaction between floes leads to ice deformation. Thin ice floes can slide one on top of the other, thicker ice floes can break apart or get compacted as they collide, while broken debris can form ridges as it piles up along floe edges.

Ice decay starts once surface ice melt begins. The main factors for the onset of ice decay are increasing air temperatures, the incoming solar radiation and the melting of the snow cover. Absorbed solar radiation together with conductive heat from the atmosphere initiate the surface melt. Because of unequal absorption of solar radiation, darker areas on

the ice are the first ones to exhibit melt. They can be the result of dust deposition or the presence of algae in the ice which have a lower albedo than the surrounding areas. The unequal snow layer distribution across the ice means that areas with thinner snow layer will be the first to exhibit surface melting. As the melt process continues, the resulting liquid water accumulates in depressions in the ice surface creating melt ponds. The presence of the lower albedo water further accelerates absorption of incoming radiation and the pond deepens and expands.

As the Arctic Ocean is semi-enclosed, floating ice does not leave the Arctic basin as easily as sea ice formed around Antarctica for example. If sea ice survives one summer melt season in the Arctic it becomes second year ice. If it survives multiple summer seasons it will become multi-year ice. This gradual transformation from first year ice into multi-year ice is accompanied by significant changes in the physical properties. Generally, the older the sea ice is the more weathered the surface aspect will be with smooth ridges and refrozen melt ponds. One consequence of surviving the melt season is that surface melt water percolates through the ice layer. If the brine pockets are connected into an effective drainage network with access to both the surface of the ice layer and to the bottom, melt water will flush out the brine pockets as long as the melt conditions continue at the surface. Once the melt seasons ends, the water in the drainage network will continue to drain aided by gravity. But without new surface melt waters some of the channels will be empty. Once freezing conditions are in place again the empty channels become air inclusions.

Another physical parameter that differentiates between first year and multi-year ice is the thickness of the ice layer. As long as the ice survives, it continues to grow through accretion at the interface with the water underneath. First year ice can reach a maximum thickness of around 2.5 m before the first melt season, multi-year ice floes can reach 6-8 m after several growth seasons [Shokr and Sinha, 2015]. Sea ice growth beyond 3 m thickness is caused by deformations and not thermodynamic growth.

Microwave radiometric measurements cannot reveal all of the subtle changes in the structure of the sea ice cover in the observation scene but enough information can be gained for a number of practical applications. For models representing the heat transfer between ocean and atmosphere the detection of sea ice cover presence is frequently considered sufficient. For navigation the thickness of sea ice is important and because of the relationship between ice thickness and its age, distinguishing between first year and multi-year sea ice from radiometric measurements is used to give an estimate of ice thickness.

The radiometric contrast between sea ice of all types and open water is very clear in winter as the emissivity of the ice is much greater than that of the open ocean. During the summer season however, because of the surface melt this contrast between the two sea ice types is reduced which increases the difficulty of differentiating between the two using radiometric measurements. In Figure 2.2 the different radiometric signatures of first year, multi-year and open ocean surfaces are shown for the frequency range between 0 and

100 GHz. The contrast between sea ice (A,B,C) and ocean surface (D) is larger at the lower end of the frequency range, while the contrast between first year (B) and multi-year ice (C) is more pronounced at the higher frequencies. The effect of melt conditions on the sea ice emissivity is also shown as a late summer sea ice (mixed first-year and multi-year) curve (A) with higher emissivity values across the whole frequency range.

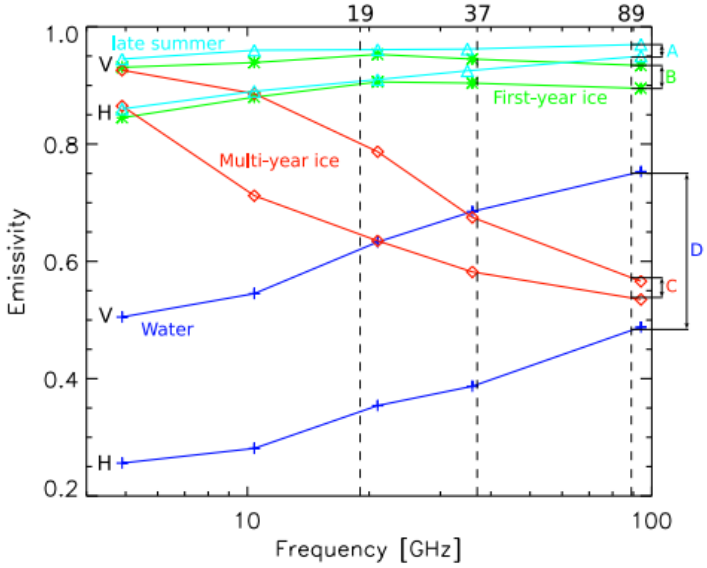

Figure 2.2: Vertical and horizontal emissivities of different surface sea ice types and open ocean between 0-100 GHz. From Spreen et al. [2008].

While penetration depth is a term more suitable for active measurements, in the context of passive microwave radiometric observations the penetration depths refers to the thickness of the layer whose emission contributes to the total surface signal which is transmitted at the ice-air interface. Because of the high variation in snow cover, salinity, shape, size and orientation of the brine inclusions, density and temperature profile of the ice layer the microwave penetration depth in this medium is also highly variable (Fig. 2.3). The dielectric loss factor of sea ice decreases with the sea ice temperature and increases with salinity. Because of this in general the penetration depth in first year ice which has higher salinity and density is lower than in multi year ice which has lower salinity and is less dense because of the air inclusions.

Surface scattering effects occur for all ice types due to irregular features on the sea ice, such as ridges and edges. For the case of first year ice, due to the low penetration depth scattering occurs mainly at the surface. The snow layer can contribute to the volume scattering effects, but in winter the snow is dry and mostly transparent to microwave radiation. For multi-year ice, once the wavelength of the radiation is close to the size

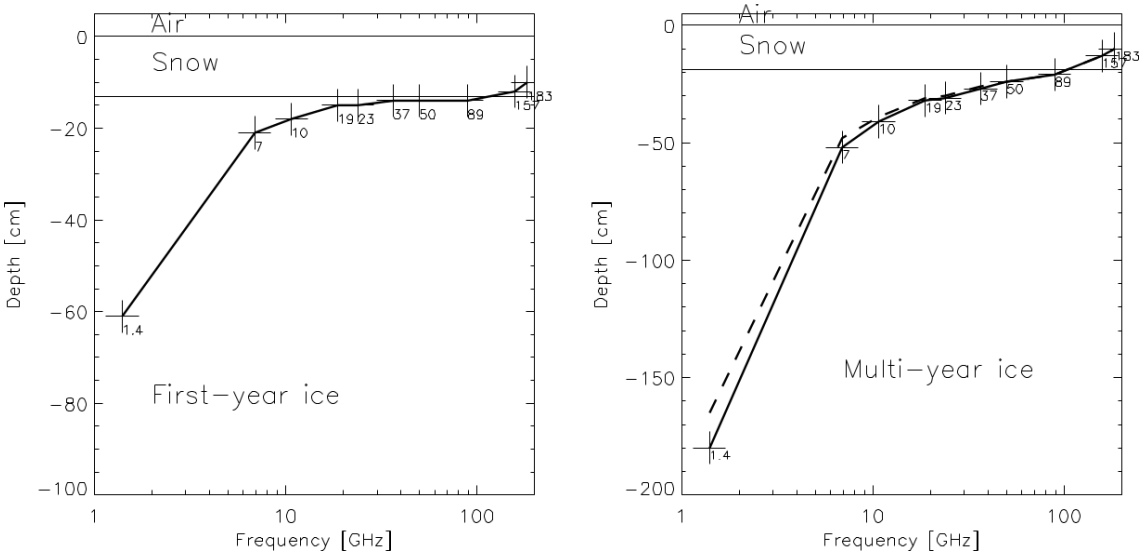

Figure 2.3: Penetration depth for frequencies between 0-100 GHz in first year and multi-year ice while assuming a snow layer of 20 cm. From Mathews [2007].

of the air bubbles trapped in the ice, coupled with the larger penetration depth typical for this ice type, volume scattering becomes significant. Besides the lower intensity of emerging radiation because of volume scattering, the multi-year ice radiometric signature is also more polarized than for first year ice (Fig. 2.2). When the melt seasons starts and the snow layer on top of ice becomes wet, the signal from the underlying sea ice can be masked by the snow layer.

3 Data

3.1 AMSR-E data

3.1.1 The instrument

The Advanced Microwave Scanning Radiometer for Earth Observing System (AMSR-E) is a passive microwave radiometer on board NASA (National Aeronautics and Space Administration) spacecraft AQUA. It has a conical scan geometry with an incidence angle of around 55°. The instrument measures microwave emissions from the Earth's surface and atmosphere in twelve channels at six different frequencies between 6.9 and 89 GHz in vertical and horizontal polarizations [Imaoka et al., 2002].

The technical details of the instrument are shown in table 3.1. Because the footprint of the 89 GHz channels is so small (3.5×5.9 km^2), in order to properly sample the Earth's surface there are two scan lines for these channels, Scan A and Scan B, that are interweaved to cover the gap between the scan lines.

3.1.2 Level-2A resampled brightness temperatures

In the initial integrated retrieval paper [Melsheimer et al., 2008] it was found that using the first ten channels of AMSR-E in their native resolutions for the retrieval caused discrepancies between the observed and the forward model simulated brightness temperatures. These discrepancies appeared in regions with strong gradients such as at the sea ice edge or in areas with high surface roughness and they are caused by mismatches between the different channel footprints. Because each channel "sees" a slightly different scene on the Earth's surface, we need to compensate for this mismatch in order to use all the channels

Table 3.1: Technical characteristics of the AMSR-E instrument, from [Imaoka et al., 2002].

Polarization	Horizontal and vertical					
Incidence angle	55°					
Swath	1445 km					
Dynamic Range (K)	2.7 to 340					
Precision	1 K (1σ)					
Center Frequency (GHz)	6.925	10.65	18.7	23.8	36.5	89.0
Bandwidth (MHz)	350	100	200	400	1000	3000
Sensitivity (K)	0.3	0.6				1.1
Mean Spatial Resolution (km)	56	38	21	24	12	5.4
IFOV (km)	74 x 43	51 x 30	27 x 16	31 x 18	14 x 8	6 x 4
Sampling Interval (km)	10 x 10					5 x 5
Integration Time (msec)	2.6					1.3
Beamwidth (degrees)	2.2	1.4	0.8	0.9	0.4	0.18

for retrieving the geophysical parameters. This issue is alleviated by using the Level 2A resampled brightness temperature data product [Ashcroft and Wentz, 2000].

The AMSR-E Level 2A dataset contains several spatially consistent subsets of brightness temperature observations resampled to the footprint sizes of the 6.9, 10.7, 18.7, 36.5, and 89 GHz channels. This is achieved by bringing the Level 1A antenna temperatures to the common spatial resolution using a set of weighted coefficients. Every Level 2A observation in a scan line is calculated using the coefficients that correspond to the relative weights of all neighboring Level 1A observations. These coefficients are unique for every position within one scan line but they do not vary between different scan lines. The weighting coefficients for the Level 1A observations are produced using the Backus-Gilbert method. The different subsets are produced by resampling the higher resolution channels to match the larger footprint size of the lower resolution channels. The available subsets are shown in table 3.2.

There are two sources of error in the resembled brightness temperature datasets. The first one represents the mismatch between the ideal antenna pattern and the constructed brightness temperature. The second one is the random measurement error that carries over into the resampled values. An important consequence of the spatial averaging of multiple small gain patterns from the high resolution channels into one large gain pattern corresponding to the low resolution channels is the reduction in the measurement noise for one constructed (resampled) observation. This noise reduction is influenced by the

Table 3.2: Spatial characteristics of AMSR-E Level 2A observations. Adapted from [Marquis et al., 2003]

Res.	**Footprint size**	**Mean spatial resolution**	**Channel frequencies [GHz]**					
			89.0	36.5	23.8	18.7	10.7	6.9
1	74 km x 43 km	56 km	•	•	•	•	•	•
2	51 km x 30 km	38 km	•	•	•	•	•	
3	27 km x 16 km	21 km	•	•	•			
4	14 km x 8 km	12 km	•	•				
5	6 km x 4 km	5.4 km	•					

number of real observations that are included in the averaging. For our application we want to use all AMSR-E channels resampled to one common resolution. This necessarily means that the common resolution is that of the lowest frequency channels, the 6.9 GHz channels. Because at this resolution the gain pattern can fit the maximum number of observations for any higher frequency channel it follows that the noise reduction will also be the highest for this resampled set of brightness temperatures. Another consequence of the spatial averaging is that the errors of neighboring observations will have a degree of correlation with each other within a given channel. It is important to note that individual channel errors are not correlated.

3.2 ECMWF data

The ECMWF model data was used in the OEM prototype as a source for the start guess position needed to start the iterative process. Eventually, this data became the source for constructing pixel wise background ensembles of WSP, liquid water path, water vapor and surface temperatures.

The European Centre for Medium-Range Weather Forecasts (ECMWF) provides forecast and reanalysis datasets that include temperature, pressure, WSP as well as cloud cover, cloud liquid water content and humidity from model runs. The particular ECMWF product we used for all the results included in this work is the ERA-Interim [Dee et al., 2011], a global atmospheric reanalysis produced by ECMWF. The majority of observation data assimilated in ERA-Interim originates from satellites which vary according to the period of interest. This assimilated data includes clear-sky brightness temperatures from orbiting and geostationary sounders and imagers, atmospheric motion vectors from geostationary satellites, scatterometer wind data and ozone retrievals. Measurements of

atmospheric refraction from GPS radio occultation are also included for the period relevant to this study. Conventional observations from radiosondes, pilot balloons, aircraft and wind profilers as well as ground measurements of surface pressure, temperature, relative humidity and surface winds are also assimilated. Direct satellite radiances over open water from channels 5-10 of AMSR-E and channels 3-5 from the AMSU-B sounder are also assimilated. Because of our local storage necessities the ERA-Interim data is gridded to a 1.5°grid with four 6 h time steps per day. For each AMSR-E swath the corresponding ERA-Interim grid points and closest time step data is extracted from the global grid and profiles of cloud liquid water and atmospheric water vapor are integrated as needed to provide columnar values which are required by the forward model.

3.3 NASA Team algorithm

The other component of the background and first guess data is represented by the surface parameters of sea ice concentration and multi-year ice fraction. These values are generated before the first iteration by a simplified implementation of the NASA Team algorithm [Markus and Cavalieri, 2000]. It can provide total ice concentration as well as multi-year ice concentration from which the multi-year ice fraction is calculated. The algorithm uses for retrieval the 18.5 GHz channel in both polarizations and the 36.5 GHz channel in the vertical polarization. The version implemented in the OEM does not use any weather filters in order to attempt a retrieval on every pixel without discarding any due to weather influences.

3.4 ASR data

In order to test the influence of different changes to the OEM on the retrieval, a consistent comparison data set was needed. The most accessible source for these parameters are ECMWF model data but since the ERA-Interim is integrated as the first guess point for the OEM a distinct data set was required. The Arctic Systems Reanalysis was selected as a benchmark against which to check how reasonable the OEM output is. This provides a high resolution ensemble of atmospheric and surface temperature parameters. ASR is produced from runs of the Polar Weather Forecast Model using the WRF-VAR and the High Resolution Land Data Assimilation systems. The data assimilation systems have been optimized for the Arctic region. The resolution of the product dataset is 30 km. Similar to the ERA-Interim, the ASR product assimilates both satellite and ground measurements from the Arctic and the authors of this data set claim that there is a high commonality with the ERA-Interim for the assimilation sources [Bromwich et al., 2001]. The output parameters from the two reanalysis products are also similar but with distinctly different distributions. The distributions of all output parameters from the two sources have been

compared using the Kolmogorov–Smirnov test and the two data sets have proven to be statistically different, it was therefore felt that ASR is a safe benchmark for comparing against.

3.5 Round Robin Data Set

In order to test the sea ice concentration retrieval of our method we used the Round Robin Data Set [Pedersen and Saldo, 2012]. This data product comprises two subsets which contains cases of validated 100% (SIC1) sea ice concentration and the other contains cases of open water near, but at a safe distance from the ice edge (SIC0). The dataset originates from the sea ice project of the Climate Change Initiative and it provides a source for validating sea ice concentration retrieval [Pedersen and Saldo, 2012, Ivanova et al., 2015] and for testing atmospheric parameter retrieval over pure surface types. The data package includes collocated ERA-Interim values for WSP, integrated columnar water vapor, liquid water path, sea surface temperature, ice skin temperature and scatterometer backscatter data from ASCAT. The temporal coverage for the RRDP version used in this work spans from 2007 to 2011. The RRDP is not recommended for use during the Arctic summer when the 100% SIC data points in the SIC1 data-set cannot be validated and so the analysis performed with this data package is limited to data points from January to April and November to December of every year.

3.6 2006 Dataset

The Arctic environment goes through many changes throughout the year. Sea ice extent, melting conditions and snow cover all influence the surface component of the microwave emission. In order to capture this variability and to measure its impact on the retrieval we created a large dataset (20 million data points) that spans the entire year 2006. In order to reduce the demand on computational and storage resources we sampled every tenth day of the year and included all AMSR-E swaths of that day into our dataset. The dataset starts on January 11^{th} 2006 and ends on January 6^{th} 2007. For this dataset we collocated both ASR atmospheric data fields as well as Advanced Microwave Sounding Unit B (AMSU-B) retrieved water vapor and ASI retrieved sea ice concentration data points.

3.7 ASI SIC data

The presence of sea ice has the largest influence on the AMSR-E measured brightness temperatures. Even low concentrations of sea ice determine a strong response in the measurements and as such correctly identifying the SIC is very important for separating the surface and atmospheric contributions in the measured TB signal. An accurate SIC

retrieval is therefore crucial for the goal of retrieving the ensemble of seven parameters and in order to test this we used an operational SIC product for comparing with the optimal estimation retrieval. This is the ARTIST Sea Ice product [Spreen et al., 2008] which uses the polarization difference between the 89 GHz V and H channels from the same AMSR-E radiometer in order to retrieve SIC at a high resolution of 6.25 km. Because of the important atmospheric influence on the TB signal at 89 GHz the presence of high water vapor or cloud liquid water can lower the polarization difference over open water scenes leading to retrieval of spurious SIC values. Weather filters are used in order to reduce the atmospheric influence over open ocean. The influence of water vapor and clouds over high sea ice areas is less pronounced than over open ocean but it cannot be filtered resulting in low scale variability in the final ASI product for high SIC values.

3.8 AMSU-B TWV data

As a validation tool for atmospheric water vapor retrieval we selected the AMSU-B total water vapor product [Melsheimer and Heygster, 2008].

This method uses passive microwave sounding channels which have similar surface emissivity but different atmospheric absorption characteristics. It uses three channels around the water absorption line at 183 GHz to detect the low water vapour values typical for the atmosphere over sea ice in the Central Arctic. A special characteristic of this retrieval product is that uncertainty increases with increasing water vapour values from about 1 mm for retrieval values below 2 mm to an uncertainty around 3 mm for retrieval values around 14 mm. For scenes with atmospheric water vapor above 15 mm the method does not retrieve anything as all channels around the 183 GHz frequency become saturated. Very important to the comparison effort with OEM is that the AMSU-B TWV retrieval was specially designed to function over sea ice which makes it ideal for testing the reliability of OEM atmospheric retrieval in the Arctic. For the comparison only those pixels were selected where both the optimal estimation retrieval and the AMSU-B product have valid values which means that only TWV values between 0 and 15 mm were included.

4 Method

4.1 Optimal estimation method (maximum a posteriori solution)

In this chapter the basic retrieval method is described starting from the theory of optimal estimation and concluding with the adaptations necessary for the specific inversion application that is the topic of this thesis. Testing and establishing a specific set-up of the retrieval method will be addressed in more detail in Section 5.

Following the basic radiative transfer theory described in Section 2 we can approximate the brightness temperatures measured at the top of the atmosphere by a passive microwave radiometer as a function of a number of geophysical parameters.

$$T_A = F(\mathbf{p}) \tag{4.1}$$

where $\mathbf{p}$ is the state vector containing both surface parameters such as SST and atmospheric profiles of temperature, humidity and liquid water, surface sea ice cover and WSP vectors. F is the forward operator (Section 4.2) that maps the functional relationship between the state vector parameters and the observed brightness temperatures. The measured brightness temperature contains information about all of these parameters. Retrieving relevant data about all of them is an under-constrained problem because several of the state vector parameters are continuous, such as temperature or pressure profiles, while the number of brightness temperature measurements is finite [Pedersen, 1994].

In order to derive the geophysical parameters from the measurements we need a forward model that can describe the measurements in terms of the required geophysical parameters and then invert it. The forward model might not be easily invertible or the errors in the

measurements together with errors in the forward model simulation can make it impossible to find a solution.

The inverse problem consists of inverting a known equation which relates thermal radiation to the state of the atmosphere and surface in order to express atmospheric parameters in terms of the measured radiation. This sort of problem is ill-posed because there is no mathematically unique solution for it. From this we follow with the estimation problem which means finding the appropriate criteria for choosing the solution that is most consistent with the measurements [Rodgers, 1976].

The estimation method used here follows [Rodgers, 2000] and is called the maximum a posteriori. Through an iterative process the prior state vector $\mathbf{p_n}$ is nudged to a new state $\mathbf{p_{n+1}}$ so that a cost function is minimized. This cost function balances the penalty of departing from the background state vector (P_a) with the penalty of deviating from the observed brightness temperatures. This ensures that at each iteration step the state vector is within a realistic distance of the background values while trying to match the measurements within a reasonable precision range. This process involves two sets of constraints. We would expect to find reasonable values for the state vectors spaced within the natural variability constraints around the the background position. These constraints for the state vector space are represented by a covariance matrix with the individual parameter variances on the diagonal and inter-parameter covariances in the off diagonal elements. This is called the a priori covariance matrix because it represents the level of knowledge about the geophysical state before the measurements are made. The background values represent long term means from climatological or other sources which together with the individual parameter variances in the background covariance matrix S_a constrain the retrieved parameters to physically realistic values. The diagonal elements of the corresponding covariance matrix should represent the natural variability of each parameter in order to allow for a consistent retrieval, but this information is limited by the quality of the prior information we have about the climate system. In order to speed up the iterative process for finding the optimal solution, the method also uses a first guess point that serves as initialization state. The first guess state can also come from a background state but that is not the only source Rodgers [2000]. According to Pedersen [1994] the retrieval accuracy is influenced by the quality of the first guess data. A similar constraint is used for the observation space. A covariance matrix contains the individual channel variances that constrain the forward model simulated brightness temperature to a reasonable accuracy. This level of accuracy is chosen based on the combined measurement, modelling and geophysical parameter errors that together influence how far from the observed brightness temperatures the simulated values are permitted to be. The shape, construction and importance of the covariance matrices that represent the constraints for the optimal estimation are discussed in further detail in Chapter 5.

4.2 Forward model (adaptations for use over sea ice)

The forward model is needed in order to translate the seven geophysical parameters into the twelve brightness temperatures corresponding to the AMSR-E radiometer channels. To this end it uses separate modules to address different components of the radiative transfer equation. The upward component uses a sea surface emissivity model that takes into account the sea surface temperature, calculates the frequency specific dielectric constant of sea water, and uses a geometric model for the wind roughened ocean surface contribution. For the atmospheric component the forward model uses frequency specific absorption and scattering coefficients. In the frequency range of the AMSR-E channels the main atmospheric absorbers are oxygen and water so that these coefficients have been calculated from compiled radiosonde flights. The amount of atmospheric water vapour and cloud liquid water is connected to the atmospheric emission temperatures through a list of regression equations. An important feature of the forward model is that the radiative transfer equation uses the absorption-emission approximation which excludes scattering from large rain drops and ice particles. This assumption is valid for clear and cloudy skies and for light precipitation conditions for the frequency range of 6 to 37 GHz. At the 89 GHz channels however, scattering by clouds is no longer negligible.

The original implementation of the forward model [Wentz and Meissner, 2000] was designed to work over open ocean surfaces only. In order to use it over the ice covered central Arctic areas the calculation of the surface emission has to be modified in order to account for the different microwave emissivity of sea ice [Melsheimer et al., 2008]. Each pixel is now considered as being formed of a mixture of open water, first year and multi-year ice. The up-welling thermal contribution of the surface will then be:

$T_S = C_{ow}E_{ow}T_{ow} + C_{fyi}E_{fyi}T_{fyi} + C_{myi}E_{myi}T_{myi}$,

where C_{ow}, C_{fyi} and C_{myi} represent the concentration of each surface type in the current pixel. The sum of these three factors must be 1. Corresponding to each surface type E_{ow}, E_{fyi} and E_{myi} are the microwave channel specific emissivities for open water, first year ice and multi-year ice respectively.

The second equation that needed to be modified is the one responsible for calculating the reflection and scattering of the atmospheric down-welling radiation. The reflectivity of a pixel will be calculated from individual reflectivities of each surface type.

$R_{eff} = 1 - E_{eff} = 1 - (C_{ow}E_{ow} + C_{fyi}E_{fyi} + C_{myi}E_{myi})$

This then opens up the necessity of having some information about the surface emissivity of sea ice. Frequency dependent emissivities are based on the empirically retrieved values from Mathews [2007]. These values represent monthly averages and the individual value for each pixel is calculated by interpolating in time between these monthly values.

4.3 Error treatment and covariance matrices

The background values represent long term means from climatological or other sources which together with the individual parameter variances in the background covariance matrix S_a constrain the retrieved parameters to physically realistic values. The diagonal elements of this covariance matrix should represent the natural variability of each parameter in order to allow for a consistent retrieval, but this information is limited by the quality of the prior information we have about the climate system. In order to speed up the iterative process for finding the optimal solution, the method also uses a first guess point that serves as initialization state. The background state can be used as the first guess state. According to Pedersen [1994] the retrieval accuracy is influenced by the quality of the first guess data. In order to test the sensitivity of the retrieval method to the background covariance matrix and to the first guess conditions, different implementations of the optimal estimation retrieval are compared. For each of these tests one reference version was kept the same. It uses a diagonal background covariance matrix (see Appendix, Table A.1) obtained from year long ECMWF ERA Interim mean variances for the atmospheric parameters and the surface temperatures. For the sea ice concentration and multi-year fraction variances, a locally processed dataset using the NASA Team algorithm Markus and Cavalieri [2000] was used for the same time period. The background state vector for all versions tested below represents the yearly mean values for each parameter (Appendix, Table A.1), and is calculated from the same sources as the reference background covariance matrix. For this reference OEM version, the start guess comes from temporally and spatially collocated ECMWF ERA Interim data.

As discussed above, the satellite measurements are connected with a measurement error due to instrumental noise and the nature of the measurements themselves. This measurement error is considered to be normally distributed and is represented in the retrieval through the covariance matrix S_e. Each of the twelve individual channels of the radiometer is represented in the error covariance matrix by the variance of its measured brightness temperature. The error covariance matrix S_e is diagonal because the measurement channels are assumed to be independent.

The covariance matrix of the geophysical parameters represents a priori information about these parameters together with the background values which represent a long term mean of these parameters. In our method, the non diagonal elements of the parameter covariance matrix are zero and the diagonal elements represent the variance of each geophysical parameter. These variances have been estimated from climatological archives and model data. For the three atmospheric parameters of integrated columnar water vapour, cloud liquid water and WSP as well as the surface temperature for both ice free ocean and sea ice, the variance values have been derived from a full year of ERA Interim reanalysis data. For the sea ice parameters, climatological averages were used.

In an attempt to add more data to the a priori, separate covariance matrices have been calculated for open water and sea ice covered areas. The switch between these two covariance matrices was implemented as a SIC threshold where the open ocean covariance matrix was used for areas with less than 75% sea ice cover. Using the specific sea ice covariance matrix was supposed to take advantage of the natural correlations that occur between the sea ice covered surface and atmospheric parameters such as TWV. These covariance matrices were calculated using three separate retrieval products that can cover the open ocean and the sea ice-covered central Arctic respectively. For the open ocean the RSS retrieval product [Wentz and Meissner, 2007] for the atmospheric parameters of WSP, total water vapor, cloud liquid water and sea surface temperature was used. For the sea ice-covered regions the ASI sea ice product [Spreen et al., 2008] was combined with the AMSU-B total water vapor product [Melsheimer and Heygster, 2008] in order to assess the covariance between these two parameters. The threshold switch for SIC was set because areas with high sea ice assure a lower uncertainty for the AMSU-B product.

After implementing these separate covariance matrices, a test was run for the RRDP dataset (Section 3.5) in both SIC1 and SIC0 situations. The results were inconclusive, the algorithm using separate covariance matrices did not show any clear advantage over the classic algorithm using one single covariance matrix with mostly diagonal elements. Because the latter version is technically simpler to implement, the initial single covariance matrix system was selected for further testing and the multiple covariance matrix approach was abandoned for the moment.

4.4 The inverse method

The iterative solution is found by inverting

$$T_A = F(\mathbf{p}) + e \tag{4.2}$$

where T_A is the vector of satellite measured brightness temperatures. F is the forward model, $\mathbf{p}$ is the state vector containing the seven geophysical parameters (WSP, TWV, LWP, SST, IST, SIC, MYIF) and e is the measurement error. The solution is found by using the Jacobian of the forward model

$$M = \frac{\partial F(\mathbf{p})}{\partial \mathbf{p}} \tag{4.3}$$

and iterating the state vector following the Gauss-Newton method

$$\mathbf{p_{n+1}} = \mathbf{p_n} + \hat{S}_n^{-1}(M_n^T {S_e}^{-1}(T_A - F(\mathbf{p_n})) + {S_a}^{-1}(p_a - \mathbf{p_n})) \tag{4.4}$$

where $M_n = M(\mathbf{p_n})$ and

$$\hat{S}_n = ({S_a}^{-1} + {M_n}^T {S_e}^{-1} M_n)^{-1} \tag{4.5}$$

is the a posteriori covariance matrix of the state vector.

The Gauss-Newton iteration nudges the state vector to follow a quadratic approximation of the cost function. In the case that the forward model is too non-linear for the Gauss-Newton method to work, the iteration step towards finding a solution needs to be chosen at each iteration in order to decrease the cost function. This can be achieved by adding an additional parameter to the iteration rule as proposed in the Levenberg-Marquardt method [Rodgers, 2000]:

$$\hat{S}_n = ((1+\gamma){S_a}^{-1} + {M_n}^T {S_e}^{-1} M_n)^{-1} \tag{4.6}$$

The key difference is that γ is chosen at each iteration step and the cost function is evaluated. If the cost function decreases the iteration values are accepted. If the cost function does not decrease then γ is increased to force the iteration on a steeper decent (and a smaller step size) towards the minimum and the same iteration step is repeated.

The convergence conditions suggested by [Rodgers, 2000] are implemented in order to stop the iteration process and output the optimal solution. The method will check whether the following is true

$$d^2 = (\mathbf{p_{n+1}} - \mathbf{p_n})^T \hat{S}_n^{-1} (\mathbf{p_{n+1}} - \mathbf{p_n}) < 7 \tag{4.7}$$

This represents the degrees of freedom of the system and seven was chosen as the dimensionality of the state vector. An additional condition for convergence to be accepted is whether the cost function Δ has been decreased following the last iteration

$$\Delta = ||T_A - F(\mathbf{p_n})||. \tag{4.8}$$

If both of these conditions are fulfilled, $\mathbf{p_n}$ is accepted as the solution and sent to output.

AMSR-

5 | Developing and testing the method

The OE method needs information about the prior state of the geophysical system in order to stabilize the results. This prior information is crucial because it constrains the possible number of solutions to the state vector that match the observations within a prescribed uncertainty. The quality and nature of the a priori data will influence the OE retrieval results. In order to find what is the sensitivity of the OE retrieval to changes in the a priori constraints a number of tests have been performed. These tests touch on all forms of a priori information used in this OE implementation and expand on the preliminary results shown in Scarlat et al. [2017]. The a priori elements are

(i) the background covariance matrix S_a - Section 5.1

(ii) sea ice surface temperature parametrization IST - Section 5.2

(iii) the background state vector P_a - Section 5.3

(iv) the first guess for the iterative process P_0 - Section 5.4

(v) the sea ice emissivities used to parametrize the sea ice surface contribution in the forward model - Section 5.5

(vi) the modelling and measurement errors included in the brightness temperature (Tb) covariance matrix S_e - Section 5.6.

The sea ice parameters form an important fraction of the state vector and affect the brightness temperature signal. Therefore the RRDP data set used for these tests is subdivided into two distinct data subsets that account for the scenario of 100% sea ice cover and for open water. This reproduces as much as possible a controlled test environment in which

we can isolate the surface specific effects on the retrieval from the effects of the changes in the a priori constraints. The goal of these tests is to find and justify the final set-up for the OEM a priori constraints which will be used in the comparison tests of Chapter 6. In all of the tests one basic OEM implementation is kept as reference. This reference version is based on the prototype OEM and uses the diagonal covariance matrix and background values shown in Table A.1. All OEM version tested in this chapter use the 10 channels between 6.9 and 37 GHz, excluding the two 89 GHz channels of AMSR-E (for more details see Section 5.5).

For every modified OEM version tested against the reference, the practical effects on the retrieval are shown in tables such as standard deviation of the output or agreement against ASR benchmark data. To completely characterise the results, we need to know if the modifications to the OEM cause statistically significant changes in the retrieval. The Kolmogorov–Smirnov (K-S) test is used for each retrieved parameter to determine whether the distribution of the modified OEM output is significantly different from that of the reference output. For most of the comparisons made the changes are found to be significant, with the lowest confidence level corresponding to 99.999% and with typical values higher than that. In the context where the size of the RRDP sample used in the comparisons is on the order of 13000 data points for SIC0 and 17000 data points for SIC1, we believe this confidence level is sufficient. There are however cases where the modifications to the OEM do not result in statistically significant changes in the retrieval parameters. In each case the K-S test result is included in the discussion along side the practical changes in the output. The p values resulting from the K-S test give the confidence level for rejecting the null hypothesis that the compared samples have the same distribution. Because in most cases this p value is very small, and showing its nominal value would not contribute to the discussion, for every comparison case the conclusion of the K-S test is discussed but the values themselves are not shown separately.

5.1 Sensitivity to the background covariance matrix (S_a)

One of the a priori components is the background covariance matrix (S_a) which constrains the space in which we expect the geophysical parameters to be found. This matrix is obtained from any prior knowledge about the climate system including climatological data, ground measurements and other retrieval sources. The diagonal elements of the covariance matrix represent the parameter variability while the off-diagonal elements show correlations between parameters. The background covariance matrix should use the best possible knowledge about the investigated climate system before the measurements are taken in order to speed up the convergence process [Rodgers, 2000] and retrieval precision by imposing realistic limits on the state space. At the same time this information should be unbiased [Merchant et al., 2008] in order to lead to an unbiased optimal retrieval. The following

tests provide insight into several aspects of selecting the background covariance matrix. The data source used for generating the elements of this matrix should be representative for the spatial and temporal domain of the OE retrieval (Section 5.1.1). The background covariance matrix influences the retrieval by imposing different restrictions depending on whether or not off diagonal elements are included (Section 5.1.2). Although the a priori information cannot be perfect and the OE retrieval is stable for small scale variability in the background covariance matrix elements, large scale changes in individual diagonal elements will have a direct impact on the retrieval precision of the corresponding state vector parameter (Section 5.1.3).

5.1.1 Data source for S_a

For testing the importance of the data source of the background covariance matrix, we compare an OEM retrieval that uses a covariance matrix based on one year of climatology data with two different OEM implementations that use climatology derived values from the Max Planck Institute for Meteorology (MPI-M) Climate model (F. Bunzel, personal communication). The main difference between the ERA-Interim and the MPI-M derived parameter variances is that the former included one year of data while the latter only data from one winter month. This means that the two data sources represent the variability of the geophysical parameters on different time scales. The year long data set includes one full cycle of seasonal variability while the winter month data set only reflects typical variations for that time window. From the two MPI-M derived matrices one is a diagonal covariance matrix of the same shape as the reference version while the other, besides the same diagonal elements, also includes the off-diagonal elements that represent covariances between parameters. These three background covariance matrices are given in the Appendix in Tables A.1, A.3 and A.4 for the reference OEM S_a, and the two MPI-M derived matrices respectively. While for the ERA-Interim based covariance matrix data from the NASA Team sea ice algorithm was required to fill in the variances for SIC and MYIF, the MPI-M data source includes all parameters except SST and MYIF. For this reason the variances for SST and MYIF are the same for all matrices.

For ease of notation in the following discussion the one year climatology based diagonal covariance matrix and the OEM version that uses it will be referred to as C-diag, the diagonal covariance matrix based on MPI-M climate model data from February will be called Feb-diag OEM and the final version that uses the full covariance matrix from the same MPI-M model data will be Feb-full.

All three versions of the OEM are run for both the RRDP SIC0 and SIC1 data sets and the standard deviations of the output parameters are compared between OEM versions. The same background values were used for all versions, the only difference between these OEM implementations being the shape of the background covariance matrix. The results are shown in Table 5.1 for the RRDP SIC0 and Table 5.2 for SIC1.

Table 5.1: Mean value and standard deviation of output parameters from OEM retrieval using different background covariance matrices. Data set used is SIC0.

Stat	Parameter	units	C-diag	Feb-diag	Feb-full
Mean value	WSP	[m/s]	9.76	7.75	9.49
	TWV	[mm]	11.16	10.86	10.96
	LWP	[mm]	0.10	0.11	0.10
	SST	[K]	278.90	278.16	278.32
	SIC	[%]	-0.97	0.68	-0.47
Standard dev.	WSP	[m/s]	4.55	3.07	3.76
	TWV	[mm]	5.44	5.18	5.30
	LWP	[mm]	0.17	0.07	0.08
	SST	[K]	2.85	3.27	3.52
	SIC	[%]	1.87	1.88	1.59
% of convergent points			99.91	97.76	99.32
Avg. no. iterations			4.10	6.07	13.66

Table 5.2: Mean value and standard deviation of output parameters from OEM retrieval using different background covariance matrices. Data set used is SIC1.

Stat	Parameter	units	C-diag	Feb-diag	Feb-full
Mean value	TWV	[mm]	2.07	2.53	4.70
	LWP	[mm]	0.20	0.16	0.17
	IST	[K]	262.26	264.08	264.40
	SIC	[%]	97.66	97.53	97.33
	MYIF	[%]	46.37	51.71	54.84
Standard dev.	TWV	[mm]	2.36	1.73	1.78
	LWP	[mm]	0.19	0.05	0.05
	IST	[K]	5.94	4.99	5.22
	SIC	[%]	2.22	2.20	2.46
	MYIF	[%]	30.45	32.02	31.57
% of convergent points			70.08	57.92	61.70
Avg. no. iterations			13.91	16.01	16.456

Both the Feb-diag and the Feb-full OEM versions determine statistically distinct distributions for all retrieval parameters in both the SIC0 and SIC1 cases, compared to the reference OEM version using the C-diag S_a. The lowest confidence level resulting from the K-S tests corresponds to a p value of 10^{-12}. Regarding the practical effects of implementing the modified background covariance matrices, larger variances do not always result in larger retrieval standard deviations. For the SIC0 comparison the largest difference between OEM version results can be seen for WSP and especially LWP retrieval which are parameters with a significant difference in variance between the three OEM versions. For TWV however there exists a big difference in the corresponding variance term in the covariance matrices, but a very small difference in the retrieval results. A similar situation is evident in the SIC1 comparison where again LWP and this time IST (in the absence of WSP retrieval over 100% SIC) display the highest differences between the OEM versions while the TWV retrieval variability between OEM versions differs more than over SIC0.

The larger values for variance and retrieval standard deviation correspond to the C-diag covariance matrix which is based on one year of data. While the variances can be explained through the fact that the yearly variability of these geophysical parameters is larger than the variability within one winter month, the retrieval differences partially stem from the reduced constraints imposed on the OEM. A larger parameter variance in the background covariance matrix can result in higher variability in the corresponding retrieval parameter but this is not always the case and will be investigated further in the Section 5.1.2.

The largest impact of the different covariance matrices on the results can be seen in the number of convergent cases and the average number of iterations required to reach convergence. Ideally the off-diagonal elements of the background covariance matrix in Feb-full should introduce more information about the state of the climate system before the measurement are taken. However, it is difficult to evaluate whether the covariances used are representative for the yearly time scales used in the retrieval testing. The results of this comparison seem to indicate that these covariances impose an additional constraint on the method which in certain cases cannot be satisfied within 50 iterations resulting in almost 10% fewer convergent results. Similarly, the diagonal matrix based on one month of data for Feb-diag imposes unrealistic constraints on the OEM as the variances it contains are not representative for the parameter variability throughout the year.

It is important to note the difference between the convergence performance over SIC0 and SIC1 for the reference OEM version. While much lower over SIC1 than over SIC0, it must be noted that this reference OEM is meant to be used in tests only, as it uses arbitrary sets of parameters which are meant to be improved as a result of these tests. The issue of the relatively low convergence rate over SIC1 will be addressed in Subsection 5.3.

5.1.2 Information content analysis for different S_a versions

The section above shows the effect of different versions of the background covariance matrix on the retrieval. The tight constraints of the Feb-full S_a entail a lower convergence rate and a higher number of iterations needed for reaching convergence (Tables 5.1, 5.2). The impact on the retrieval is however harder to interpret from looking at the parameter standard deviations only. In the case of TWV for example, a variance difference between S_a versions does not trigger a significant increase in output standard deviation. For a more complete understanding of the effects of improper constraints on the OEM we studied the change in the information content for different versions of the background covariance matrix. The information content of a measurement as described by Rodgers [2000] represents the change in the logarithm of the number of distinct states of the system that is being measured. This is based on the original definition by Shannon and Weaver [1949]. For the sake of clarity all references to information content used throughout this thesis are meant to be understood in the context of the Shannon definition for information. The number of distinct states that the measured system can take is called the system entropy. If we take the base 2 logarithm of this change in entropy then the information content can be measured in bits.

A probability distribution function P can characterise the possible states of the system, then the information content of a measurement of this system depends on the entropy of the system $S(P)$. The change in entropy as a result of the measurement can be written as

$$H = S(P_a) - S(P_p), \tag{5.1}$$

H is the information content of the measurement, P_a is the state of the system before the measurement is performed and P_p is the state after. The decrease in entropy is equivalent to a decrease in the uncertainty about the state of the system and it represents the new knowledge that the measurement brings.

If we assume Gaussian distribution the entropy of the system is then

$$S(P) = \frac{1}{2} ln|S|, \tag{5.2}$$

with $|S|$ being the determinant of the background covariance matrix which describes our knowledge about the system before the measurements are made. The change in entropy following the measurement or the information content of the measurement will then be

$$H = -\frac{1}{2} ln|S_p S_a^{-1}|, \tag{5.3}$$

S_p being the covariance matrix of the system after the measurement, and S_a the system covariance matrix before the measurement.

A different tool for studying the information content of a measurement is the number of degrees of freedom of the system. One degree of freedom of the measurement represents

one independent component which contains information on the state of the system and the information uncertainty is smaller than the measurement error of the component [Ulaby et al., 2014]. If the total number of degrees of freedom of a set of measurements is smaller than the number of measurements, only a part of the measurement components will bring in independent pieces of information that can be observed above the noise level. The degrees of freedom for signal can be written as the trace of the matrix product

$$d_s = tr(S_p S_a^{-1}). \tag{5.4}$$

Following Rodgers [2000], the retrieval system can be described as

$$y = Kx, \tag{5.5}$$

where y represents the observations, x the variables and K the weighting function of the forward model that relates the variables to the observations. The purpose of the information content analysis is to determine if the measurement error allows the retrieval of the desired variables by comparing this error to the natural variability of the variables. Any component for which the natural variability is higher than the measurement error can be retrieved. In order to calculate the information content and the degrees of freedom for signal, the weighting function matrix K has to be scaled according to the errors contained in the measurement error covariance matrix S_e and the natural parameter variability represented by the a priori covariance matrix S_a

$$\widetilde{K} = S_e^{-1/2} K S_a^{1/2}. \tag{5.6}$$

Rodgers [2000] concludes that the number of independent measurements that can be made at better than the measurement error threshold is equal to the number of singular values of this scaled weighting function matrix which are greater than 1. These singular values λ_i can be used to calculate the information content H

$$H = \frac{1}{2} \sum_i ln(1 + \lambda_i^2) \tag{5.7}$$

and the degrees of freedom for signal

$$d_s = \sum_i \frac{\lambda_i^2}{(1 + \lambda_i^2)}. \tag{5.8}$$

Table 5.3 shows the difference in information content statistics between two OEM versions with different background covariance matrix shapes. These are the two diagonal background covariance matrices discussed in the previous section, the C-diag matrix based on a one year climatological mean and the Feb-diag matrix using means from only one month of data. This gives a difference in how representative each set of variances is for the

Table 5.3: Singular values (λ_i), degrees of freedom (d_s) and information content (H) for the singular vectors. The different OEM configurations were run for the SIC1 dataset.

	C-diag			Feb-diag		
i	λ_i	d_s	H	λ_i	d_s	H
1	39.884	0.999	3.686	25.870	0.999	4.694
2	10.138	0.990	2.321	3.917	0.939	2.015
3	1.373	0.654	0.530	1.116	0.555	0.583
4	0.512	0.207	0.116	0.338	0.102	0.078
5	0.299	0.082	0.043	0.179	0.031	0.023
6	0.012	0.000	0.000	0.012	0.000	0.000
7	0.001	0.000	0.000	0.004	0.000	0.000
Total		2.933	6.696		2.626	7.394

natural variability of the state vector parameters. Naturally the long term based matrix has higher values that show the parameter variability throughout the year, while the other one has smaller values which translate into tighter constraints on the OEM retrieval. The differences between the two OEM versions are to be seen in the number of degrees of freedom and the total information content. While both have three significant singular vectors with singular values above 1, the C-diag achieves a total of 3 degrees of freedom which represent 3 independent quantities being measured. The Feb-diag OEM cumulates around 2.6 degrees of freedom which signifies that 2 and a half quantities can be measured independently. When looking at the total information content available from the two retrievals, OEM C-diag achieves 6.7 bits of information while OEM Feb-diag has 7.4 bits. This means that for C-diag there are $2^{6.7} = 103.7$ different geophysical states that can be distinguished at the precision level set by the background covariance matrix. Feb-diag OEM can distinguish $2^{7.4} = 168.2$ distinct states for its precision level. This is explained by the fact that the retrieved parameters for Feb-diag achieve better precision when under the stricter constraints of the background covariance matrix. In this case more geophysical profiles retrieved with higher levels of precision can fit inside the constraints at the cost of fewer independent measurements.

More detail about the differences between two OEM versions can be understood from Figure 5.1. Even though both OEM versions have 3 significant vectors, the contributions to the simulated Tbs that these vectors represent are different. While in both cases the first two significant vectors show the largest contribution from sea ice concentration and multi-year ice fraction, the third significant singular vector in Figure 5.1 left column (C-diag S_a matrix) shows a higher contribution from cloud liquid water while for the Feb-diag S_a version there is only little influence from the atmospheric parameters of LWP and especially TWV. This explains also why for TWV despite the increased constraints imposed on the retrieval the differences in output statistics are small between the three OEM version in Table 5.2.

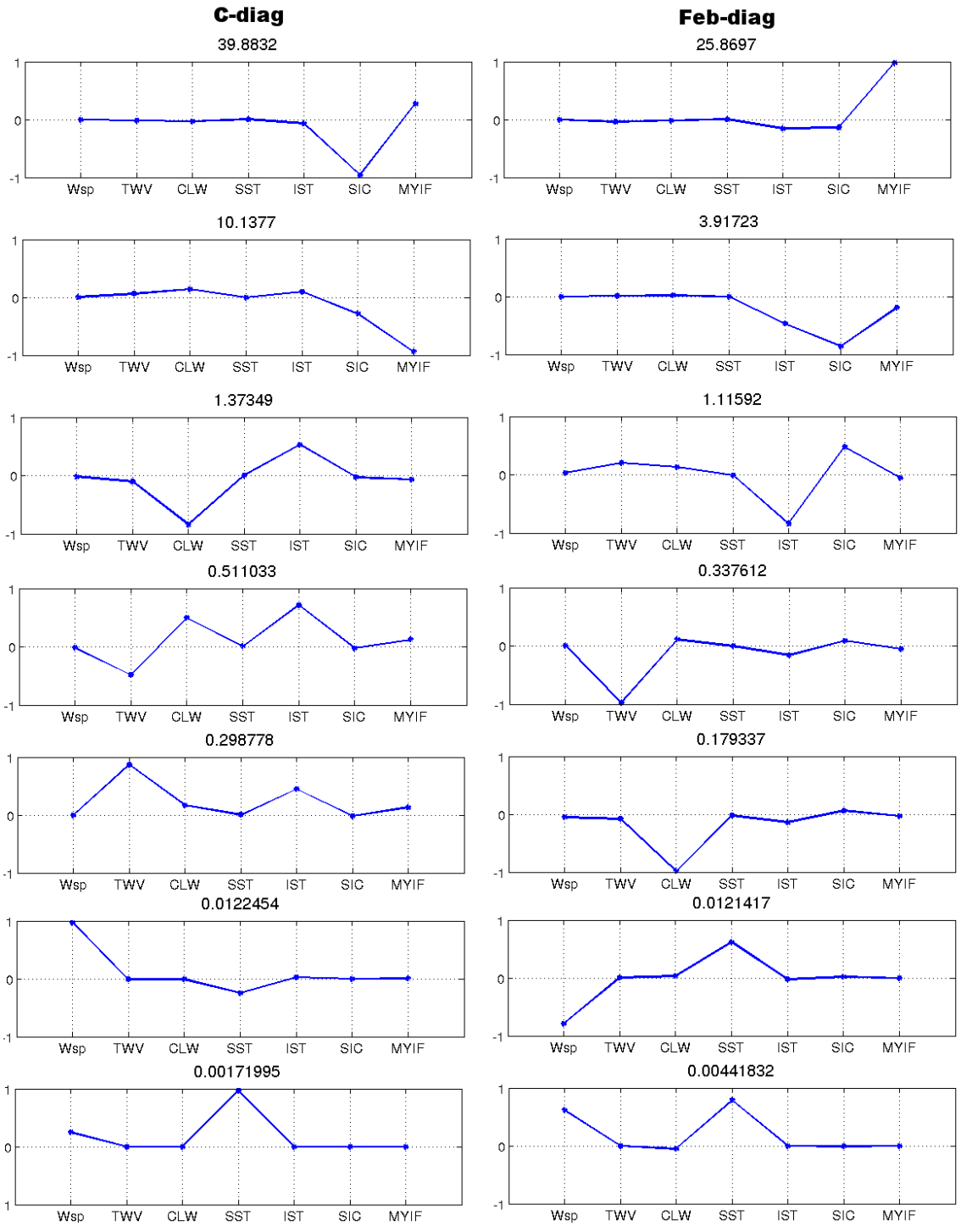

Figure 5.1: Singular vectors and the corresponding singular values for two OEM versions based on different background covariance matrices. The singular vectors are arranged from top to bottom in decreasing order of their corresponding singular values. Left column represents the long term climatology based matrix C-diag, right column is 1 month based matrix, Feb-diag.

In conclusion this comparison showcases the balance that has to be achieved when choosing the background covariance matrix. In the case of the strict constraints in the Feb-diag version the precision seems to be improved as the variability is reduced in some of the retrieved parameters but this is achieved because the number of independent retrieval parameters decreases and the OEM repeats the static background values. The relaxed constraints in the C-diag case allow for more variability in the output parameters but also more independent parameters can be retrieved as the noise threshold is relaxed. An adequate background covariance matrix should not impose a precision threshold that is lower than the natural parameter variability. This can result in improved output precision but also a bias towards the background.

5.1.3 Variations in S_a elements

The C-diag and Feb-diag background covariance matrices tests presented in the previous sections demonstrate how the OEM retrieval is affected by using a priori data that is not representative for the entire temporal domain it covers. In order to observe more clearly what are the effects on the retrieval output when individual elements of the S_a matrix are changed beyond the limits of climatological data sets the following test has been performed. Starting from the C-diag background covariance matrix, the equivalent standard deviation for the S_a elements corresponding to a single parameter has been halved (1/2 σ), then doubled (2 σ) and the effects on the standard deviation of the retrieval output have been recorded. This large variation in the S_a variance is an exaggerated forcing meant to determine a clear impact on the retrieval but otherwise it is not realistic to have such large differences between variances calculated from different data sources. This test was performed individually for TWV as an atmospheric parameter (refered to as versions 1/2 σ TWV, and 2 σ TWV respectively) that is valid over both SIC1 and SIC0 and then for surface temperature of the ocean surface and of the sea ice surface (refered to as versions 1/2 σ SST/IST and 2 σ SST/IST over SIC0 and SIC1, respectively).

In Table 5.4 the standard deviations of the output parameters are shown for different OEM version where the constraints on the TWV parameter are different. As expected, the tighter constraints in the 1/2 σ version determine the lowest standard deviation of the output, while the relaxed constraints for the 2 σ case result in the highest standard deviation for TWV. Over SIC0 the standard deviation values are overall larger than over SIC1 but the differences between 1/2 σ and 2 σ are much smaller. Over open ocean the water vapour parameter is much more important for the brightness temperature calculation and as such the constraints that force it closer to the background state are balanced by the constraints of matching the brightness temperatures. In this case, even with more relaxed background matrix constraints, the water vapour retrieval precision varies little between the three σ cases. This implies that the TWV impact on the simulated brightness temperatures is important enough that even the unrealistically strict constraints of the 1/2 σ case will be

compensated by the brightness temperature cost function. Over SIC0 the K-S test confirms that the 1/2 σ modification to the TWV constraint determines a significant change in the results over SIC0. This is not the case however for the 2 σ TWV change where only the output SST shows a distribution different from the reference with a high confidence level (»99.999%). By relaxing the constraint on TWV most retrieval parameters are not changed in a statistically significant way. This supports the idea that the TWV retrieval is more dependent on the observed brightness temperatures than on the background. It is worth mentioning that even though all of the parameters in the 1/2 σ TWV case and the SST parameter in the 2 σ TWV case show a statistical difference from the reference distribution, the practical impact of this difference is very small as can be seen in Table 5.4 where the parameter variabilities change very little. Over SIC1 however, the brightness temperatures are less sensitive to TWV as variations in the constraints determine significant changes in the distribution of retrieved TWV while the other parameters do not show differences from the reference distribution. This means that the retrieval depends more on the background for TWV over SIC1.

For surface temperature the difference between the minimum σ case and the maximum one triggers a large variation in retrieval standard deviation which more than doubles both over SIC0 and SIC1. Of note is the influence this variability has on the TWV parameter which varies in the opposite direction over SIC1, the TWV standard deviation decreases when IST σ increases and vice-versa. The atmospheric water vapour contributes little to the degrees of freedom for retrieval in the SIC1 case and as such it is more closely connected to the background state. In this case brightness temperature variability due to the atmosphere is then attributed to variability in IST because the latter is not properly constrained. The reverse also happens when the surface temperature is over-constrained and then an increase in TWV variability compensates for the IST parameter which is forced too close to the background value. The larger variability in the retrieved parameters over SIC1 is mirrored in the K-S test results that indicate all parameters using modified constraints for IST show distinct distributions from the reference.

Overall, for SIC0 the differences between σ versions are significant but smaller in absolute value than over SIC1. This indicates that the constraints to the background state are less influential over open water where the method has enough information from the atmospheric and surface parameters to not fall back on the background state.

5.2 Sea ice surface temperature correction

In addition to simply selecting as a priori the most representative data source for the region of interest and allowing for a reasonable constraint for each individual retrieval parameter, there are particular concerns relating to the physics of passive microwave measurements to be accounted for when constructing the a priori. In this section the surface temperature

Table 5.4: Standard deviations of the retrieved parameters after applying different constraints on the TWV and separately on the surface temperature parameter. The σ column represents the reference OEM version without any modifications on the constraints (constraint is one standard deviation). The second column (0.5σ) is the OEM version where the standard deviation constraint has been halved and the third column (2σ) is the OEM version where the constraint has been doubled.

Modified constraint for			None	TWV		Surf. T	
Scenario	Parameter	Unit	σ	0.5σ	2σ	0.5σ	2σ
	TWV	[mm]	1.97	1.05	2.82	2.44	1.55
	LWP	[mm]	0.15	0.16	0.15	0.18	0.12
SIC1	IST	[K]	6.87	6.99	6.81	5.02	12.44
	SIC	[%]	4.00	3.04	3.03	3.03	3.15
	MYIF	[%]	28.05	34.25	33.32	34.10	33.81
	WSP	[m/s]	4.20	4.34	4.15	4.25	4.10
	TWV	[mm]	5.23	4.39	5.51	5.24	5.20
SIC0	LWP	[mm]	0.12	0.14	0.12	0.12	0.12
	SST	[K]	1.06	1.22	1.07	1.06	2.41
	SIC	[%]	2.10	2.29	2.07	2.17	2.00

parameter is investigated in more detail as it poses a number of characteristics specific to passive microwave remote sensing over sea ice and snow covered regions. Microwave radiation is emitted from a layer of a certain depth in the snow and ice pack. The depth of this layer is dependent on the observation frequency. Besides the surface emissivity, the upwelling radiation also depends on the temperature of the material. In the case of a snow and sea ice pack there is a temperature gradient where typically the snow is colder than the ice below it, while the ice is in turn colder than the ocean water underneath. This temperature gradient will influence the microwave emission. In order to calculate the frequency dependent emission of first year and multi-year ice types, in Mathews [2007] the quantity of integrated emitting layer temperature is derived to account for the temperature gradient inside the snow and ice layers. For retrieving this quantity a set of regression coefficients specific for each frequency and ice type are derived from an analysis of snow and ice temperature profiles that relate the lowest level air temperature to the emitting layer temperature [Mathews, 2007]. Coefficient sets have been derived for first year and multi-year ice for all 12 AMSR-E channel frequencies. Seasonal variations in snow cover and temperature profiles have been accounted for by grouping the months with similar characteristics together. These sets of coefficients for winter conditions are given in Table A.6 in the Appendix. The regression equation for relating the lowest level air temperature to the emitting layer temperature is

$$T_{emitting} = aT_{air} + b \tag{5.9}$$

where T_{air} is taken from ERA-Interim temperature data. The coefficients a and b used

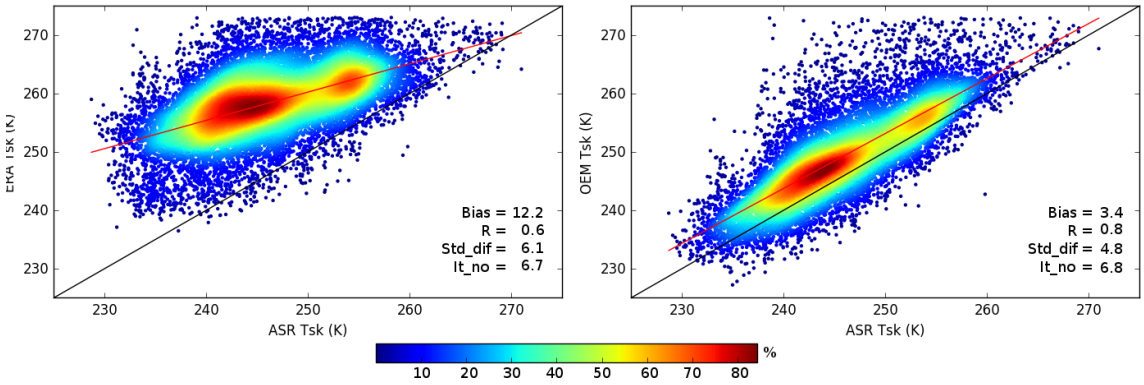

Figure 5.2: Scatterplots comparing the OEM retrieved ice surface temperature before and after implementing the effective surface temperature correction.

for first year and multi-year ice are given in Table A.6 in the Appendix. The coefficients have been implemented in the OEM forward model in order to calculate an equivalent surface temperature for each channel. These effective surface temperature values are used as background values for IST.

In order to test the impact of using the effective surface temperatures in the retrieval, an OEM version that uses the regression coefficients to calculate the channel specific emitting layer temperatures as a background value is compared with the reference OEM version which uses one single background IST value for all channels, evaluated internally using the brightness temperature of the 6.9 V channel. The correction coefficients are applied to the lowest level air temperature supplied from ERA-Interim data.

The scatterplot in Figure 5.2 shows the difference between the reference static OEM version and the version which uses the effective temperature of the emitting layer as background value and first guess for the iterative process. The biggest difference is in the distribution of the retrieved ice surface temperature. The OEM version that uses effective temperature has a larger range of variability which matches the ASR model values better than the reference OEM version. Especially observable at very low temperature, the massive bias of 12 K from the reference version is reduced to just 3.4 K while the correlation is increased from 0.55 to 0.8. The difference between the IST before and after the correction is mirrored by the results of the K-S test which confirms that the corrected retrieval output has a significantly different distribution than the reference one. While there is a statistical difference between output distributions, there is little change in variability for the other retrieved parameters of the state vector. This is a situation similar to that in Section 5.1.3 where statistical differences do not necessarily imply practical differences in the output. This lack of an impact on the variability of the other output parameters and the fact that there is little change in the average number of iterations suggests that improving IST does not have a large impact on the brightness temperature difference between simulations and

observations.

5.3 Sensitivity to the a priori background state (P_a)

In the previous sections the impact of the constraints that limit the OEM to a space around the a priori known background state has been shown. Now the influence of this background state itself on the retrieval will be investigated.

The purpose of the a priori background state vector is to give the OEM the best possible knowledge about the climate system before the measurements are taken. This information can come from other retrieval methods, models, or climatological records. In tests it will be shown what is the impact on the results if the background state vector is based on previous knowledge of different quality levels similar to the different background covariance matrices presented in Section 5.1.1. One scenario is based on having one static state vector that is constructed from a long time average of the seven parameters from climatological records and will be referred to as static-P_a. In the other scenario a different background state vector is constructed for each retrieval pixel with temporally and spatially collocated data from the ERA-Interim model and will be called collocated-P_a. The static background state vector is given in the Appendix in Table A.1. Although normally the background state (P_a) and the background covariance matrix (S_a) are extracted from the same data source, in this section we want to focus on the influence of the background state vector (P_a) alone. The two compared OEM versions use the same background covariance matrix (S_a) based on a year long reanalysis dataset shown in the Appendix. The static and dynamic background state vectors are constructed from the same dataset, with the static version representing the mean values for each parameter.

The retrieval values are compared against a common benchmark taken from ASR model data (Section 3.4). As it is a reanalysis product, ASR has similar data assimilation sources to the ERA-Interim product used for the dynamic background state vector version. The output of the two models is very similar but have distinctly different distributions according to the Kolmogorov–Smirnov test. In the scatter plots in Figures 5.3 and 5.4, the OEM output for the two versions is compared with the ASR model data for each of the atmospheric parameters and surface temperatures for the SIC0 and SIC1 cases respectively. These are the parameters that are most affected by this test because in both scenarios the SIC and MYIF always use a collocated background value obtained from the NASA Team algorithm, while the IST parameter is evaluated inside the forward model. In the scatterplots the main difference between the static and collocated background vectors can be easily seen from the shape of the data point distribution. When using the static background array, the retrieved parameter values tend to be close to the background value which is shown as a horizontal solid green line in the plots. The dashed green lines show the limits imposed by the background covariance matrix constraints on the space around the background state

vector values. The retrieval can move outside of these constraints only if there is a need to balance the difference between the simulated and observed brightness temperatures.

Over SIC0 the constant background array only slightly influences the retrieval results because the atmospheric parameters have a large impact on the simulated brightness temperature so that the OEM results will move away from the background values in order to match the measured Tbs. This is visible over all atmospheric parameters but especially in the case of water vapour distribution, where even with a static background the OEM retrieved values are well distributed over the entire range, matching the variability of the ASR model. In the case of LWP, the parameter variability is so low in the ERA-I data that using collocated model values or a static value as background does not make much of a difference. In the case of WSP and sea surface temperature there is in addition a noticeable improvement in reducing the spread of the retrievals. The shape of the area of maximum density is also changed to reflect a broader distribution of values along the identity line as would be expected from the natural variability of these parameters. The biggest impact can be seen for SST where the static background retrieval can be found within constraints of the a priori, with only a small positive gradient following the ASR distribution. This can be interpreted as SST having a small impact on the simulated brightness temperatures and thus not triggering a move away from the background. In the dynamic background OEM retrieval, SST follows the ASR distribution much more closely with the maximum density of data points on the identity line. For SIC, even though there was no change in the corresponding background data between the two OEM versions, there is an improvement in that the mean retrieved value is closer to 0. This is the true value for the SIC0 data set. In addition to this, the standard deviation of the retrieval has been reduced by half after implementing the collocated P_a. This is explained by the fact that part of the sea ice surface variability can be masked and incorrectly attributed to variability in the atmospheric parameters where this can result in the same values for the simulated Tbs. These are cases of local minima of the cost function condition but do not represent the true solution of the retrieval problem. By attributing more accurately the atmospheric influence to the atmospheric parameter values through the use of the dynamic background, the SIC retrieval variability is reduced as well.

For SIC1 (Fig. 5.4) where the atmospheric parameters' influence on the simulated brightness temperatures is lower over sea ice, the OEM results do not move away from the static P_a as much. This results in more of the retrieved values being close to the background. This is especially true for TWV where there is one area of high data point density close to the static P_a value of 2.86 mm and a cloud of negative values along the lower limit of the background constraint. These negative TWV values have no physical meaning but indicate that the OEM had to compensate for a Tb difference in the cost function and that this was the local minima found within the constraints. After implementing the collocated P_a, the TWV values show much lower variability around the identity line and

they match much better with the ASR data. The variability of LWP has been decreased, but because the model data for this parameter are not very accurate there is little agreement between the OEM retrieval and the ASR model data. For IST the correction method described in the previous section has been used, as it combines the collocated P_a data with the empirical emission layer coefficients in order to obtain a more physically consistent result. The final IST retrieval is similar to that shown in Figure 5.2, however they are not identical. Because of changes in the retrieval of the other parameters, the IST output shows slight differences versus the ASR benchmark, when compared to the one presented in the previous section. This will be discussed in more detail below, based on the statistics in Table 5.6. Another interesting feature of the IST plots is that the intra-seasonal variability can be seen in the two high density areas. The area of higher IST value corresponds to the months of March and April from the SIC1 data set which are warmer than the rest. With a static P_a, the IST distribution is more flat with a lower variability than when implementing the ERA-Interim collocated P_a. Similar to the SIC0 test, the SIC parameter in the SIC1 scenario has a decrease in standard deviation by around 40% after using dynamic background points for the atmospheric parameters. For the MYIF parameter compared to Advanced SCATterometer (ASCAT) backscatter data included in the RRDP (Section 3.5), there has been no change in the P_a treatment. The background value is based on collocated NASA team data for both cases where the atmospheric parameter use static values or collocated ERA-Interim as background. There is however a change in the high MYIF pixels where a better differentiation can be seen between pixels with MYIF >95% and those flagged as <85% than in the case where the atmospheric parameters use a static P_a. These flags are based on NASA Team MYIF values and ASCAT backscatter data and have been included in the SIC1 RRDP data set (J. Lu, personal communication).

Table 5.5: Intercomparison between static background OEM, collocated background OEM and ASR model data over SIC0.

Statistic	Method	WSP [m/s]	TWV [mm]	LWP [mm]	SST [K]
Bias vs ASR	C-Pa	0.22	-0.23	0.06	-2.04
	ERA-I Pa	0.88	0.04	0.06	0.05
Stdev diff to ASR	C-Pa	2.79	1.84	0.11	2.46
	ERA-I Pa	1.74	1.37	0.11	0.80
Correlation vs ASR	C-Pa	0.75	0.94	0.36	0.59
	ERA-I Pa	0.91	0.97	0.38	0.95

The SIC0 statistics in Table 5.5 confirm the improvement in agreement between the OEM retrieval and the ASR model data after implementing the collocated ERA-Interim as background value. For WSP, even though the dynamic background OEM version scores a slightly higher bias against ASR than the static background version, the standard deviation of the difference decreases to almost half and the correlation increases from 0.73 to 0.91. For TWV the improvement is visible in all statistics with bias and standard deviation of the

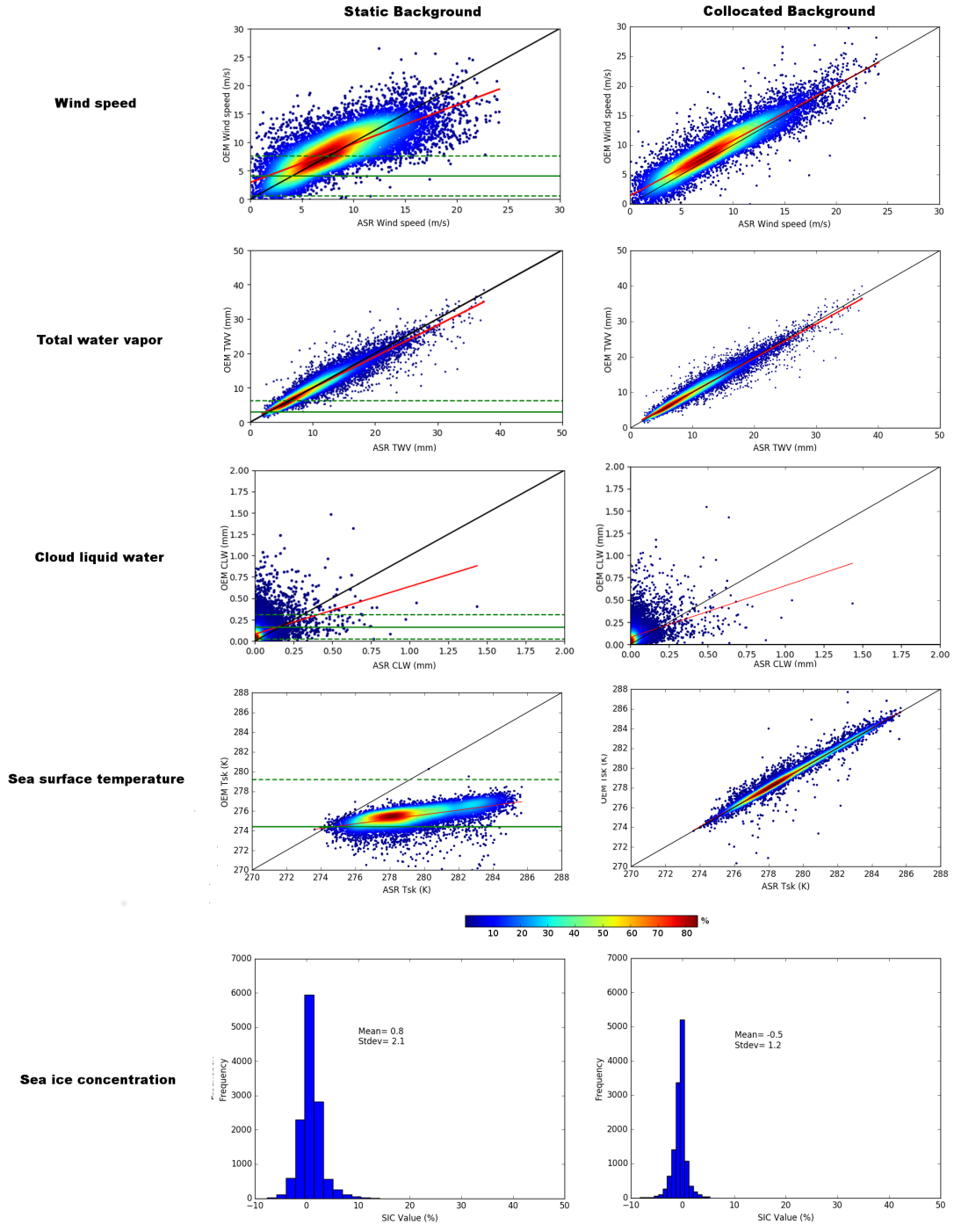

Figure 5.3: Scatter plots comparing the OEM output parameters from a static background and a collocated background OEM version with ASR data for the SIC0 data set. For WSP, TWV, LWP and SST the green continuous line represents the static background value, while the green dotted lines represent the constraints imposed by the background covariance matrix.

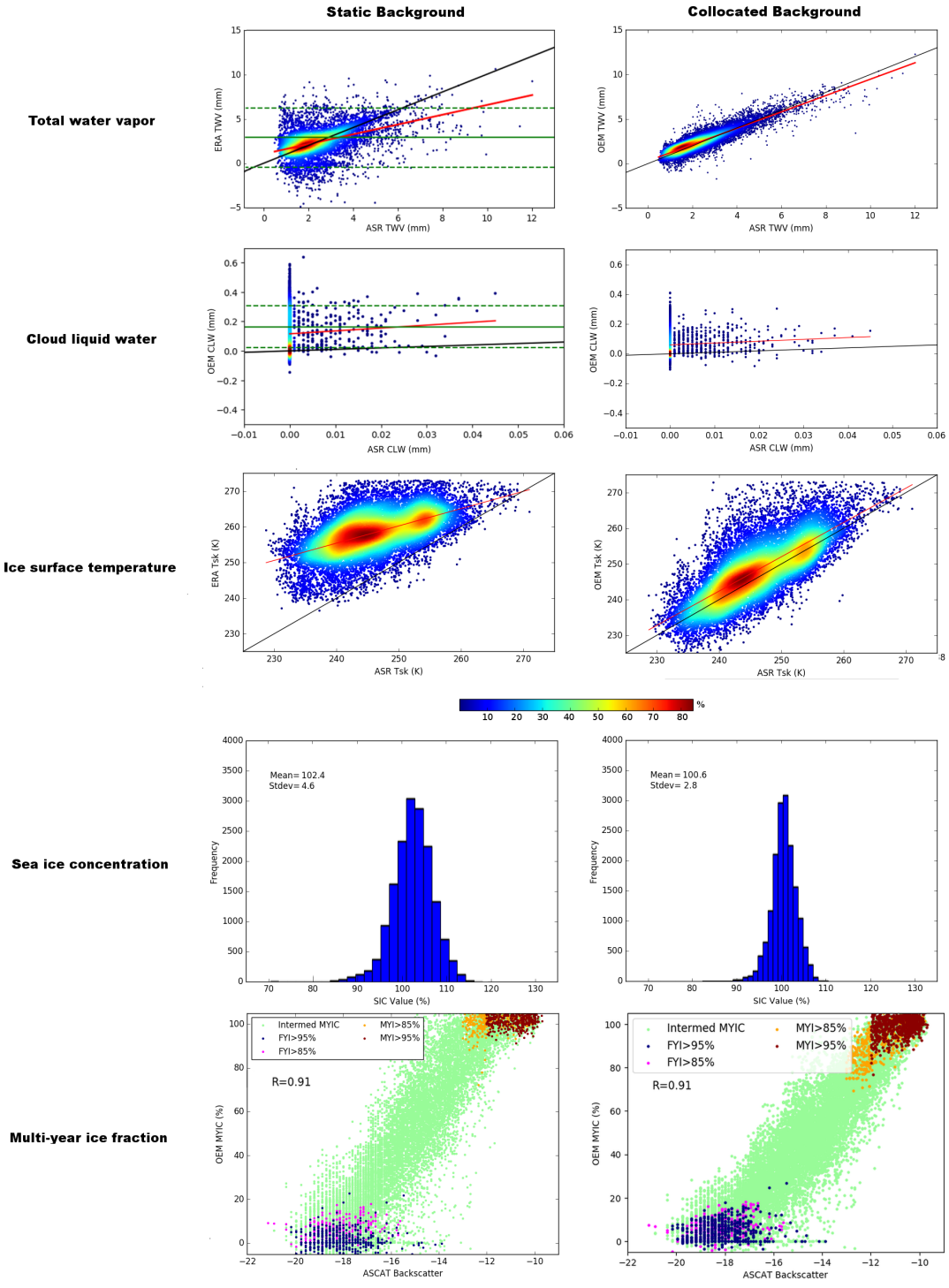

Figure 5.4: Scatter plots comparing the OEM output parameters from a static background and a collocated background OEM version with ASR data for the SIC1 data set. For TWV and LWP the green continuous line represents the static background value, while the green dotted lines represent the constraints imposed by the background covariance matrix.

Table 5.6: Intercomparison between static background OEM, collocated background OEM and ASR model data over SIC1.

Statistic	Method	TWV [mm]	LWP [mm]	IST [K]
Bias vs ASR	C-Pa	-0.08	0.12	12.24
	ERA-I Pa	0.11	0.06	2.16
Stdev diff to ASR	C-Pa	1.62	0.13	6.06
	ERA-I Pa	0.55	0.07	5.78
Correlation vs ASR	C-Pa	0.43	0.04	0.55
	ERA-I Pa	0.90	0.03	0.75

difference both decreasing and correlation increasing. The LWP comparison confirms that there is little difference between one static background value and dynamically collocated values from ERA-Interim most of which are close to 0. The statistics change little when compared to ASR over SIC1. Similar as over open water, LWP representation in circulation models at the exact time and space of the satellite overflight is poor and there are few other reliable data sources for this parameter in the Arctic. The K-S test results indicate that WSP, SST and SIC have a statistically different distribution after implementing the collocated P_a while TWV and LWP do not. This supports the results in Section 5.1.3 and confirms that TWV does not depend much on the background values or constraints over SIC0. Together with TWV, LWP is shown in Figure 5.3 and in Table 5.5 to be the parameters with the smallest difference to the reference which indicate that, in SIC0 conditions, the background has little influence on them when compared to the influence of the brightness temperatures.

The statistics for the comparison over SIC1 (Table 5.6) confirm the better agreement of the collocated ERA-Interim background OEM retrieval version with the ASR model. The bias, standard deviation of the difference and correlation for both TWV and IST improve with TWV showing the biggest change. The difference to the reference distribution is also significantly different across all parameters after implementing the collocated P_a, according to the K-S test. This underlines the importance of the background for the OEM retrieval in SIC1 conditions.

Of all the tested changes to the OEM a priori, using collocated ERA-Interim values as background state shows the biggest improvement in terms of bringing the retrieval nearer to the benchmark model data. One parameter which is not shown in Table 5.6 is the percentage of convergent data points. This is because while the reference OEM convergence values have already been shown in Table 5.1 for SIC0 and Table 5.2 for SIC1, after implementing the collocated P_a, all data points result in convergence over both SIC0 and SIC1. By providing a background position that is closer to the real geophysical state by using the ERA-Interim values, the OEM manages to always find a retrieval ensemble that matches the Tb observations within the constraints.

5.4 Sensitivity to the first guess value (P_0)

The first guess value is a technical parameter which is chosen in order to start the iteration process. In order to study the influence of this parameter on the retrieval we performed a test in which the standard deviations of the output parameters of two OEM versions are compared. The reference OEM uses collocated ERA-Interim data as start guess, and the test version uses one single set of values for all pixels for both SIC1 and SIC0 subsets of the RRDP data set. The static start guess vector is identical to the background state vector. For the test OEM version this means that every iterative process starts with a minimal cost for the difference to the background and the changes in the state vector values are only dictated by the cost of diverging from the observed brightness temperatures.

The differences between the best case scenario and the static first guess are minimal. Over SIC1 the differences are observable for water vapour and liquid water path which are highly variable parameters that also have a small impact on the simulated brightness temperatures over sea ice covered regions. Using a single start guess position causes the OEM to search longer for a set of parameters that satisfies the cost function and the convergence criteria which is mirrored in the increase in the average number of iterations needed for the test OEM version when compared to the reference case (Table 5.7). Over SIC1, all output parameters distributions have significant differences to the reference.

For the SIC0 comparison the differences between the two OEM versions are minimal for all seven parameters. The standard deviation of the output parameters is almost identical in both cases which indicates that over open water, the OEM will find approximately the same solutions regardless if the iteration starting point is fixed or dynamic. The WSP, TWV, SST and SIC output distributions do not show significant differences from the reference. While the distribution of LWP is different, the practical aspect of retrieval variability is unchanged. The small increase in the average number of iterations is the only significant impact of the static starting point over the OEM.

We conclude that the starting point position does not influence the OEM retrieval in scenarios of low or no sea ice presence, while it does have some influence on the atmospheric parameters of TWV and LWP in situations of high sea ice concentration.

5.5 Sea ice emissivity correction

Because sea ice dominates the microwave signal at the instrumental frequencies, it is important that the forward model can simulate unbiased brightness temperatures when compared to the measurements. Any bias in the simulations will influence the retrieved geophysical parameters because the optimal estimation method will try to compensate for the brightness temperature difference by adjusting the predicted state vector. In order to test whether a bias is present, we calculated the mean differences between the retrieval step

Table 5.7: Standard deviation of output parameters from OEM retrieval using different first guess versions. REF uses collocated ERA-I as first guess for the 3 atmospheric parameters plus surface temperatures. C-Sg uses one static set of 5 values for these parameters. SIC, MYIF are given by the NT algorithm.

Parameter	Unit	SIC0		SIC1	
		REF	C-Sg	REF	C-Sg
WSP	[m/s]	3.73	3.74	-	-
TWV	[mm]	5.38	5.38	1.67	2.39
LWP	[mm]	0.11	0.11	0.04	0.14
SST/IST	[K]	2.95	2.93	7.21	6.61
SIC	[%]	1.69	1.71	4.45	4.67
MYIF	[%]	-	-	38.58	38.17
No. iterations		2.8	3.53	5.22	6.03

simulated brightness temperatures and the AMSR-E measurements for the SIC1 data set (Table 5.8 Reference columns). The highest discrepancies occur in the two 89 GHz channels and for now we have discontinued including these two channels in any retrieval scheme and also in the test cases described in the previous section. Excepting the 89 GHz channels, high biases are also present in the horizontal polarization channels while the lowest bias at 18.7V is still around 1 K. In order to compensate for these biases over sea ice, we assume that the difference in brightness temperatures is entirely caused by the surface component through the prescribed emissivities. Assuming the difference between simlations and measurements should be zero, an offset is calculated for each channel speciffic emissivity. Using averages of these channel wise offsets for the whole RRDP test dataset we calculate a set of corrected emissivities that minimise the channel wise difference between the simulated and observed brightness temperatures.

In order to minimise the influence of monthly variations throughout the winter season, the corrected emissivities are calculated as winter averages, even though a slight improvement may be obtained by using temporally varying emissivities. The original set of empirical emissivities as well as the corrected set are given in Table A.5 in the Appendix.

The mean differences between measured and simulated brightness temperatures after correction are shown for each AMSR-E channel for the whole SIC1 data set in the "Corrected" columns of Table 5.8. The average difference over all 10 channels and all winter data points of SIC1 has decreased from 0.69 to 0.14 K. In order to investigate the effects of the correction over pure ice types the data set has been separated according to the NASA Team result for multi-year ice type fraction. For pixels with more than 90% MYIF there is a large decrease in the average Tb difference from 2.77 to 0.57 K. For the set with less than 10% MYIF the initial difference is lower but there is still a decrease from 0.9 to 0.44 K. The distributions of the retrieval step simulated brightness temperatures show statistically significant differences to the reference after implementing the corrected

Table 5.8: Mean differences (in K) between simulated and observed brightness temperatures. The reference version uses the original emissivities averaged over the entire winter data set for each ice type. The corrected OEM version uses the new set of averaged winter emissivities.

SIC1 subset	Average all winter pixels		Multi-year ice		First year ice	
Channel	Reference	Corrected	Reference	Corrected	Reference	Corrected
6.9V	0.36	-0.17	4.62	0.09	-0.16	-0.28
6.9H	-0.12	0.2	0.6	-0.06	0.36	0.45
10.7V	1.16	-0.07	4.77	0.27	0.4	-0.29
10.7H	0.97	0.39	0.55	0.03	1.23	0.48
18.7V	-0.67	-0.23	1.13	0.31	-1.58	-0.72
18.7H	-1.12	0.04	-2.89	-0.56	-1.1	0.14
23.8V	-0.35	-0.02	-0.58	-0.35	-0.71	-0.18
23.8H	-1.08	-0.16	-3.14	-1.32	-1.36	0.25
36.5V	0.31	0.09	-4.41	-1	1.98	0.46
36.5H	-0.72	0.07	-5.02	-1.66	0.17	1.11
89V	-16.39	13.41	-21.11	-2.21	-11.82	19.38
89H	-20.34	16.94	-21.77	-2.78	-18.39	24.15

sea ice surface emissivities. Even though the initial assumption was that the prescribed emissivities are the only parameter that determine the discrepancy between the modeled and the measured brightness temperatures, there are also other factors involved in the modelling error which are not accounted for. These can be the model input parameter uncertainties or errors in the model parameterizations and they can explain the residual difference between simlations and measurements.

Even after the correction, the 89 GHz channels are not included in the retrieval. Even though the difference between simulated and measured Tbs at this frequency has also decreased on average, we have decided to exclude it from the retrieval because of the remaining forward model deficiencies in modelling scattering effects at this frequency. As mentioned in the forward model description, the scatterers relevant at this frequency are difficult to account for in the simulations because of their unknown profiles of distributions in size, shape and orientation. Further testing regarding the use of the 89 GHz channels is presented in Chapter 7.

5.6 Sensitivity to the brightness temperature covariance matrix (S_e)

The satellite measurements are connected with a measurement error due to instrumental noise. In addition, the simulations contain modelling errors. These error sources need to be taken into account when constructing the constraints under which the OEM has to match the measurements. Following the testing done for the background covariance matrix

and the start guess position, we compared four different brightness temperature covariance matrices (S_e) in order to assess the impact on the retrieval. The reference run is based on the pre-launch AMSR-E radiometric error values. A second S_e matrix is constructed from the variances of the differences between observed and modelled brightness temperatures. Tb differences are expected to be highest in the SIC1 retrieval scenario because of the high variability of the sea ice surface contribution, with any differences occurring over open ocean conditions expected to be lower than over sea ice. Because of this the differences over the entire RRDP SIC1 data set were used to construct this matrix. These variance values include the modelling error as well as the errors of the forward model input parameters and the measurement errors of the instrument. These values are obviously larger than the pre-launch radiometric errors so that this covariance matrix is named L S_e for short reference. In order to test the sensitivity of the retrieval to changes in the brightness temperature covariance matrix we also tested one version that uses all values in the L S_e multiplied by two and one that uses the same elements but divided by two. The elements of these brightness temperature covariance matrices are given in the Appendix in Table A.2. The results of comparing these retrieval runs against ASR are shown in Table 5.9

Table 5.9: Mean value and standard deviation of output parameters from OEM retrieval using different brightness temperature covariance matrices. Data set used is SIC1.

Stat	Parameter	Unit	Reference Se	L Se	2L Se	1/2L Se
Mean value	TWV	[mm]	0.80	1.10	1.39	0.76
	LWP	[mm]	0.09	0.08	0.07	0.09
	IST	[K]	258.84	258.05	257.17	258.66
	SIC	[%]	102.37	102.94	103.45	102.61
	MYIF	[%]	53.88	52.92	51.17	54.24
/hline Standard dev.	TWV	[mm]	2.23	1.71	1.37	1.94
	LWP	[mm]	0.119	0.103	0.092	0.12
	IST	[K]	6.70	6.39	5.96	6.77
	SIC	[%]	4.59	4.54	4.26	4.76
	MYIF	[%]	38.35	36.80	36.58	37.06
Avg. no. iterations			6.721	5.201	4.197	6.47

In general larger variances in the S_e matrix mean less strict constraints on matching the simulated to the measured Tbs. These constraints on the Tbs are what causes the OEM to move away from the background state vector. Thus the tendency for the number of iterations is expected to decrease because of the relaxed constraints. At the same time the variability of the output is slightly reduced as more importance is given to the constraint to conform to the background. The reduction is especially noticeable for the atmospheric parameters over SIC1 which have the least influence on the simulated Tbs. As such they will default more often towards the P_a if the constraints on the Tbs are relaxed. The surface parameters SIC and MYIF show little influence under the changes in the S_e matrix. MYIF does however stand out in the K-S test results. Where the other output

parameters show significant changes from the reference for every change in S_e, the MYIF retrieval distribution for the 1/2 L S_e OEM version does not. This implies that there is little impact on MYIF retrieval between using the reference constraints on the S_e matrix or the 1/2 L S_e constraints.

While it is necessary to account for the TB modelling error in the constraints to ensure an unbiased retrieval, and because the background constraints have not changed, it follows that the method output will move closer to the ERA-Interim data when relaxing the brightness temperature constraint (Section 5.6).

Going forward after this test, the brightness temperature covariance matrix S_e used is constructed from the variances of the retrieval step simulated brightness temperature difference to the measured brightness temepratures as is described for the L S_e matrix version. Because these differences will change after each modification implemented in the OEM configuration, the S_e matrix has to be recalculated as a last step in these implementations. The channel wise variances of the Tb difference is used on the matrix diagonal while the non-diagonal elements are zero. Like for the background covariance matrix S_a, this represents the minimum requirement for constraining the method however it avoids possible bias problems when using the covariances that result from the forward model simulations.

5.7 Conclusions on the testing of the OE retrieval

Based on the results of the testing presented in this chapter the OEM set-up used in the subsequent chapters includes the following modifications over the prototype OEM version:

(i) A climatological background covariance matrix (C-diag S_a) based on a long 9 years SIC0 data set using ERA-Interim data for WSP, TWV, LWP and SST and on the SIC1 ERA-Interim for IST is used. This background covariance matrix is shown in Table A.7 in the Appendix.

(ii) Collocated ERA-Interim data is used as background values (P_a) for each pixel instead of one static set of parameters.

(iii) The start guess position (P_0) is identical to the background state vector for all pixels in order to speed up the convergence process, and increase convergence rate.

(iv) The effective surface temperature of the frequency dependent emitting layer correction has been included in the forward model, so that this emitting layer temperature is calculated for each channel individually as opposed to using one surface temperature value for all channels.

(v) Sea ice surface emissivity correction has been applied to the mean seasonal emissivities in order to reduce the difference between the simulated and measured Tbs.

The set of emissivities for first year and multi-year ice are shown in Table A.5 in the Appendix.

(vi) After including all of the changes above, the differences between the retrieval step simulated Tbs and the AMSR-E measurements are calculated. The mean variances of these differences are then used as a final brightness temperature covariance matrix

This OEM setup is based on tests run in the conditions of absolute sea ice cover from the RRDP SIC1 and SIC0 data sets. This whole chapter is dedicated to presenting the tools developed for improving the method over the preceding prototype, tools which can also be used for adapting the method after any future change in the retrieval configuration. Pending further testing using even larger data sets, some of the a priori parameters are subject to change in the future such as the covariance matrices or the sea ice surface emissivities. This concluding OEM version represents a configuration suitable for further testing, with the expectation that the constraints and parameterizations can be tuned and expanded. One example of this is presented in Section 6.1 where the constraint for the SST parameter had to be relaxed after testing the method in a more realistic scenario.

6 | Comparing with state of the art

The tests presented in the previous chapter have been performed over the controlled environment of the RRDP with known sea ice conditions in order to develop the improvements needed to address the OE retrieval over sea ice where the surface emissivity and effective surface temperature are key parameters for the forward model. However the two scenarios of 0 and 100% SIC present in the RRDP are not representative for the entire spatial domain that the OEM should cover and so we proceed with testing the retrieval over a realistic Arctic dataset without any sea ice cover limitations. Using the final OEM configuration described in the previous chapter, the retrieval is applied to 16 winter days in 2006 over the entire Arctic domain north of 60 °latitude. The 16 test days are spread between January and May, with a 10 day interval between any two days in the set in order to cover a wide array of different winter surface conditions. This dataset only contains winter days because the summer surface melt has a detrimental effect on all passive microwave retrieval due to the high variability of the surface microwave emission. Because of this it is difficult to perform any retrieval tests over sea ice in surface melt conditions.

In this chapter a series of comparisons are performed between the OE retrieval and a number of state of the art retrieval products. While different atmospheric retrieval products over open ocean have been developed and reached a satisfactory level of maturity, the same cannot be said for products over sea ice so that the comparisons can primarily be performed over ice free areas. In addition a test for TWV retrieval over sea ice is performed against the AMSU-B retrieval product (Section 3.8). Moreover, as SIC is the most important geophysical parameter for passive microwave remote sensing, a comparison with the ASI SIC retrieval product (Section 3.7) is performed for the entire test dataset.

In order to avoid repetition for each comparison case, we can state from the start that

all of the statistical results presented in this chapter are significant for a p value lower than 0.01. This is expected as the sample size for each test varies between hundreds of thousands for the RSS comparison (3-700.000), around 17 million for the ASI comparison and around 13 million for the AMSU-B TWV comparison because of availability of valid data points in the comparison sets.

6.1 Comparing with RSS data products

The state of the art for atmospheric passive microwave remote sensing over open ocean is represented by the Remote Sensing Systems Ocean Product [Wentz et al., 2014].

It retrieves WSP, TWV, LWP and SST through direct inversion of the AMSR-E brightness temperatures measured at the channel frequencies between 6.9 and 37 GHz. The OEM uses both ERA-Interim data fields as a priori data and AMSR-E brightness temperature measurements in order to retrieve the state vector. While the ERA-Interim is our best knowledge on the geophysical state before the measurements are taken, we considered the RSS results as the best reflection of the Tb measurements without the use optimal estimation techniques. The purpose of the OEM is to take advantage of both sources of information and produce a retrieval that is balanced between the result of inverting the measurements and within the constraints given by the a priori. If the background and brightness temperature covariance matrices are consistent the OEM values will fall between the Tb based RSS retrieval product and the ERA-Interim model data.

Table 6.1: Intercomparison between OEM, RSS and ERA-Interim data over open water scenes in the winter 2006 data set.

Stat	Method	WSP (m/s)	TWV (mm)	LWP (mm)	SST (K)
Mean value	OEM	10.10	6.42	0.08	274.67
	ERA	9.18	6.36	0.03	274.54
	RSS	10.93	6.83	0.06	277.60
Std dev	OEM	3.54	3.28	0.087	2.98
	ERA	4.24	3.28	0.053	3.06
	RSS	4.57	3.27	0.065	2.99
Bias	OEM-RSS	-0.83	-0.41	0.017	-2.94
	OEM-ERA	0.92	0.06	0.050	0.12
	ERA-RSS	-1.75	-0.47	-0.032	-3.06
Std dev diff	OEM-RSS	2.88	1.10	0.055	2.58
	OEM-ERA	2.14	1.52	0.089	0.42
	ERA-RSS	3.97	2.32	0.074	2.79
Correlation	OEM-RSS	0.78	0.94	0.78	0.63
	OEM-ERA	0.86	0.89	0.28	0.99
	ERA-RSS	0.60	0.75	0.24	0.58

In Table 6.1 the statistics for comparing the three data sets with each other are pre-

sented. The RSS data is gridded and processed as daily average of the ascending and respectively descending swaths. These were collocated with the closest in space OEM retrieved pixel also sorted by ascending or descending orbits. The mean value and standard deviation for each parameter and method allow estimating for how close the three data sources are to each other. For comparing them the combinations between any two methods are given for bias and standard deviation of the difference. These show how the agreement between the ERA-Interim and the brightness temperature based RSS product changes after applying the OE retrieval.

When comparing them with each other, the three methods show different degrees of agreement with ERA-Interim having the lowest agreement with RSS. As the optimal estimation process balances the a priori against the measurements, the OEM moves closer to the RSS values. Still the best agreement is between the OEM and the ERA-Interim that represents its a priori. In terms of bias, the OEM has a slight negative bias towards RSS values, and an almost equally large positive bias versus ERA-Interim WSP. This places the OEM values in between the ERA-Interim and RSS results. The lowest variability (standard deviation) of the difference between any two methods also occurs between OEM and the ERA-Interim, followed by a higher value for the OEM-RSS comparison. The largest difference is registered between ERA-Interim and RSS. Overall the WSP comparison shows that the OEM is constrained towards the model a priori values but it manages to improve the agreement with the brightness temperature regression results of RSS.

The TWV comparison shows a different picture where all three methods are closely matched, with the two retrievals having the best agreement. In terms of mean value and standard deviation the three sources are almost identical within 0.4 mm of each other for mean value and within 0.02 mm in variability. The biases are small with a low negative bias between ERA-Interim and RSS which reduces further between OEM and RSS while the OEM is practically unbiased towards ERA-Interim values. When looking at the variability of the difference, the ERA-Interim and RSS have the highest disagreement which is reduced by half between OEM and RSS. The lowest correlation is between ERA-Interim and RSS which increases by 25% in the OEM-RSS comparison. Over all statistics the OEM water vapor retrieval demonstrates a good match with the Tb regression results from RSS while still showing good agreement with the model data. For bias, standard deviation of the difference and correlation the OEM falls right between the ERA-Interim data and the RSS retrieval.

For the LWP comparison, the two retrievals show a clear departure from the model. While this is expected because the RSS is a validated retrieval system for this parameter and the model data are acknowledged to be unreliable, it is encouraging to note that the OEM can depart from the a priori when the Tb measurements require it. LWP is a highly variable parameter where the standard deviation is higher than the mean value for all three methods. The statistics show that the pull of the measured brightness temperature

is enough to counterbalance the constraints to the a priori. This is the desired effect of this mechanism when the a priori has a high uncertainty as is the case with modelled LWP data, or when an error in the Tb measurements would force the retrieval into extreme values for the state vector.

When comparing the sea surface temperature data the OEM seems to be too tightly constrained to the a priori by the background covariance matrix. The results show good agreement between OEM and ERA-Interim, while both differing from the RSS values. The mean values show this clearly where OEM and ERA-Interim have an almost equal mean SST while both being lower than the RSS mean value. For bias the OE retrieval and ERA-Interim show a similar negative bias against RSS while being practically unbiased towards each other. The correlation values gives a tight match between OEM and ERA-Interim at 0.99 while ERA-Interim has only a moderate correlation with RSS at 0.58 which is slightly improved by the OEM vs RSS to a value of 0.63. It is clear that the OEM set-up tested here is following the a priori too closely, leading to a biased retrieval when compared to the direct Tb regression results of RSS. This issue was addressed by modifying the background covariance matrix to allow for a larger departure from the background. This is discussed in more detail below.

To accompany the statistics in Table 6.1 the density plots in Figure 6.1 give a graphical representation of the distribution of data points from the three methods used in the comparison. The plots on the left side show the ERA-Interim plotted against RSS data points which represent the a priori state that constrains the OEM. The column on the right shows the OEM retrieval results plotted against RSS.

For the WSP and water vapour plots the large scatter and lower correlation between ERA-Interim and RSS are clearly visible in the dispersed clouds of higher point density. These features are improved in the corresponding OEM plots where the correlation is improved and the width of the data point cloud is reduced. The behaviour of the data cloud also varies with parameter value. For both WSP and water vapour a slight overestimation on the OEM side can be seen at low values, which is coupled with a slight underestimation towards the higher values in the range. In the case of LWP the nature of ERA-Interim values can be seen as most of the data points are close to 0, without any clear structure to the cloud. The agreement with RSS values is improved in the OEM plot where the high density cloud becomes more elongated along the identity line. The OEM overestimation when compared to RSS is visible throughout the range of values but the correlation is greatly improved when compared to the left side ERA-Interim data plot. From the statistics, the ERA-Interim and OEM SST values are similar which is also confirmed by the two plots. The scatter of the data and correlation with RSS is almost unchanged between the two plots. What does change however is the distribution of the high density areas. While the overall variability of the SST values is similar to that of ERA-Interim, the OE retrieval points are concentrated in a few areas of higher density. The underestimation

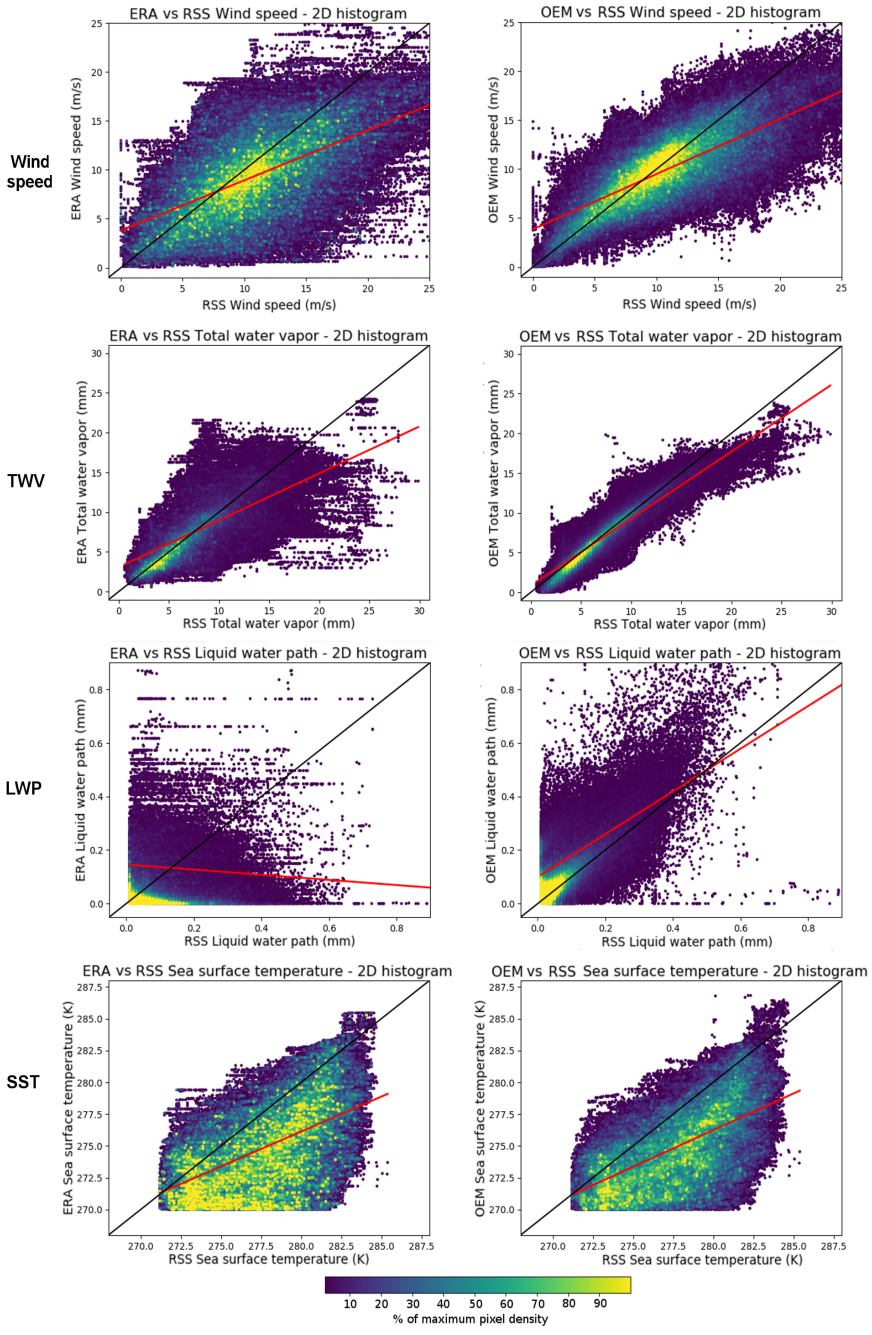

Figure 6.1: Density plots (2D histograms) of the four parameters retrievable from RSS. The column on the left shows ERA-Interim data vs RSS, column on the right shows OEM vs RSS. The black line is the identity line and the red line is the linear regression of the data points. The colour indicates the relative density of data points. Time frame used were the 16 winter days in the 2006 data set.

in ERA-Interim and OEM data versus RSS is visible throughout the entire value range. In general, when comparing the OEM vs RSS plots to the ERA-Interim vs RSS plots the cloud of data points becomes more consistently structured along the identity line confirming the improvements in correlation shown in Table 6.1. The cloud also becomes narrower in width which represents the decrease in the standard deviation of the difference between OEM and RSS when compared to the ERA-Interim vs RSS comparison. The change is most visible in the LWP comparison where OEM is much better aligned with the brightness temperature retrieval of RSS and least visible in the case of SST where OEM clearly follows the data distribution of ERA-Interim albeit with a reduction and re-positioning of areas with high point density towards the identity line. For the retrieval over open ocean of the atmospheric parameters of WSP, TWV, LWP and SST we can conclude that the OEM can improve on the a priori information from ERA-Interim and move closer to the results of a direct Tb regression represented by the RSS data.

To emphasise the parameter specific behaviour of the OEM data when compared to the ERA-Interim and the benchmark RSS retrieval one day examples are shown for the four atmospheric variables in Figures 6.2, 6.3, 6.4, and 6.5. An apparent time offset between the AMSR-E measurement and the closest ERA-Interim time step provides for a good case study to demonstrate the balance that the OEM must achieve between the satellite measurements and the model provided background values.

As suggested by the statistics, the OEM WSP retrieval is situated in between the ERA-Interim and the RSS retrieval values and this is visible in the example maps from Figure 6.2. The shapes of the larger features are recognisable in all three maps, with OEM showing the largest values overall. Out of all the state vector parameters, WSP is one of the most variable on short time scales. The ERA-Interim data represents the closest 6 hour step from the OEM swath start time. The OEM data is processed swath wise and the values on the map represent the latest swath superimposed on the previous ones in areas of overlap. RSS data has two data segments one daily average of all ascending swaths and one for the descending ones. This can cause shifts in features between the three methods if the temporal differences are considered. After testing different constraints for this parameter we conclude that the differences apparent in the map between OEM and the other two methods are caused by the temporal collocation. Because of this features that match both ERA-Interim, such as the the high WSP features south and east of Greenland, and RSS are recognisable in the OEM map. Such issues are difficult to solve in the current setup that uses the 6 hour step data from ERA-Interim as background but they could be mitigated in the future by using a higher temporal resolution product as background.

In the TWV example of Figure 6.3 the effects of a balanced constraint to the background can be seen. Because of the same temporal collocation issue, the high value region south of Iceland seems to be offset between the ERA-Interim data and the two retrievals. Both OEM and RSS use the same AMSR-E Tbs so are tightly collocated with each other. The

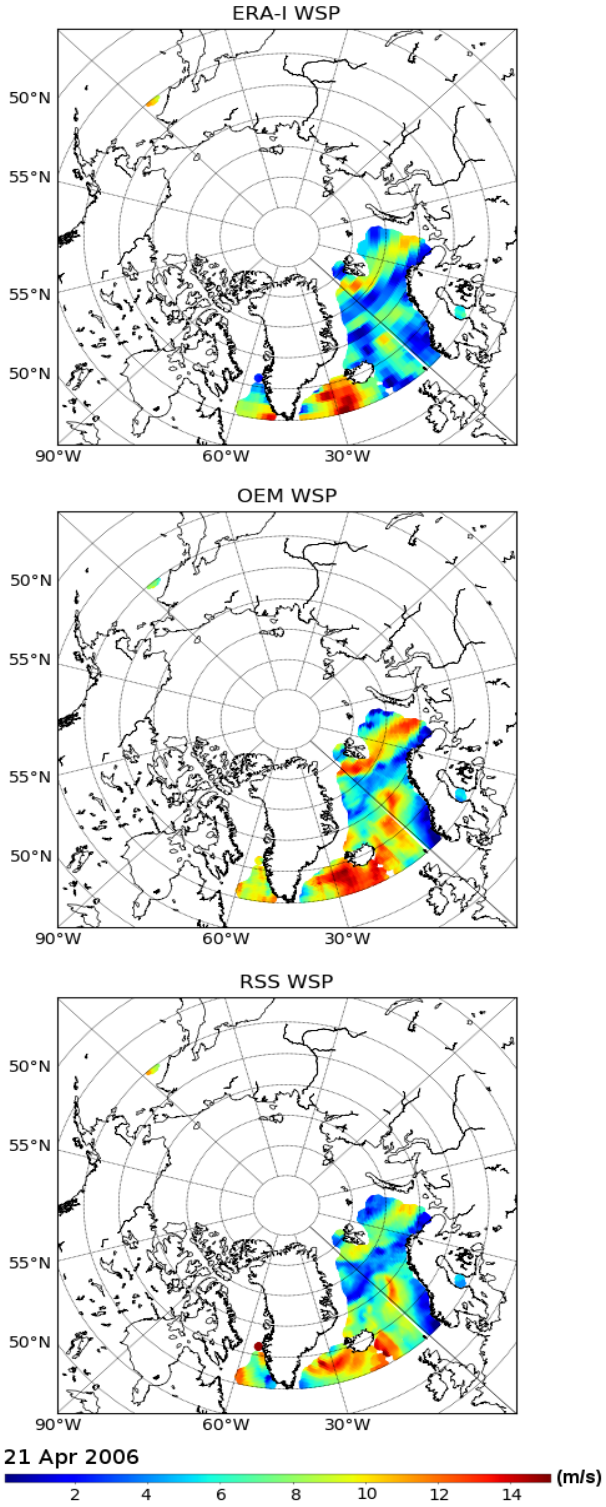

Figure 6.2: Map showing one day of WSP retrieval data from the ERA-Interim data, OEM retrieval and RSS retrieval respectively. The ERA-Interim data is the a priori used for the OEM retrieval. All data sets are restricted to the common valid domain of ice free open water ocean regions.

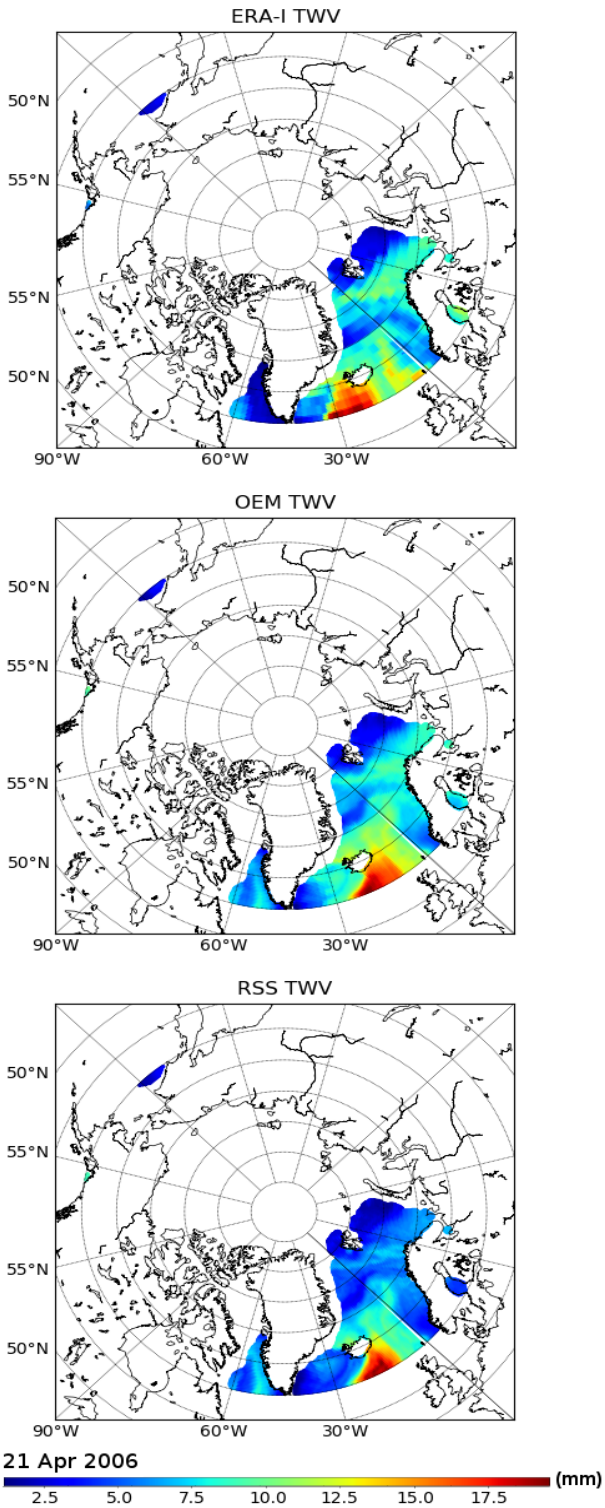

Figure 6.3: Map showing one day of TWV retrieval data from the ERA-Interim data, OEM retrieval and RSS retrieval respectively. The ERA-Interim data is the a priori used for the OEM retrieval. All data sets are restricted to the common valid domain of ice free open water ocean regions.

OEM retrieval matches the shape and location of the RSS data for both this high value region and for the lower value areas to the south west of Greenland. This shows that for relatively large values in TWV which influence the match between the simulated and the measured Tbs, the OEM can move away from the background values and retrieve the value that corresponds to the satellite measurements.

For the case of LWP retrieval (Figure 6.4) the OEM map mirrors most of the map features in the RSS product without showing any echoes from the maximum values present in the ERA-Interim map.

In the example map for SST retrieval (Figure 6.5) the tight constraint of the OEM towards the background data is most evident as even the shape of the large ERA-Interim pixels are present with some variations in the OEM SST values. While this parameter does not vary as fast in time as WSP or water vapour, and all three data sources show good agreement, the OEM bias towards the ERA-Interim data is clear, especially in the northern most regions of the map where the SST values are lower and the corresponding effect on Tb matching will also be lower.

This sort of comparative testing with a direct Tb inversion product shows that using constraints based on ERA-Interim parameter variability within a selected data set like the long term RRDP SIC0 can lead to some biased retrieval cases. This is the case of the SST retrieval were the ERA-Interim SST variability throughout the whole SIC0 data set was so low that the resulting variability constraint on the OE was just 1.4 K. After relaxing this constraint to a variability of 5 K as given by the climatological mean, the OEM SST retrieval can diverge more easily from the ERA-Interim background and get closer to the RSS result. All of the comparison statistics between OEM and RSS SST have improved after allowing for a standard deviation of 5 K from 1.4 K in the SST parameter as is shown in Table 6.2.

A visual example of how the constraints influence the retrieval can be seen in Figure 6.6. The over-constrained SST retrieval clearly shows the large pixel structures of the ERA-Interim background, while the SST retrieval with relaxed constraints has a smother structures and even slightly different distribution of values.

6.2 Comparing with ASI SIC

In order to evaluate the OEM SIC retrieval another suitable comparison benchmark is needed. The ARTIST Sea Ice algorithm uses the brightness temperatures from AMSR-E to retrieve SIC at a high spatial resolution of 6.25 km (Section 3.7). For the centre coordinates of every OEM retrieved SIC pixel the corresponding ASI SIC pixel value is selected. The comparison is then run for the entire 16 winter days of the 2006 data set. The necessary OEM background value for the sea ice parameters of SIC and MYIF are obtained by running the NT algorithm on the same AMSR-E Tb measurements. Similar

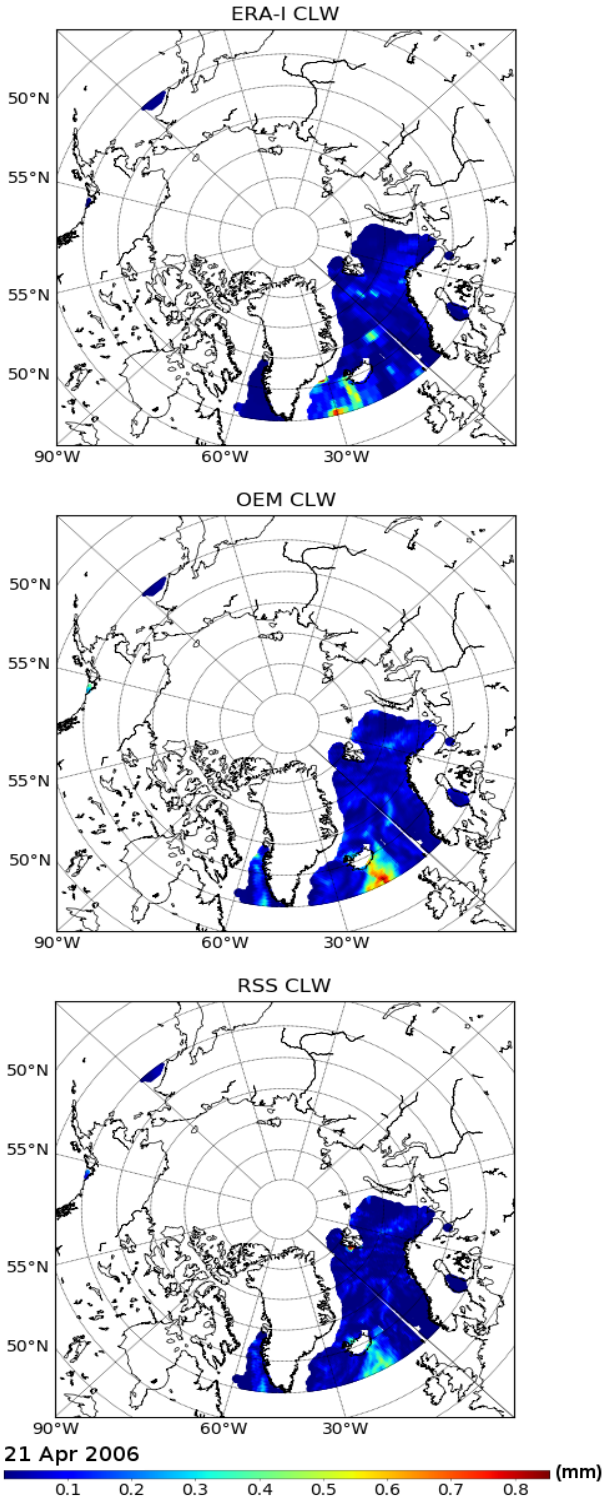

Figure 6.4: Map showing one day of LWP retrieval data from the ERA-Interim data, OEM retrieval and RSS retrieval respectively. The ERA-Interim data is the a priori used for the OEM retrieval. All data sets are restricted to the common valid domain of ice free open water ocean regions.

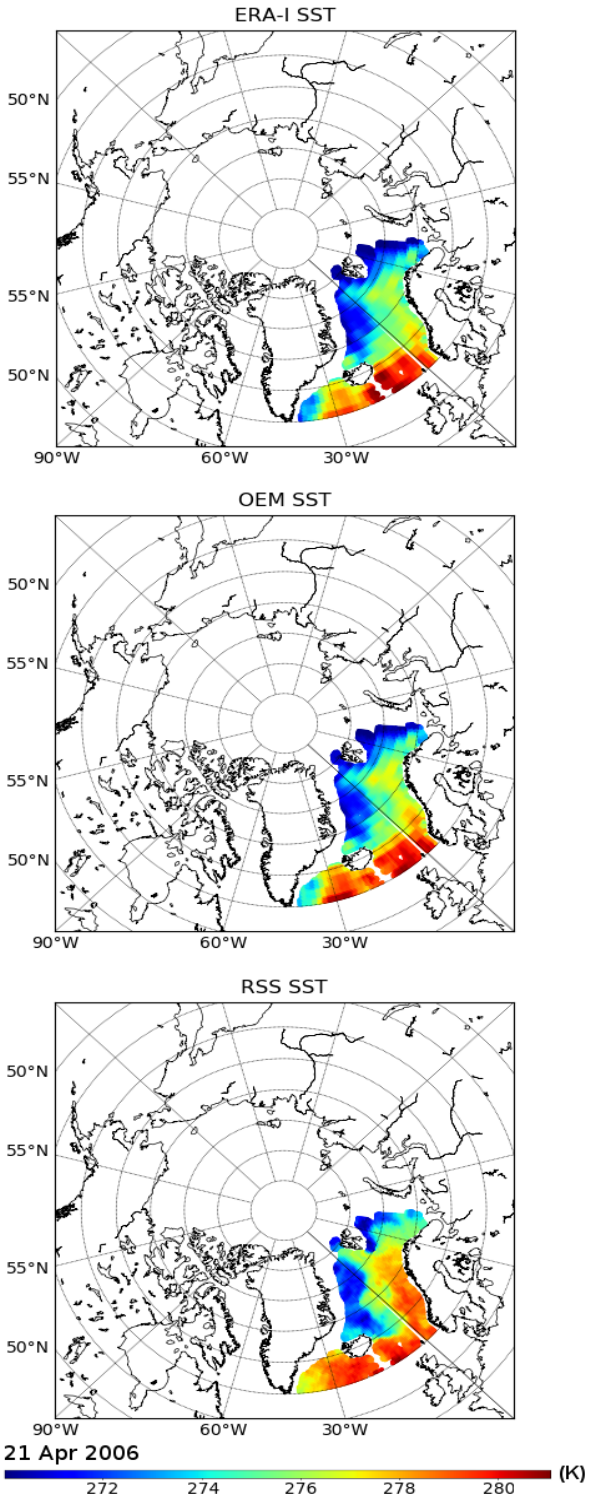

Figure 6.5: Map showing one day of SST retrieval data from the ERA-Interim data, OEM retrieval and RSS retrieval respectively. The ERA-Interim data is the a priori used for the OEM retrieval. All data sets are restricted to the common valid domain of ice free open water ocean regions.

Table 6.2: Intercomparison between OEM with different background covariance matrix constraints for the SST parameter in the winter 2006 data set.

Stat	Method	SST over-constrained (K)	SST relaxed (K)
Mean value	OEM	274.67	275.29
	ERA	274.54	274.15
	RSS	277.60	277.29
Std dev	OEM	2.98	2.87
	ERA	3.06	2.89
	RSS	2.99	2.92
Bias	OEM-RSS	-2.94	-2.00
	OEM-ERA	0.12	1.14
	ERA-RSS	-3.06	-3.14
Std dev diff	OEM-RSS	2.58	1.67
	OEM-ERA	0.42	1.68
	ERA-RSS	2.79	2.75
Correlation	OEM-RSS	0.63	0.83
	OEM-ERA	0.99	0.83
	ERA-RSS	0.58	0.55

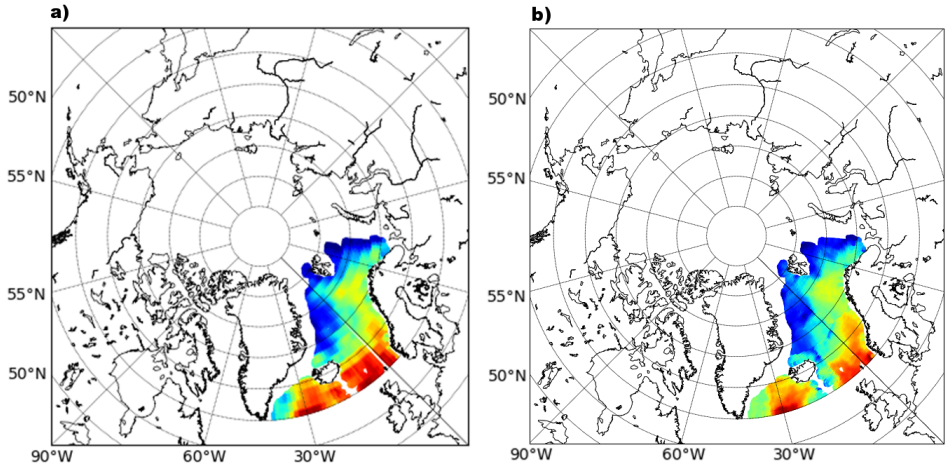

Figure 6.6: Map showing one day of SST retrieval data from OEM with an over-constrained (a) and a relaxed constraint (b) on the SST parameter. The day shown is the 21st of April, 2006.

to the comparison in the previous section, the a priori NT data is compared to OEM SIC and to the reference ASI SIC retrieval products in order to determine the relationships between the three. Ideally, the OEM can improve on the a priori information and show a better agreement to the reference ASI benchmark than the NT data. In Table 6.3 the statistics of the comparison between the NT, OEM and ASI SIC products are presented.

Table 6.3: Intercomparison between NT, OEM and ASI SIC retrievals. The comparison is done for all winter days of the 2006 data set.

Stat	Method	Value (%)
Mean value	OEM	77.35
	NT	76.38
	ASI	77.27
Std dev	OEM	38.04
	NT	34.25
	ASI	40.17
Bias	OEM-ASI	0.08
	OEM-NT	0.97
	NT-ASI	-0.89
Std dev diff	OEM-ASI	7.17
	OEM-NT	8.23
	NT-ASI	11.15
Correlation	OEM-ASI	0.99
	OEM-NT	0.98
	NT-ASI	0.97

Of the three methods only NT stands out with a mean value 1 percentage point smaller than the other two which are almost equal at 77.3% SIC. In terms of standard deviation NT has the lowest value and ASI the highest with OEM being in between the two. When comparing them in pairs, the biases between all three methods are small with values within +-1%. The NT has the largest discrepancy from ASI which decreases by more than a third between OEM and ASI. The correlations show good agreement between all methods. The three methods all agree well with each other and, though small, an improvement over the a priori NT is brought on by the OEM when compared to the operational ASI SIC data.

In order to gain more insight over how the three methods compare with each other, the histograms of SIC values from each data source are presented in Figure 6.7. Although the statistics do not indicate large differences, the histograms show that the distribution of SIC values differs between the three retrieval methods. The NT algorithm retrieves more intermediary value SIC data points with the largest number situated between 0 and 30% SIC at the lower end and between 70 and 100% at the higher end of the SIC range. The OEM SIC shows a value distribution more concentrated between the extreme points with the low SIC values distributed mainly between 0 and 10% while the high SIC values are spread between 80 and 100%. The ASI SIC retrieval shows an even peaked distribution

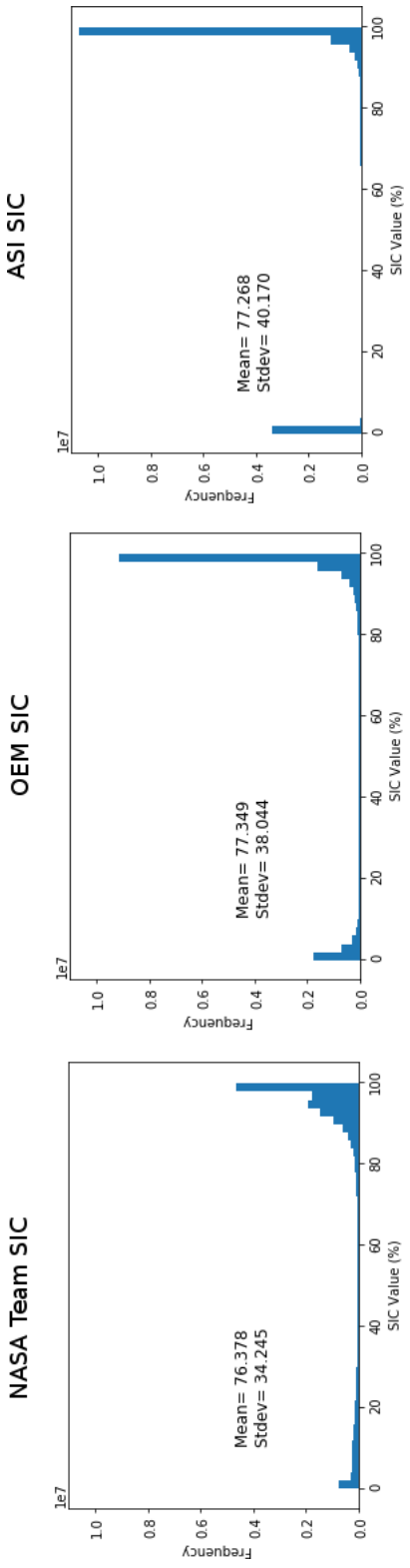

Figure 6.7: Histograms for SIC from three retrieval methods. Basic NT is on the left, OEM SIC is in the centre and ASI SIC is on the right.

with the majority of data points clustered around the 0% value and between 90 and 100% at the high end. From this comparison the OEM SIC retrieval is situated between the NT distribution with many intermediary values and the ASI distribution with two sharp peaks at 0 and 100% and few values in between. This behaviour can be explained by the difference in resolution between the three methods as well as the different weather filters included. While the NT set-up used as a source for background values does not use any weather filters for the sake of simplicity this means that spurious ice over open ocean as well as weather induced variability over the ice pack will appear in the histogram as a wider distribution of values between 0 and 100% SIC. The OEM retrieves the weather influence separately as state vector parameters and so the retrieved SIC parameter has a clearer distribution with two peaks at the extreme values of the SIC range. The difference between OEM and ASI SIC is then given by the resolution of the two products. Each large OEM pixel (75x43 km) is associated with a single ASI pixel with the same centre coordinates. This selection of ASI pixels biases the SIC values towards an even sharper distribution between the 0 and 100% peaks. An OEM pixel of intermediary SIC value is associated with a smaller ASI pixel which due to its smaller size can completely cover only an open ocean or a pack ice area inside the large OEM pixel. This is not the ideal way to perform such a comparison but the purpose was not to validate the OEM SIC retrieval but to test how reasonable the results are and use a simple approach where both methods have a common number of comparison pixels instead of asigning an average of ASI pixels for each large OEM one.

In Figure 6.8 three example daily maps of SIC data are shown from the three data sources. The data point distribution seen in the histograms from Figure 6.7 is confirmed by the details in the SIC maps. The NT implementation provides a background value for the OEM retrieval and does not benefit from any weather filters. As such, there are large areas of spurious ice caused by weather contamination just south of Iceland in the example maps. The values around the sea ice edge display intermediary SIC values so that there is a more gradual decrease from the 100% SIC in the centre of the ice pack towards the areas of open oceans. In the middle of the ice pack there are also weather contaminated areas with lower than 100% SIC which contribute to the number of intermediary SIC value pixels. The spurious sea ice over open ocean and the weather contaminated ice pack regions are almost completely eliminated in the OEM SIC retrieval. A feature of the OEM SIC however is the presence of intermediary SIC values at the edge of the ice pack similar to the NT results. This feature is absent in the ASI SIC map where there is a sharp drop from the 100% areas to the 0% open ocean. This is evident all along the marginal ice zone and in the south west of Novaya Zemlya island. In this area especially the ASI retrieval resolves three clear sea ice floes with open water between them, while the OEM SIC registers a more homogeneous zone with SIC values between 50% in the spaces between the floes and 90% values coinciding with the position of the floes in the ASI map. Here the big difference

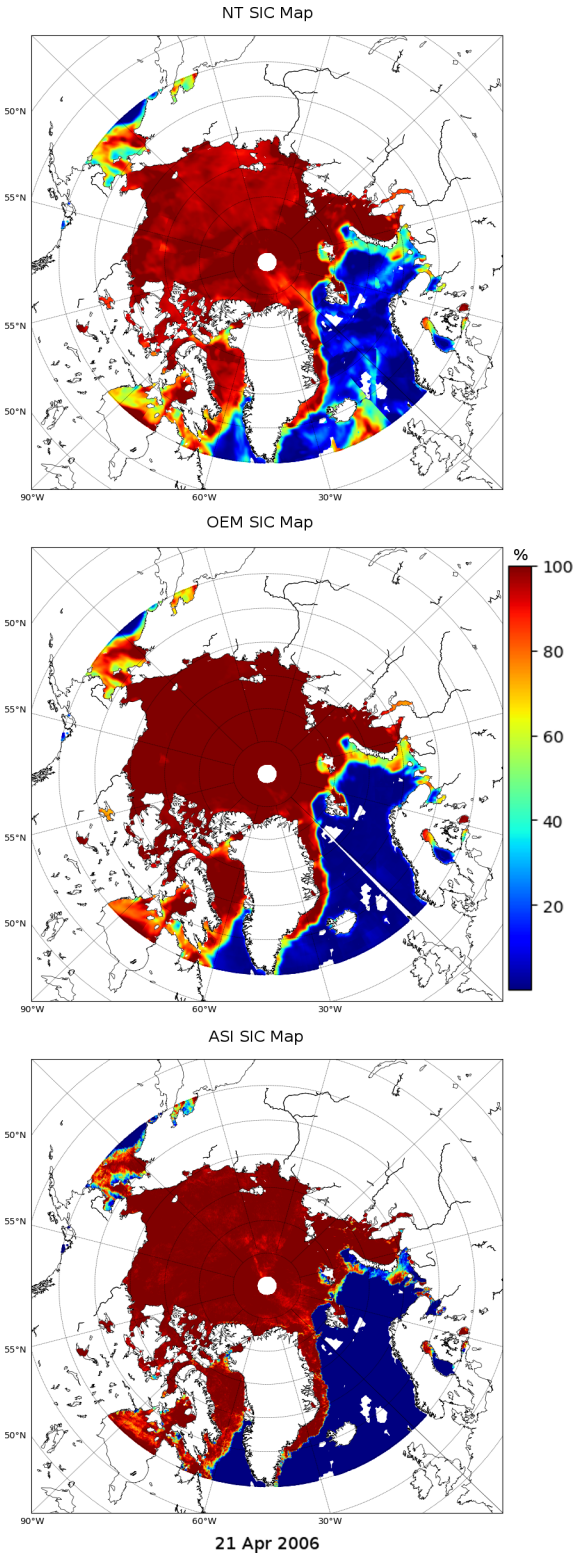

Figure 6.8: SIC maps for the Arctic above 60° N.

in resolution between the methods plays a role. While the OEM retrieval is limited to the spatial resolution of its lowest frequency channel at 56 km, the ASI retrieval benefits from using the highest frequency AMSR-E channels at 89 GHz and has a resulting spatial resolution of 6.25 km in the gridded daily product shown here. A downside of using the 89 GHz channels is that the SIC retrieval is more susceptible to weather influences which albeit reduced by weather filters and less pronounced than in the simple NT retrieval are still present in the final ASI SIC map over the ice pack. To conclude, the OEM does improve on the simple NT retrieval used as background and achieves a result close to the high resolution ASI SIC product. Moreover through its nature of simultaneously retrieving the relevant atmospheric parameters, the OEM SIC retrieval is weather filtered by default.

6.3 Comparing with AMSU-B TWV

The most challenging task for proving the reliability of the OE retrieval as an Arctic wide retrieval is testing the results for the atmospheric parameters over sea ice. The RSS product used in the previous section only works over ocean as the surface emissivity there can be parametrized as a function of SST and WSP while over sea ice the surface emissivity is much higher and highly variable and dependent on a larger number of parameters which are difficult to assess. One atmospheric retrieval method that can work around the problem of sea ice surface emissivity is the AMSU-B total water vapour product (Section 3.8). The retrieval range of the AMSU-B method is limited to values below 15 mm as the 183.3 GHz sounding channels become saturated. This means that the spatial domain over which a comparison with OEM can be done is restricted to mostly sea ice regions which are typically less moist, although in the winter season such low TWV values can also be encountered over open water at high latitudes. The OEM comparison with the AMSU-B TWV retrieval is seen as complementary to the RSS comparison done over open water because it focuses on atmospheric retrieval in areas where sea ice is present. The AMSR-E instrument used by the OEM has two channels around the weak water absorption line at 22 GHz, so that the information content available to the two methods is different, with higher sensitivity to water vapour available to the AMSU-B method which uses channels around the strong water absorption line at 183.3 GHz. This comparison is important however because the AMSU-B method is to date the most reliable retrieval that can daily cover the sea ice regions of the Arctic.

There are two main features that can be observed in the scatter plots. In Figure 6.9(a) there is a number of data points with TWV values covering the entire retrieval range of AMSU-B which are seen as 0 in the ERA-Interim data. Presumably this is a weakness of the ERA-Interim data because it shows a gap in the TWV data point distribution between 0 and 2 mm, which otherwise would be difficult to explain. Some of these 0 value pixels are still present in the OEM retrieved data but their number is greatly reduced with the high

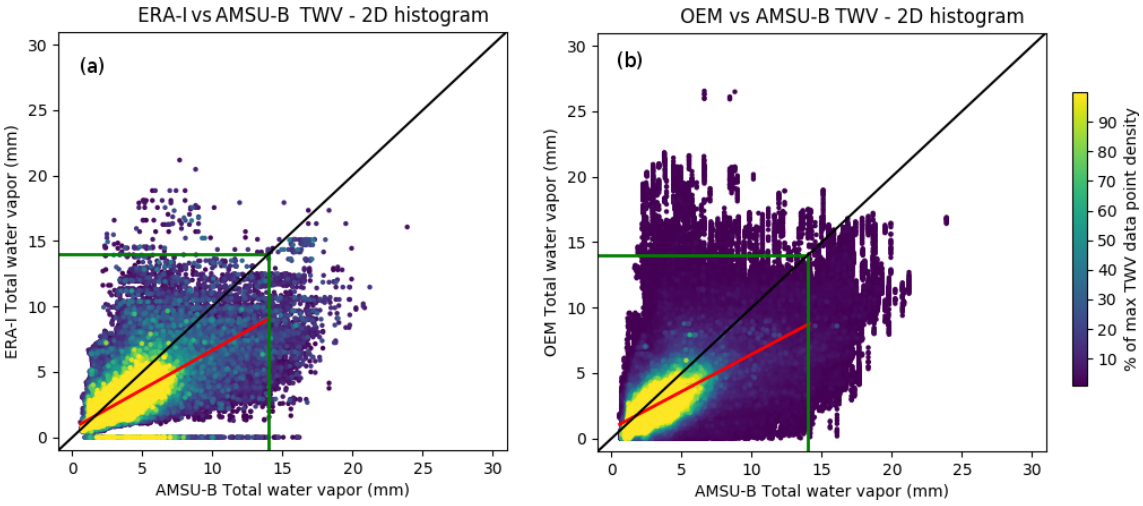

Figure 6.9: Scatter plots showing the distribution of AMSU-B retrieved TWV data versus collocated ERA-Interim data (a) and OEM retrieval TWV (b) respectively. The green lines represent the 14 mm limit above which AMSU-B retrieval channels starts to saturate. The red lines show the regression between the data sets. Data is based on the 16 winter days in the 2006 data set.

pixel density regions being confined only to the 0-6 mm interval region. Another difference for the ERA-Interim comparison with AMSU-B is the high scatter of data points. The largest density of points is registered at TWV values between 1 and 7 mm with the scatter increasing for values higher than 7 mm. In the OEM TWV retrieval the maximum data density is kept in the same value range but with far less points scattered at higher values. From the scatter plots we can conclude that the OEM retrieval moves away from the a priori when ERA-Interim data gives values of 0 mm TWV and retrieves values that are in better agreement with the AMSU-B product. For values above 7 mm the spread of the data scatter is reduced even though the negative bias versus AMSU-B data is present in both the comparison with ERA-Interim and OEM data.

The scatter plots in Figure 6.4 are complemented by the comparison statistics over the winter days of the 2006 data set in Table 6.4. While the three data sources show similar mean TWV values, there are differences in the standard deviations of each method. When comparing the three sources, the OEM retrieval agrees best with the ERA-Interim data. This is to be expected as the collocated ERA-Interim values are used as the a priori background from which the OEM will move away only if the brightness temperature difference is large enough. For every statistic, the OEM is behind ERA-Interim for testing agreement with the AMSU-B retrieval. The standard deviation of the difference and bias value are higher and the correlation lower between OEM and AMSU-B when compared to the ERA-Interim comparison with the AMSU-B retrieval.

In the one day example maps from Figure 6.10 the three data sources show similar

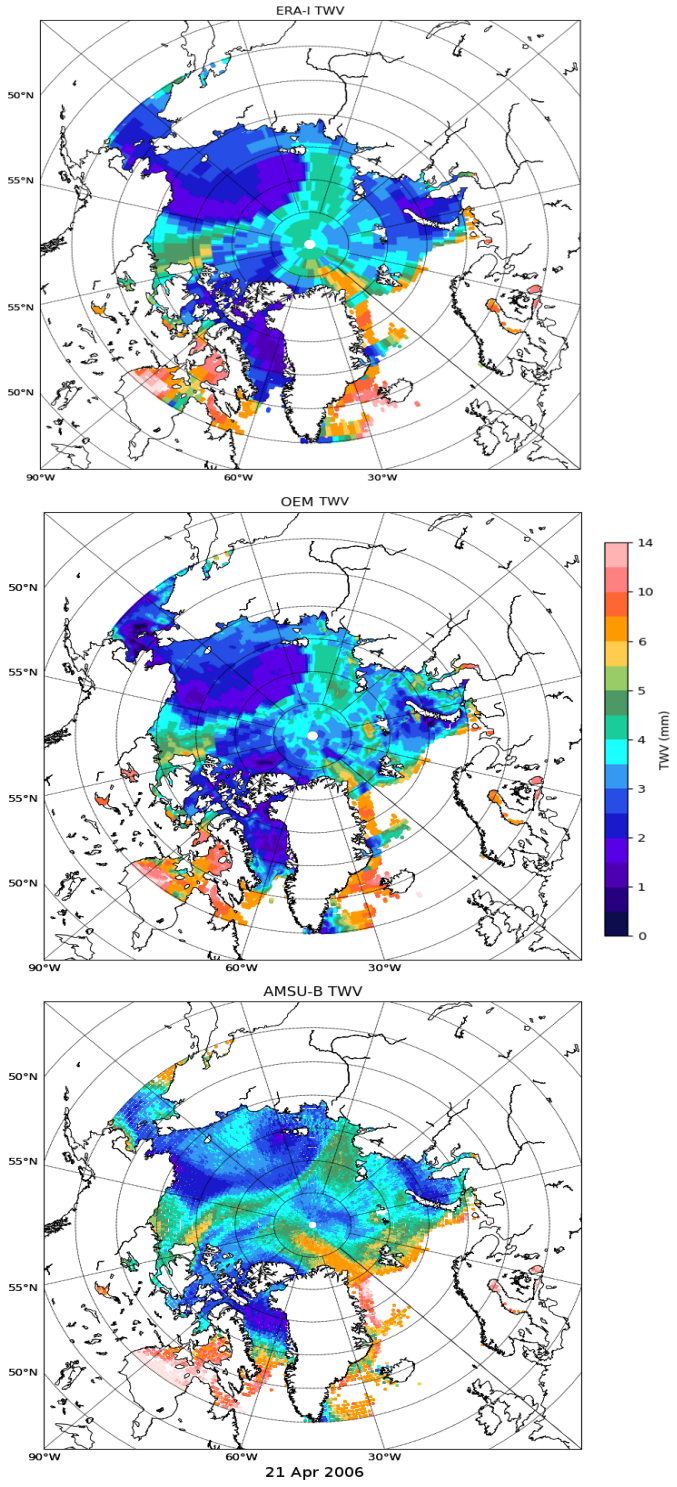

Figure 6.10: Map showing one day of TWV data from the ERA-Interim data, OEM retrieval and AMSU-B retrieval respectively. The ERA-Interim data is the a priori used for the OEM retrieval and they are both restricted to the sea ice covered and open water ocean regions while the AMSU-B retrieval coverage is only restricted by the TWV value. The day shown here is the 21st of April, 2006.

Table 6.4: Comparison statistics between OEM TWV retrieval, ERA-Interim data used as a priori and AMSU-B TWV retrieval.

Stat	Method	Value (mm)
Mean value	AMSU-B	3.58
	OEM	3.72
	ERA-Interim	3.69
Std dev	AMSU-B	1.93
	OEM	2.68
	ERA-Interim	2.62
Bias	OEM-AMSU-B	-0.81
	OEM-ERA-I	0.03
	ERA-Interim - AMSU-B	-0.78
Std dev diff	OEM-AMSU-B	1.46
	OEM-ERA-Interim	1.05
	ERA-I- AMSU-B	1.33
Correlation	OEM-AMSU-B	0.67
	OEM-ERA-I	0.92
	ERA-Interim - AMSU-B	0.73

TWV values over the common spatial domain. Big features are easily recognisable such as the low TWV region north of the Chukchi Sea and the one west of the Greenland coast. While the shapes are similar, the values are lower in the ERA-Interim and the OEM retrieval maps. This confirms the negative bias of these two data sources versus AMSU-B TWV data shown in Table 6.4. The three methods agree better in regions with higher TWV loads like in the north of Hudson Bay, and on the eastern coast of Greenland. It is important to note that there are significant differences between the three data sources. The AMSU-B TWV data represents a daily average map the same as the AMSR-E based OEM retrieval while the ERA-Interim data is the closest model step to the collocated AMSR-E measurement. As TWV is a parameter with high temporal variability, the time difference between the three sources can explain shifts that appear in the map features. An important difference between the two retrieval methods is that the AMSU-B methods benefits from using the high water absorption line at 183 GHz while the OEM implementation based on the lowest 10 frequency channels of AMSR-E depends only on the weak water absorption line around 22 GHz. This means that the AMSU-B TWV retrieval is more reliable for low values as it has a higher sensitivity. The forward model used by the OEM to translate the state vector to simulated AMSR-E brightness temperatures uses parametrizations that were derived from radiosonde measurements taken in more southerly latitudes where TWV values are higher. The resolution is also an important factor. The ERA-Interim data is gridded on a 1.5 °grid, the OEM retrieval is limited to the resolution of its lowest frequency channel at 56 km spatial resolution and the AMSU-B daily retrieval is gridded to a 50 km spatial resolution. Despite the higher resolution of the AMSR-E sensor, the OEM retrieval

reproduces the large pixel structures found in the ERA-Interim data. This is because the TWV values are small, and their influence on the simulated brightness temperatures is lower than the surface sea ice parameters that the OEM does not move away from the background data source.

7 | Different channel combinations

In order to determine the best set-up for the OEM, the constraints, a priori information and forward model have been tested in the previous chapters. The tests run on the OE in Chapter 5 and the comparisons made in Chapter 6 have used the ten AMSR-E channels between 6.9 and 37 GHz as input for the retrieval. As stated in Chapter 5, this was done because the forward model has a known limitation regarding the interaction with Mie scatterers at frequencies above 37 GHz and this will result in a higher uncertainty for the simulated Tbs at the 89 GHz channels. On the other hand, these channels are also known to be the most sensitive ones out of the set of 12 for TWV and LWP and including them in the OEM can potentially improve the retrieval of these atmospheric parameters. In order to test this approach, an OEM version that uses all 12 AMSR-E channels has been developed. This OEM set-up has been tested over the whole RRDP set and the results have been explored through information content analysis and compared to the reference 10 channel version. This analysis is similar to that presented in Section 5.1.2 and it shows if and by how much the knowledge on the state vector parameters can be improved by adding the 89 GHz channels while taking into account the increased uncertainty of the simulated Tbs.

A different point of interest for the development of the OEM is the potential for improving the horizontal resolution of the output. By using the AMSR-E Level 2a resampled Tb data product the retrieval is limited to the spatial resolution of the lowest frequency channel. This means that the only retrieval resolution supported by the current implementation of the OEM is the 56 km spatial resolution of the 6.9 GHz channels. One approach for increasing the retrieval resolution of the OEM is to discard the 6.9 GHz channels from the input and use the Level 2a product resampled at the 38 km spatial resolution of the

10.65 GHz channels. Similarly to the analysis for including the 89 GHz channels, an information content analysis was done for an OEM version that uses only the ten highest frequency channels of AMSR-E. This shows the impact on the retrieved knowledge of discarding the 6.9 GHz channels.

7.1 The forward model Jacobian

One way to predict the potential impact of each individual AMSR-E channel on individual parameter retrieval is to check the forward model Jacobian matrix. It indicates the change in the individual channel Tb for a small perturbation in an individual state vector parameter. In order to compare the relative influence of the state vector parameters with each other and across different channels the elements of the Jacobian have been normalised by the a priori parameter uncertainty (standard deviation) derived from the S_a matrix variances. The full set-up for the a priori parameters is discussed in more detail below. For a better insight into how these parameter sensitivities vary depending on the surface conditions, the Jacobian results are averaged separately for all RRDP SIC1 and SIC0 scenes respectively.

For both SIC1 and SIC0 cases all 12 channels have been used in the retrieval. In order to extend all of the findings of Chapter 5 to all 12 channels, the effective sea ice surface temperature correction coefficients and surface emissivity corrections include the 89 GHz channels. The corresponding brightness temperature covariance matrix S_e has been calculated to account for the increased uncertainty of the 89 GHz channels. As the sea ice surface emissivity correction is calculated for the retrieval step modeled brigthness temepratures and the cost function accounts for the brightness temperature differences across all channels, the retrieval will have some differences from the OEM version which excludes the high frequency channels. By including the higher uncertainty 89 GHz channels the retrieval is influenced and indirectly the emissivity correction corresponding to this OEM configuration has change so that the resulting variances across some of the channels have also increased. This means that the S_e elements for the 12 channel OEM version will be larger than the elements for the 10 channel OEM which excludes the 89 GHz channels. In order to observe only the effects of using different channel combinations on the information content separate from any effects that the different S_e matrix would have, the same brightness temperature matrix is used for both SIC0 and SIC1 tests and across all OEM versions tested in this chapter. The equivalent standard deviation values for each channel are shown in the Appendix in Table A.8 side by side with the equivalent values for the 10 channel OEM without the 89 GHz channels in order to showcase the impact on all Tb uncertainties of including the high frequency channels. On average the standard deviation of the difference between simulated and observed Tbs has increased from 1.64 K to 2.77 K after including the 89 GHz channels. The attempt to use separate S_a matrices for

SIC1 and SIC0 cases respectively, showed in Chapter 6 that the resulting variances from a long term SIC0 data set can lead to overconstraining some of the retrieval parameters to the background. A second attempt to create a SIC0 specific S_a matrix was made using ERA-Interim parameters from the 16 winter days of the 2006 data set for SIC values below 5%. The results were very close to the climatology based S_a matrix described in Section 5.1.1. In order to avoid confusion, the same climatology based diagonal background covariance matrix described in Table A.1 in the Appendix is used for both the SIC1 and SIC0 tests.

In Figure 7.1 let side the Jacobian for the SIC1 tests is shown. Out of the seven state vector parameters some are not represented over SIC1 such as SST and WSP as they do not impact the surface emitted brightness temperatures. Out of the remaining five parameters that can influence the simulations, SIC shows the strongest sensitivity. It determines large Tb responses across all channels with the relative sensitivity decreasing with frequency. The other parameter that triggers a response in all channels is the MYIF where the Tb change increases with frequency up to 37 GHz. The 6.9 GHz channels show the highest sensitivity to SIC changes in both polarizations but are closely followed by the 10.65 GHz channels. This means that removing the 6.9 GHz channels would decrease the sensitivity to SIC but this could potentially be supplemented by the other channels. This aspect will be further investigated in Section 7.2.

For the atmospheric parameters, the 89 GHz channels stand out as the most sensitive ones to both LWP and TWV. This is particularly important as these atmospheric parameters determine very low responses in the lower frequency channels. For the case of SIC1 including the 89 GHz channels can add greatly increased atmospheric sensitivity to the OEM with the downside of the increased uncertainty for the simulated Tbs.

On the right side of Figure 7.1 the corresponding Jacobian values are plotted for the SIC0 test scenario. The SIC is again the most influential parameter followed by LWP, TWV and WSP with SST being the least important for the forward model calculations. Over SIC0 the atmospheric parameters determine Tb responses over all channels. This is important because it means that the retrieval sensitivity is not affected too much by the channel combination if all channels can provide some measure of sensitivity to all significant parameters. The 89 GHz channels provide the best sensitivity for LWP while the 6.9 GHz channels are most sensitive to SIC but in both cases there are adjacent frequency channels which provide similar sensitivities. Based only on the Jacobian we can say that changing the channel combination will have a lower impact on the OEM over SIC0 regions than over SIC1 over open water there is more redundancy for atmospheric parameter sensitivity while over sea ice the signal is dominated by SIC and MYIF with only the 89 and to a lesser extent 37 and 22 GHz channels still offer some sensitivity to LWP and TWV. This is however without taking into account the different channel accuracies which is what the information content analysis can provide as is described in the introduction of Section 5.1.2.

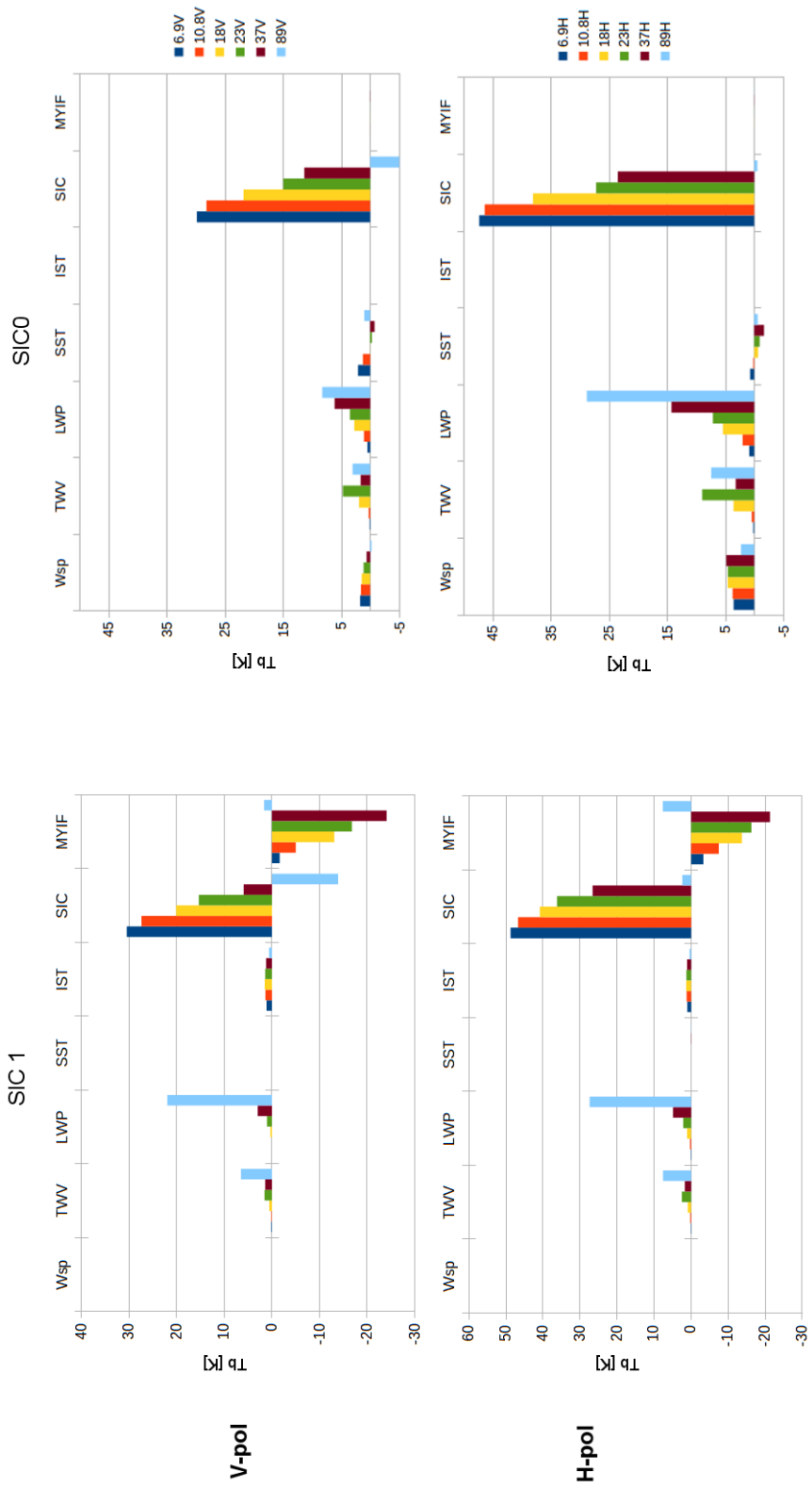

Figure 7.1: Mean Jacobian values for the RRDP SIC1 on the left side, and SIC0 on the right side for all winter data points.

7.2 Testing over RRDP SIC1

In order to determine how suitable for retrieval different channel combinations are an information content analysis of the retrieval is performed for three different version of the OEM. The reference version is the OEM set-up used throughout Chapter 6. It uses the AMSR-E channels between 6.9 and 37 GHz including all of the improvements listed in Section 5.7 and the relaxation of the SST S_a matrix constraint described at the end of Section 6.1. For ease of notation throughout this section, this OEM version will be called 10c-low as it uses the ten lowest frequency channels of AMSR-E. Another version, called 12c, uses all 12 AMSR-E channels with corresponding adaptations for emissivities and sea ice surface temperature. A third version, called 10c-high, uses the channels between 10.65 and 89 GHz thus discarding the 6.9 GHz channels. Besides the input channel combination all three versions are identical, using the same a background data and constraints.

Table 7.1: Singular values (λ_i), degrees of freedom (d_s) and information content (H) in bits for the singular vectors of the three OEM versions. Test was done over RRDP SIC1.

	10c-low			10c-high			12c		
i	λ_i	d_s	H	λ_i	d_s	H	λ_i	d_s	H
1	43.17	0.999	3.77	36.74	0.999	3.6	42.75	0.999	3.76
2	14.1	0.995	2.65	12.11	0.993	2.5	14.16	0.995	2.65
3	1.23	0.602	0.46	2.93	0.896	1.13	8.64	0.987	2.16
4	0.6	0.266	0.16	0.64	0.29	0.17	0.62	0.278	0.16
5	0.36	0.113	0.06	0.29	0.077	0.04	0.5	0.199	0.11
6	0	0	0	0.01	0	0	0	0	0
7	0	0	0	0	0	0	0	0	0
Total		2.975	7.09		3.255	7.44		3.459	8.85

For SIC1 Table 7.1 gives the results of the information content analysis. It shows the individual contribution of each singular vector as well as the total information content for each of the three channel combinations. The total information content gives the number of bits of independent information with which the retrieval improves on the a priori knowledge. The information content associated with each singular vector gives a measure of the retrieval sensitivity to the parameters represented by that particular singular vector. The degrees of freedom are also shown for each OEM version and they give the number of independent measurements that can be made at higher precision than the noise threshold. For understanding the differences in information content between the different OEM versions the value in the table need to be viewed alongside the singular vector plots shown in Figure 7.2, where the singular vectors are shown in decreasing order of their singular values. The singular vectors can be seen as reflections of how the forward model calculates the parameter contributions to the simulated brightness temperatures and the higher the information content for a singular vector, the larger the OEM retrieval sensitivity to the

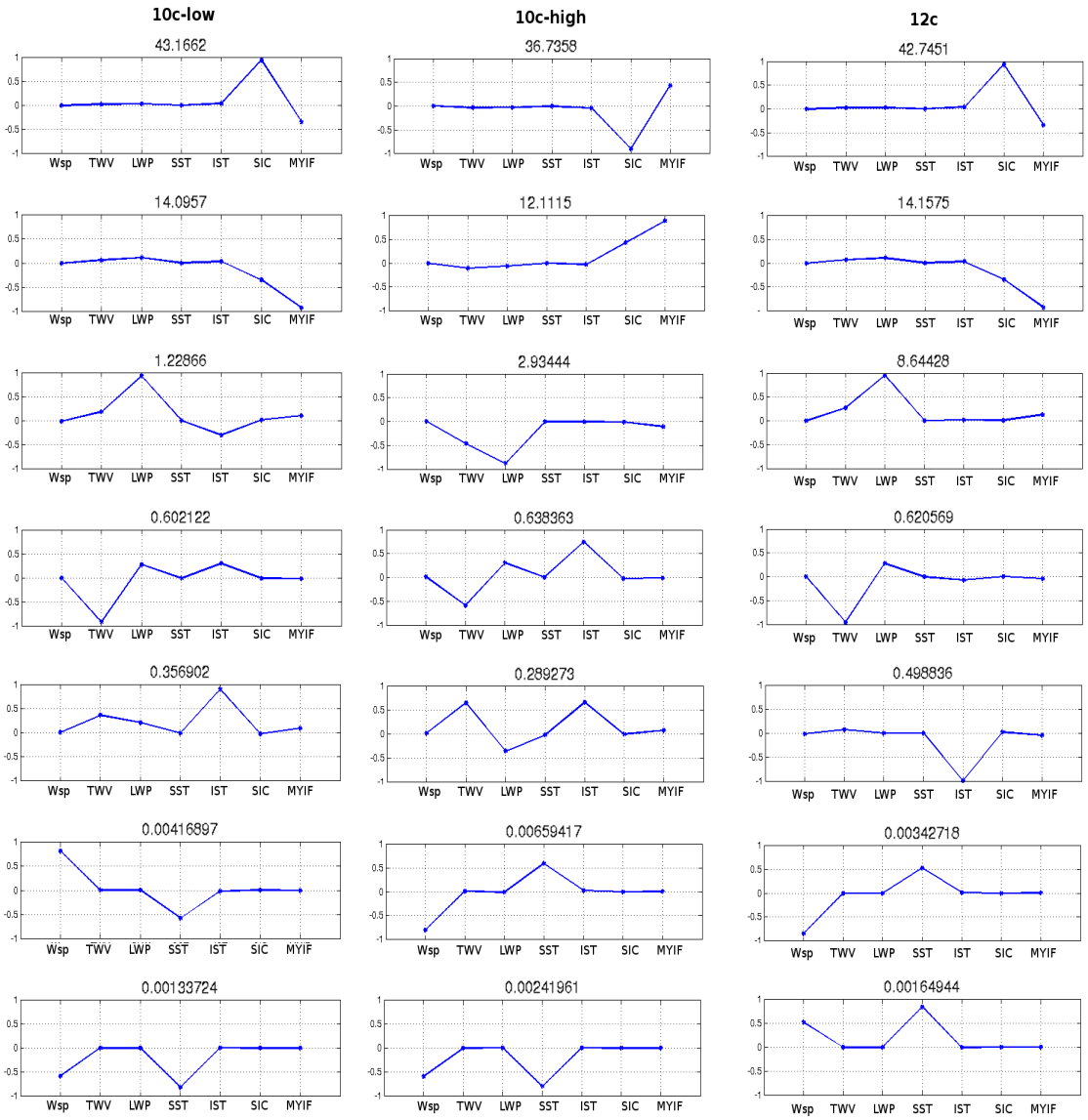

Figure 7.2: Singular vectors for the three OEM versions based on different input channel combinations tested over the SIC1 data set. The left most column represents the 10c-low version, the middle column is the 10c-high version, while the right most column represents the 12c version.

parameters that contribute to that particular singular vector.

The 12c channel combination has the highest information content. This is to be expected as it includes the maximum number of input information from Tb measurements. It is interesting to watch how the information content varies when the 6.9 GHz or the 89 GHz channels are not included in order to gauge the impact these channels have on the retrieval. The influence of the 6.9GHz channels can be seen in the first two singular vectors which represent the combined contributions from SIC and MYIF (Fig. 7.2, top two rows). As the 6.9 GHz channels have the highest sensitivity to SIC (Fig. 7.1) it makes sense that the OEM versions which include these channels (10c-low and 12c) will have the highest information content in the singular vectors that depend on this parameter. When 6.9 GHz channels are discarded, the higher frequency channels can contribute enough information to achieve one degree of freedom for each of these singular vectors, however the information content for the first two singular vectors is reduced (Table 7.1, 10c-high column, top two rows) when compared to the other two OEM versions.

The third singular vector has the strongest influence from the LWP and TWV contributions (Fig. 7.2, top two rows) and its information content is increased (Table 7.1, 12c column, third row) by almost a factor of 5 in the 12c version compared to the 10c-low version, from 0.46 to 2.16 bits as the 89 GHz channels offer higher sensitivity to these parameters (Fig. 7.1). This shows that the main benefit of the the 89 GHz channels is in improving the OEM information content for LWP and TWV while the increased noise they introduce determines has very little effect on the surface parameter information content compared to the 10c-low OEM version (Table 7.1, 10c-low column and 12c column, top two rows).

The inclusion of the 6.9 GHz channels ensures the highest information content among the three versions for the retrieval of SIC. The total information content of the retrieval decreases by 16% (or 1.41 bits) between the 12c and the 10c-high versions as a consequence of discarding the 6.9 GHz channels. However given the precision levels for SIC set by the background covariance matrix, the remaining mid-frequency channels provide enough sensitivity to ensure the retrieval of one degree of freedom for each of the first and second singular vectors. This means that the OEM can retrieve SIC as an independent parameter with a precision level above the noise threshold even without the 6.9 GHz channels if the OEM application requirements ask for a higher resolution. The reverse is that for applications that require the most accurate OEM SIC retrieval, with the highest information content for this parameter, and without concern for the resolution difference, the 6.9 GHz channels must be included.

At the opposite end of the channel frequency range, excluding the 89 GHz channels (10c-low) has a more dramatic effect on atmospheric parameter retrieval as the sensitivity they provide is unique among the AMSR-E channels. The total information content of the 12c version is greater by 25% (or 1.76 bits) than that of the 10c-low version. The

OEM versions that included the 89 GHz channels, 10c-high and 12c, achieved almost one degree of freedom for the third singular vector which means that if retrieving independent information about the atmospheric parameters of LWP and TWV over sea ice is a priority, the 89 GHz channels have to be included in order to beat the precision levels set by the background covariance matrix.

7.3 Testing over RRDP SIC0

Just as over SIC1, the first singular vector for all versions over SIC0 (Fig. 7.3) is dominated by the contribution from SIC. The second and third singular vectors however give mixed contributions from an ensemble of surface and atmospheric parameters. TWV and LWP are the most important parameters for these singular vectors but to a lesser degree also WSP, SST and SIC contribute to the information content. This is important because the 6.9 GHz channels are the most sensitive channels for SIC, WSP and SST (Fig. 7.1). The information content is reduced (Table 7.2) by 28% (2.2 bits) between the 12c and the 10c-high version.

For the 12c version, when compared to the 10c-low version, the contribution the 89 GHz channels bring for the atmospheric parameters of LWP and TWV is reflected in the increase in information content for the second and third singular vectors (Table 7.2, 12c column, second and third top rows). The inclusion of the 89 GHz channels improves the knowledge on the atmospheric parameters LWP and TWV, however the additional information is quantified to just 10% (0.7 bits) more than the 10c-low OEM (Table 7.2). The number of degrees of freedom is increased only slightly. In practice both versions should achieve a retrieval of between 3 and 4 independent parameters over SIC0 while the 10c-high version can achieve less than 3 independent parameters.

Overall the impact of removing the 6.9 GHz channels is more important over SIC0 scenes because the surface parameters WSP and SST influence all significant singular vectors. The impact of including these channels is less dramatic as over SIC1 because over ice free regions there are other channels with relatively large sensitivities to LWP and TWV. Over SIC1 only the 37, 23 and to a small extent, 18 GHz offer some sensitivity to LWP and TWV but significantly lower than the 89 GHz channels (left side Fig. 7.1). Over SIC0 all channels offer sensitivity for LWP and all except 6.9 GHz for TWV. While the 89 GHz channels are still the most sensitive for LWP, and second most sensitive for TWV, the differences to the other channels are not as dramatic as over SIC1 (Fig. 7.1).

For the forward model calculations, over open water the parameter contributions are interconnected more than over sea ice and as such the WSP and SST parameters influence all of the singular vectors. Removing the 6.9 GHz channels reduces the method sensitivity to these parameters and in turn this reduces the information content of the retrieval overall. Over SIC1, the loss of the 6.9 GHz channels is compensated for by the adjacent frequency

channels, with a small decrease in the information content and almost no change in the number of degrees of freedom for the first two significant singular vectors. As predicted by the parameter sensitivities shown in the forward model Jacobian (Fig. 7.1), the inclusion of the 89 GHz channels contributes more information about the atmospheric parameters of LWP and TWV. It is important to note once again that the downside of including these channels in the OEM is represented by increased uncertainty in the simulated brightness temperatures. Even though the uncertainty of the 89 GHz channels is about double that of the lower frequency channels as shown in Table A.8, a gain in knowledge is still achieved. The impact of the high frequency channels is larger over SIC1 as the retrieval sensitivity for the atmospheric parameters is greatly improved despite the added noise from the larger Tb uncertainty. Over SIC0 the contribution of the 89 GHz channels is also present but its impact is reduced as the other channels also offer reasonable sensitivity for the two atmospheric parameters.

Table 7.2: Singular values (λ_i), degrees of freedom (d_s) and information content (H) in bits for the singular vectors of the three OEM versions. Test was done over RRDP SIC0.

	10c-low			10c-high			12c		
i	λ_i	d_s	H	λ_i	d_s	H	λ_i	d_s	H
1	39.11	0.999	3.67	32.53	0.999	3.48	39.05	0.999	3.67
2	6.52	0.977	1.89	4.62	0.955	1.55	9.91	0.990	2.30
3	2.77	0.885	1.08	1.12	0.557	0.41	3.11	0.906	1.18
4	1.02	0.511	0.36	0.61	0.269	0.16	1.33	0.640	0.51
5	0.66	0.305	0.18	0.33	0.099	0.05	0.73	0.348	0.21
6	0.00	0.000	0.00	0.01	0.000	0.00	0.01	0.000	0.00
7	0.00	0.000	0.00	0.00	0.000	0.00	0.00	0.000	0.00
Total		3.677	7.17		2.879	5.65		3.883	7.87

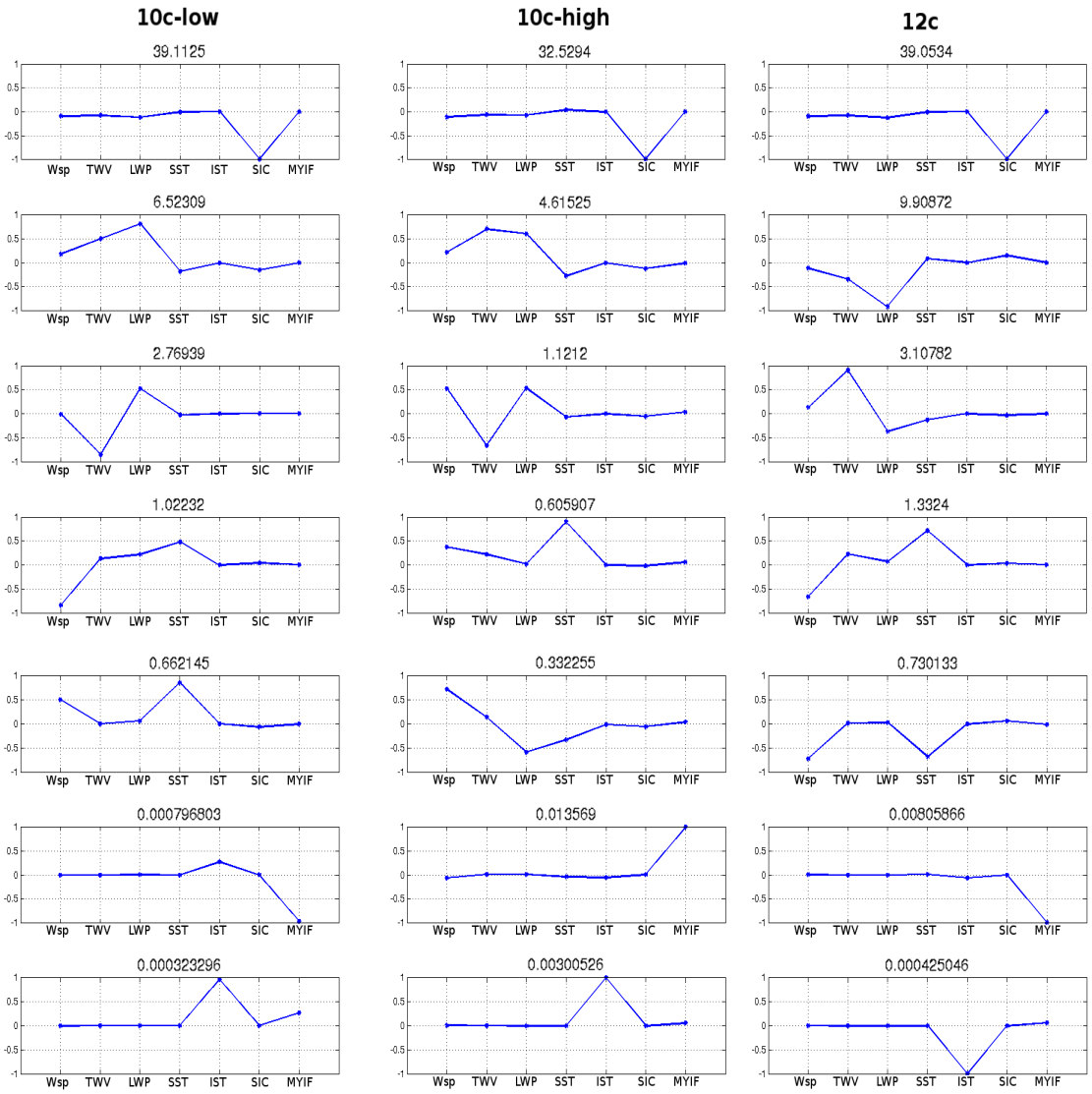

Figure 7.3: Singular vectors for the three OEM versions based on different input channel combinations tested over the SIC0 data set. The left most column represents the 10c-low version, the middle column is the 10c-high version, while the right most column represents the 12c version.

8 | Conclusions

8.1 Sensitivity tests and improvements

The aim of this study was to explore and further develop the performance of the OEM prototype [Melsheimer et al., 2008] for an integrated retrieval of seven atmospheric and surface parameters in the Arctic described in Chapter 4. The method sensitivity to the a priori parameters has been tested in Chapter 5. The main findings are:

(i) The OEM is resilient to small scale changes in the background covariance matrix elements. When these elements are changed to unrealistic levels there is a resulting bias in the retrieval. This means that the OEM is reliable as long as the a priori is based on reasonable data which allows for natural parameter variability.

(ii) The representability of the a priori data is important. A priori constraints based on short term data sets can be too strict if the retrieval is run for longer time series. A background covariance matrix based on model data from a single winter month proved to be too restrictive for a retrieval data set that covered the winter season across five years.

(iii) The previous point about the representability of the constraints is further supported by an analysis of the retrieval information content. By looking at the degrees of freedom of the retrieval, the OEM version using the one month based constraints has been shown to retrieve fewer independent parameters than the one using the long term background covariance matrix.

(iv) The presence of non-diagonal elements in the background covariance matrix (S_a) has an important effect on the retrieval. It is shown that for the OEM version that

uses an S_a based on a short term data set which includes non-diagonal elements, the number of iterations has increased dramatically. This means that the off-diagonal elements impose additional constraints that require more iterations to be satisfied. An additional challenge is that the covariances between parameters are difficult to extract from climatological data, and these relationships can vary in time and space [Pedersen, 1994]. The potential for bias is strong, resulting from overconstraining the retrieval in conditions where the covariances do not hold true, for example any covariances relating to the atmospheric parameters over sea ice. It was decided that a simplified implementation where no covariances are used is preferable. By discarding the off-diagonal elements altogether, the resulting diagonal background covariance matrix is the minimum required according to Rodgers [2000], but sufficient for the OEM to function and the potential bias issues are avoided.

(v) A dynamically collocated set of background parameters for each retrieval pixel ensures a faster convergence rate, full convergence for all tested datapoints, and a better agreement with the ASR model data. ERA-Interim data is used for the parameters WSP, TWV, LWP and SST. Both over open water and over 100% SIC the use of collocated ERA-Interim as background causes an improvement in the retrieval agreement with the benchmark data for all parameters except for LWP. It is a known feature of reanalysis data that LWP fields from model data do not exactly represent the cloud situation at the place and time of the satellite overflight. When using one static set of background parameters the retrieval is constrained to this single position resulting in an unrealistic distribution of the output data points clustered around the static background position. By using collocated background data the data distribution of the retrieval is normalised. It is an interesting consequence that by improving the atmospheric parameter retrieval and thus correctly attributing their contributions to the simulated Tb signal, a better result for the SIC parameter is achieved (Fig 5.3, 5.4). The SIC retrieval using collocated reanalysis data for the atmospheric parameters has a lower standard deviation and a narrower distribution around the extreme values of 100 and 0% for the SIC1 and SIC0 data sets respectively. By correctly attributing the contributions by the atmospheric parameters to the simulated Tb, the retrieved SIC standard deviation is decreased from 2.1% to 1.2% for SIC0 and from 4.6% to 2.8% over SIC1.

(vi) Related to the collocated ERA-Interim background data is the treatment of the effective ice surface temperature. Because each of the AMSR-E channels used in the OEM has a different frequency dependent penetration depth inside the snow and ice pack, the surface temperature parameter needed in the forward model should be different for each channel. To address this issue, channel wise regression coefficients determined by [Mathews, 2007] were used in order to relate the ERA-Interim 2 meter

air temperature to individual channel effective surface temperatures. An OEM version that includes the sea ice surface effective temperature correction and a reference OEM are compared against ASR skin surface temperatures for the RRDP SIC1 set. The OEM that includes the correction has shown a massive improvement in terms of IST bias reduction from 12 K to 3.4 K, as well as an increase in correlation with the model data from 0.55 to 0.8.

(vii) Another parameter to which the OEM sensitivity was tested is the start guess value. Initially, collocated ERA-Interim data was used for this first guess, in order to place the OEM as close to the solution as possible. Alternatively, an OEM implementations was tested which used a static start guess array for all RRDP pixels. Comparing the two versions showed that the start guess value has some influence on the atmospheric retrieval over SIC1 areas and almost none at all on retrieval over SIC0. The largest influence of the start guess is in the number of iterations required by the OEM to reach convergence. In both SIC1 and SIC0 scenarios the static start guess OEM version needed on average 0.8 more iterations per pixel than the dynamic start guess version. This means that the start guess is not that important and the OEM is resilient against the position of the initialization point.

(viii) One important aspect of forward model calculations in the Arctic is the contribution of the sea ice covered surface. Empirical sea ice surface emissivities calculated by [Mathews, 2007] are used in the OEM prototype. Individual channel biases were found in the simulated brightness temperatures calculated over SIC1 scenes when compared to the AMSR-E measurements using this set-up. To reduce the biases a correction was applied to the empirical emissivities. Under the assumption that the differences between the simulated and the measured brightness temperatures are caused by the sea ice surface component of the forward model, a set of corrected emissivities has been calculated that minimises these differences (Table A.5). While before the correction the emissivities had monthly values and each pixel wise set of emissivities was interpolated in time depending on the date of the retrieval, the corrected emissivities are averaged for the winter season in order to reduce the influence of monthly variations. For testing the effect of the correction on the OEM, two versions of the retrieval have been compared. The differences between simulated and measured Tbs for the corrected OEM version are decreased over all channels. The largest impact of the emissivity corrections is over high MYIF regions where the Tb difference is decreased from 2.8 K to 0.6 K on average. Over FYI the final result is less drastic with a decrease in the average Tb difference from 0.9 K to 0.4 K.

(ix) The sensitivity to the brightness temperature covariance matrix S_e has been investigated. This matrix describes the uncertainties that can cause the simulated brightness temperatures to deviate from the measured brightness temperatures as-

suming the state vector parameters are correct. This matrix restricts the space in which the simulated brightness temperatures can be found within acceptable limits of the measurements. Four different S_e versions have been tested based (i) only on radiometric noise values of 1 K for each AMSR-E channel which would ignore any modelling errors in the simulated Tbs, (ii) on the variances of the differences between the simulated and the measured Tbs after one OE retrieval run using only the first S_e version. This version also includes the modelling errors of the forward model. In order to test the sensitivity of the retrieval results to variations in S_e, two other version are developed from the second by (iii) halving and respectively by (iv) doubling the value of each element.

Larger S_e values relax the pull towards the measurements and shift the retrieval towards the background values as seen for the version using the doubled values. If the S_e values are too low, like in the version using halved values, they overconstrain the simulations to match the measurements up to an unrealistic precision level which results in a biased retrieval as the OE compensates for errors in the simulation with changes in the state vector parameters. For all subsequent OEM versions, the second version of the brightness temperature covariance matrix was used from the four described above. As good practice for future development, every change introduced to the method should be reflected in the brightness temperature covariance matrix by using the same procedure. First a test run of the modified OEM is performed with a generic S_e with large enough values to avoid overconstraining the method. Then the variances of the differences between the retrieval step simulated Tbs and the measurements are taken as the components of the new S_e matrix. In this way the brightness temperature covariance matrix includes the measurement error, the channel wise combined modelling error and the forward model parameter error after implementing the modifications in order to allow for a good balance between the background state vector values and the measured Tbs.

8.2 Comparison with state of the art

The RRDP test data set represents isolated scenes with extreme SIC values, 100% or 0%. In order to test how the method behaves after implementing the changes detailed above, a more realistic data set of AMSR-E measurements in the Arctic is used which covers the whole polar region north of 60 °N and 16 individual winter days spaced every 10 days in 2006. The purpose of this second data set is to include more variety in the surface conditions than the RRDP set provides. In addition, the OEM retrieval results are compared with state of the art retrieval products. While not a true validation effort, this comparison shows how reasonable the OE output is in a realistic retrieval environment. The results of these comparison tests are:

(i) The first comparison product used was the RSS Ocean Data product which is a state of the art retrieval method that uses a direct Tb inversion to retrieve WSP, TWV, LWP and SST over open ocean. The OEM retrieval result was positioned in the parameter space between the background data of the ERA-Interim and the RSS retrieval. For WSP, TWV and LWP, the OEM retrieval improves on the previous knowledge represented by the ERA-Interim data and achieves a better agreement with the RSS benchmark (Table 6.1). The SST retrieval is shown to have been over constrained to the background using a SIC0 derived covariance matrix. After the constraint on SST is relaxed back to climatological values the OEM moves away from the background towards the RSS values.

(ii) The SIC is the most important parameter because it dominates the microwave signal over all AMSR-E channels (Fig. 7.1). As a benchmark for SIC state of the art retrieval the ASI SIC product was used for the comparison with OEM retrieved SIC. The OEM results improved on the NASA Team background data and moved closer to the ASI benchmark both in the distribution shape of the retrieved data and standard deviation of the difference between results. Despite that the NASA Team SIC data used as background by the OEM is not weather filtered, the OEM SIC output does not contain the spurious ice over open water or cloud patterns above pack ice that appear in the a priori (Fig. 6.8). In this sense, by correctly attributing the individual contributions to the simulated Tb from each state vector parameter, the OEM achieves automatically a weather corrected SIC retrieval where the weather influences are retrieved as separate parameters, making the statistically based weather filters obsolete.

(iii) Testing the atmospheric retrieval over sea ice is difficult because there are few comparable retrieval products over sea ice. The state of the art for TWV retrieval over sea ice is represented by the AMSU-B TWV product [Melsheimer and Heygster, 2008], and it has been used as a benchmark in this case. The comparison shows that the OEM TWV output is reasonable, with a correlation of 0.7. The daily average map examples indicate that the differences can be caused by the temporal collocation. The TWV fields are clearly shifted in position between the OEM output and the AMSU-B TWV retrieval, although similar in shape (Fig. 6.10). Also of note is that the impact of very low TWV values on the Tbs at channels between 6.9 and 37 GHz can be so small that the OEM will just repeat the background as the Tb difference is not big enough to determine a change in this parameter (Fig. 7.1 left side). The OEM sensitivity to TWV over sea ice can be improved by including the 89 GHz channels. This is further discussed in Section 8.3, (ii).

8.3 Testing different input channel combinations

The testing summarized above was based on the OEM implementation using the AMSR-E channels between 6.9 and 37 GHz. In addition to this version, different channel combinations have been explored through information content analysis in order to provide avenues for further development of the method. The main improvements of the OEM that can be addressed by changing the combination of input channels are the resolution of the output and the sensitivity to atmospheric parameters over sea ice.

(i) The resolution of the OEM retrieval is limited to that of the lowest involved frequency channels so that the resolution can only be improved if the 6.9 GHz channels are discarded from the retrieval. Depending on the surface conditions some limitations to the retrieval performance are observed (Fig.7.1). The performance reduction is highest over the open ocean as the sensitivities to WSP, SIC and SST are reduced by discarding 6.9 GHZ channels. Over sea ice covered regions the drop in sensitivity is less noticeable as the signal information content is dominated by contributions from SIC, the ice type and LWP. While most of the remaining channels provide good sensitivity for SIC and MYIF, the inclusion of the 89 GHz channels ensures good sensitivity for LWP. Depending on the application, this version of the OEM can be used if the higher resolution is required and the retrieval spatial domain consists of sea ice covered regions.

(ii) The 89 GHz channels provide the best sensitivity to the atmospheric parameters TWV and LWP which are lacking in current retrieval products over sea ice. At the same time, limitations in the forward model regarding scattering calculations at frequencies above 37 GHz argue against including the 89 GHz channels. OEM versions that include the 89 GHz channels either in a set of 10 channels after discarding the 6.9 GHz channels or as a full set of all 12 AMSR-E channels have been tested in Chapter 7. The increased sensitivity to LWP and TWV is evident both over open ocean and sea ice covered regions. Over SIC1 cases the impact of the additional sensitivity is more important than over SIC0 as in the latter other channels (37, 23, 18 GHz) that provide sensitivity. In both SIC1 and SIC0 cases however the OEM version using the full set of 12 channels has the highest information content even while taking into account the increased uncertainty of the simulated Tbs. For applications where the surface parameter retrieval requires the most information content, the 89 GHz channels can be excluded as they increase the uncertainty of the simulated brightness temperatures. However if the priority is on retrieving atmospheric parameters, especially over sea ice, and the increased noise level in the simulations is acceptable, the 89 GHz channels have to be included.

8.4 Outlook

Of immediate concern for the development of the method is a thorough validation of as many state vector parameters as possible. Parameters over open water are easier to approach than over sea ice. Depending on the length of the validation time series such data can be used to update the background covariance matrix which is crucial to the retrieval performance as has been shown in Chapters 5 and 6. Further testing of the OEM using all 12 AMSR-E channels could yield better performance for the retrieval of atmospheric parameters over sea ice as indicated by the information content analysis (Tables 7.1, 7.2). As a direct consequence of using the 12c OEM version, the treatment of the 89 GHz channels can be improved by a newer implementation of the radiative transfer model (currently Wentz and Meissner [2000] with the adaptations for sea ice described in Section 4.2) with updated atmospheric coefficients for the high frequency channels or by switching to a different forward model like RTTOV (Radiative Transfer for TOVS) [Saunders et al., 2017] or the CRTM (Community Radiative Transfer Model) ([Weng et al., 2005]). These models include Mie scattering calculations that become relevant at these frequencies. The additional challenge will then be in providing input parameters about the drop size distribution.

8.5 Summary

The OEM takes advantage of the sensitivities of multi-channel microwave radiometers to retrieve an ensemble of geophysical parameters which are currently unavailable or obtained from single parameter retrievals. A number of improvements have been implemented over the OEM prototype including (i) a sea ice surface temperature treatment that accounts for the channel specific penetration depth, (ii) surface sea ice emissivities that minimise the differences between simulations and observations, (iii) using collocated reanalysis data as background to improve the convergence rate and (iv) tools for testing and tuning the a priori constraints to minimise the biases in the retrieval. The OEM depends on many variables and can be run in a multitude of configurations. The most important ones have been explored and a retrieval scheme is suggested that can match the performance of existing multi-parameter retrievals over open ocean with the added benefit of reliable surface parameter and reasonable atmospheric parameter retrieval over sea ice. Based on these results and the tools identified in this work the method can be developed in a variety of channel combinations depending on the intended use. For applications that require the best information about surface parameters the 6.9 GHz channels need to be includedq. If a spatial resolution higher than 56 km is required, the 6.9 GHz channels can be excluded with a small loss in retrieval performance over sea ice but higher degradation over open water. For applications that prioritise the retrieval of atmospheric parameters, especially over sea ice, the 89 GHz channels have to be included.

A | Appendix

Below are the detailed parameters of different OEM implementations used throughout this thesis. The reference OEM used for the tests presented in chapter 5 uses the background covariance matrix and the static background state vector shown in Table A.1. The sea ice surface emissivities used are seasonal averages (only winter used here) of the original empirical values from [Mathews, 2007] shown in Table A.5. The reference brightness temperature covariance matrix used for constraining the difference between the simulations and the measurements is given in Table A.2. This reference S_e uses only the radiometric error of 1 K for each channel.

Table A.1: Elements of the background covariance matrix and static elements of the background state vector of the reference OEM version. The values shown here represent the standard deviations of the state vector parameters. For IST, SIC and MYIF the background values are not fixed but evaluated once for every data point.

Parameter	WSP	TWV	LWP	SST	IST	SIC	MYIF
Units	[m/s]	[mm]	[mm]	[K]	[K]	[%]	[%]
S_a equivalent σ	3.51	3.32	0.14	4.89	4.89	32	54
P_a elements	4.11	2.86	0.17	274.50	evaluated	evaluated	evaluated

As a conclusion to Chapter 5, an improved OEM version is constructed for use in further testing in subsequent chapters. The background covariance matrix is constructed from a large RRDP set of 9 years of data for the SIC0 scenario where ERA-Interim data was used for calculating the variances of wind speed, TWV, LWP and SST. The ERA-Interim skin temperature from the entire SIC1 data set was used for IST variance and NASA Team data for the same set was used for the SIC and MYIF variances. The diagonal elements of the final S_a matrix are shown in Table A.7.

Table A.2: Diagonal elements of the brightness temperature covariance matrix - S_e for different versions of the OEM. Shown here are the standard deviations (K).The column labeled "Final" represents the S_e matrix calculated in the same manner as the LS_e but after implementing all of the improvements described in Chapter 5.

Channel	Ref.S_e	1/2LS_e	LS_e	2LS_e	Final S_e
6.9V	1	1.46	2.92	5.85	1.54
6.9H	1	1.21	2.42	4.84	2.20
10.7V	1	0.93	1.86	3.71	1.27
10.7H	1	0.64	1.28	2.56	2.34
18.7V	1	0.61	1.21	2.42	0.99
18.7H	1	1.01	2.02	4.04	2.22
23.8V	1	0.28	0.56	1.17	1.02
23.8H	1	0.92	1.83	3.66	1.63
36.5V	1	2.19	4.37	8.75	1.59
36.5H	1	1.84	3.67	7.34	1.63

Table A.3: Background covariance matrix of the Feb-diag OEM version. The diagonal elements are variances of each parameter, and the values are based on MPI model output from the month of February in the Arctic.

Parameter	WSP	TWV	LWP	SST	IST	SIC	MYIF
Units	$[m/s^2]$	$[mm^2]$	$[mm^2]$	$[K^2]$	$[K^2]$	$[(\% \cdot 10^{-2})^2]$	$[(\% \cdot 10^{-2})^2]$
WSP	8.66	0	0	0	0	0	0
TWV	0	1.6	0	0	0	0	0
LWP	0	0	0.0003	0	0	0	0
SST	0	0	0	23.95	0	0	0
IST	0	0	0	0	46.8	0	0
SIC	0	0	0	0	0	0.0007	0
MYIF	0	0	0	0	0	0	0.30

Table A.4: Background covariance matrix of the Feb-full OEM version. The diagonal elements are variances of each parameter, while the off-diagonal elements are covariances between parameters and the values are based on MPI model output from the month of February in the Arctic.

Parameter	WSP	TWV	LWP	SST	IST	SIC	MYIF
Units	$[m/s^2]$	$[mm^2]$	$[mm^2]$	$[K^2]$	$[K^2]$	$[(\% \cdot 10^{-2})^2]$	$[(\% \cdot 10^{-2})^2]$
WSP	8.66	0.81	-0.005	0	6.22	-0.008	0
TWV	0.81	1.6	0.003	0	7.02	-0.003	0
LWP	-0.005	0.003	0.0003	0	0.033	-0.00005	0
SST	0	0	0	23.95	0	0	0
IST	6.22	7.02	0.033	0	46.8	-0.05	0
SIC	-0.008	-0.003	-0.00005	0	-0.05	0.0007	0
MYIF	0	0	0	0	0	0	0.30

Table A.5: Empirical sea ice surface emissivities differentiated by ice type. The original values represent the averages of the winter season values given in Mathews [2007]. The corrected values are obtained from the original set (Section 5.5).

Channel	Multi-year ice pixels		First year ice pixels	
	Original	Corrected	Original	Corrected
6.7V	0.954	0.958	0.955	0.972
6.7H	0.854	0.868	0.861	0.866
10.7V	0.953	0.960	0.930	0.948
10.7H	0.860	0.879	0.840	0.845
18.7V	0.964	0.965	0.884	0.885
18.7H	0.875	0.887	0.808	0.799
23.8V	0.960	0.960	0.848	0.839
23.8H	0.875	0.882	0.775	0.763
36.5V	0.936	0.946	0.761	0.731
36.5H	0.851	0.864	0.699	0.675

Table A.6: Emitting layer temperature regression coefficients, as taken from Mathews [2007].

Frequency [GHz]	First year ice winter pixels		Multi-year ice winter pixels	
	a	b	a	b
6.9	0.23	-5.5	0.27	-11.5
10.7	0.26	-5.2	0.34	-10.5
18.7	0.29	-5	0.42	-9.5
23.8	0.29	-4.9	0.43	-9.2
36.5	0.3	-4.9	0.45	-8.9
89	0.37	-4.2	0.49	-8.4

Table A.7: Equivalent standard deviations for background covariance matrix elements based on ERA-Interim and NASA Team data from the extended 9 years SIC0 dataset.

WSP [m/s]	TWV [mm]	LWP [mm]	SST [K]	IST [K]	SIC [%]	MYIF [%]
2.39	1.17	0.3	1.42	5.02	20	32

The brightness temperature covariance matrices used for the 12 channel and the 10 channel OEM versions are discussed in Section 7.1 as needed for testing the impact of including the 89 GHz channels in the retrieval. These channels have a higher uncertainty because of the deficiencies of the forward model at these frequencies. By including these channels with higher uncertainty in the OEM, all values of the S_e matrix will increase.

Table A.8: Equivalent standard deviations (σ) of the diagonal elements of the brightness temperature covariance matrix S_e for the 12 channel (σ_{12ch}) and the 10 channel (σ_{10ch}) OEM version respectively. The 10 channel version is shown here for comparison only.

Channel	σ_{12ch} [K]	σ_{10ch} [K]
6.9V	2.25	1.53
6.9H	2.78	2.20
10.65V	2.22	1.27
10.65H	2.86	2.34
18.7V	2.05	0.99
18.7H	2.73	2.22
23.8V	1.99	1.02
23.8H	2.33	1.63
36.5V	2.20	1.59
36.5H	2.76	1.63
89V	4.99	
89H	4.03	

List of acronyms

AMSU-B	Advanced Microwave Sounding Unit B
AMSR2	Advanced Microwave Scanning Radiometer 2
AMSR-E	Advanced Microwave Scanning Radiometer - EOS
ASCAT	Advanced SCATterometer
ASR	Arctic System Reanalysis
ECMWF	European Centre for Medium-Range Weather Forecasts
EM	electromagnetic
EOS	Earth Observing System
IUP	Institute für Umweltphysik
IST	ice surface temperature
LWP	liquid water path
MYIF	multi-year ice fraction
OE	optimal estimation
SIC	sea ice concentration
SSM/I	Special Sensor Microwave Imager
SST	sea surface temperature

TWV total water vapor

WSP wind speed

Bibliography

P. Ashcroft and F. Wentz. Algorithm theoretical basis document, AMSR Level 2A algorithm. *RSS, Santa Rosa, CA, Tech. Rep*, 121, 2000.

D. Atlas. Advances in radar meteorology. *Advances in Geophysics*, 10:317–478, 1964.

D. H. Bromwich, K. M. Hines, and L.-S. Bai. Arctic System Reanalysis. 2001.

J. C. Comiso, D. J. Cavalieri, C. L. Parkinson, and P. Gloersen. Passive microwave algorithms for sea ice concentration: A comparison of two techniques. *Remote Sensing of Environment*, Volume 60(Issue 3):357–384, 1997.

D. P. Dee, S. Uppala, A. Simmons, P. Berrisford, P. Poli, S. Kobayashi, U. Andrae, M. Balmaseda, G. Balsamo, d. P. Bauer, et al. The ERA-Interim reanalysis: Configuration and performance of the data assimilation system. *Quarterly Journal of the royal meteorological society*, 137(656):553–597, 2011.

S. J. English and T. J. Hewison. A fast generic millimeter-wave emissivity model. *Proceedings of SPIE*, 3503:288–300, 1998.

K. Imaoka, T. Sezai, T. Takeshima, T. Kawanishi, and A. Shibata. Instrument characteristics and calibration of AMSR and AMSR-E. In *Geoscience and Remote Sensing Symposium, 2002. IGARSS'02. 2002 IEEE International*, volume 1, pages 18–20. IEEE, 2002.

N. Ivanova, L. Pedersen, R. Tonboe, S. Kern, G. Heygster, T. Lavergne, A. Sørensen, R. Saldo, G. Dybkjær, L. Brucker, et al. Inter-comparison and evaluation of sea ice algorithms: towards further identification of challenges and optimal approach using passive microwave observations. *The Cryosphere*, 9, 2015.

C. Kongoli, S.-A. Boukabara, B. Yan, F. Weng, and R. Ferraro. A new sea-ice concentration algorithm based on microwave surface emissivities—application to AMSU measurements. *IEEE Transactions on Geoscience and Remote Sensing*, 49(1):175–189, 2011.

T. Markus and D. J. Cavalieri. An enhancement of the NASA Team sea ice algorithm. *IEEE Transactions on Geoscience and Remote Sensing*, 38(3):1387–1398, 2000.

M. C. Marquis, R. L. Armstrong, P. Ashcroft, M. J. Brodzik, D. Conway, S. J. S. Khalsa, E. Lobl, J. Maslanik, J. Stroeve, and V. Troisi. Research applications and opportunities using Advanced Microwave Scanning Radiometer-Earth Observing System (AMSR-E) data. In *Third International Asia-Pacific Environmental Remote Sensing Remote Sensing of the Atmosphere, Ocean, Environment, and Space*, pages 434–445. International Society for Optics and Photonics, 2003.

N. Mathews. *Retrieval of Surface Emissivity of Sea Ice and Temperature Profiles over Sea Ice from Passive Microwave Radiometers*. PhD thesis, University of Bremen, 2007.

C. Melsheimer and G. Heygster. Improved retrieval of total water vapor over polar regions from AMSU-B microwave radiometer data. *IEEE Transactions on Geoscience and Remote Sensing*, 46(8):2307–2322, 2008.

C. Melsheimer, G. Heygster, and L. T. Pedersen. Integrated retrieval of surface and atmospheric parameters over the Arctic from AMSR-E satellite microwave radiometer data using inverse methods. In *IGARSS 2008-2008 IEEE International Geoscience and Remote Sensing Symposium*, volume 4, pages IV–986. IEEE, 2008.

C. Merchant, P. Le Borgne, A. Marsouin, and H. Roquet. Optimal estimation of sea surface temperature from split-window observations. *Remote Sensing of Environment*, 112(5): 2469–2484, 2008.

R. Msadek, G. Vecchi, M. Winton, and R. Gudgel. Importance of initial conditions in seasonal predictions of Arctic sea ice extent. *Geophysical Research Letters*, 41(14):5208–5215, 2014.

R. K. Pachauri, M. R. Allen, V. Barros, J. Broome, W. Cramer, R. Christ, J. Church, L. Clarke, Q. Dahe, P. Dasgupta, et al. *Climate change 2014: synthesis Report. Contribution of working groups I, II and III to the fifth assessment report of the intergovernmental panel on climate change*. IPCC, 2014.

L. T. Pedersen. Merging microwave radiometer data and meteorological data for improved sea ice concentrations. *EARSeL Advances in Remote Sensing*, 3(2-XII):81–89, 1994.

L. T. Pedersen and R. Saldo. *Sea Ice Concentration (SIC) Round Robin Data Package*, November 2012.

C. D. Rodgers. Retrieval of atmospheric temperature and composition from remote measurements of thermal radiation. *Reviews of Geophysics*, 14(4):609–624, 1976.

C. D. Rodgers. *Inverse methods for atmospheric sounding: theory and practice*, volume 2. World scientific, 2000.

R. Saunders, J. Hocking, D. Rundle, P. Rayer, S. Havemann, M. Matricardi, A. Geer, C. Lupu, P. Brunel, and J. Vidot. *RTTOV-12 Science and Validation Report*. Met. Office, NWP Division, 2017.

R. C. Scarlat, G. Heygster, and L. T. Pedersen. Experiences with an optimal estimation algorithm for surface and atmospheric parameter retrieval from passive microwave data in the Arctic. *IEEE Journal of Selected Topics in Applied Earth Observations and Remote Sensing*, 10(9):3934–3947, 2017.

R. C. Scarlat, C. Melsheimer, and G. Heygster. Retrieval of total water vapour in the Arctic using microwave humidity sounders. *Atmospheric Measurement Techniques*, 11 (4):2067, 2018.

N. Selbach. *Determination of Total Water Vapour and Surface Emissivity of Sea Ice at 89 GHz, 157 GHz and 183 GHz in the Arctic Winter*. PhD thesis, University of Bremen., 2003.

M. C. Serreze, M. M. Holland, and J. Stroeve. Perspectives on the Arctic's shrinking sea-ice cover. *Science*, 315(5818):1533–1536, 2007. ISSN 0036-8075. doi: 10.1126/science.1139426. URL `http://science.sciencemag.org/content/315/5818/1533`.

C. Shannon and W. Weaver. The mathmatical theory of information. *Urbana: University of Illinois Press*, 1949.

M. Shokr and N. Sinha. *Sea ice: physics and remote sensing*. John Wiley & Sons, 2015.

M. Shokr, A. Lambe, and T. Agnew. A new algorithm (ECICE) to estimate ice concentration from remote sensing observations: An application to 85-GHz passive microwave data. *IEEE Transactions on Geoscience and Remote Sensing*, 46(12):4104–4121, 2008.

G. Spreen, L. Kaleschke, and G. Heygster. Sea ice remote sensing using AMSR-E 89-GHz channels. *Journal of Geophysical Research: Oceans*, 113(C2), 2008.

J. Stroeve, M. M. Holland, W. Meier, T. Scambos, and M. Serreze. Arctic sea ice decline: Faster than forecast. *Geophysical Research Letters*, 34(9):n/a–n/a, 2007. ISSN 1944-8007. doi: 10.1029/2007GL029703. URL `http://dx.doi.org/10.1029/2007GL029703`. L09501.

J. C. Stroeve, V. Kattsov, A. Barrett, M. Serreze, T. Pavlova, M. Holland, and W. N. Meier. Trends in Arctic sea ice extent from CMIP5, CMIP3 and observations. *Geophysical Research Letters*, 39(16), 2012.

E. Svendsen, C. Matzler, and T. C. Grenfell. A model for retrieving total sea ice concentration from a spaceborne dual-polarized passive microwave instrument operating near 90 GHz. *International Journal of Remote Sensing*, 8(10):1479–1487, 1987.

F. T. Ulaby, D. G. Long, W. J. Blackwell, C. Elachi, A. K. Fung, C. Ruf, K. Sarabandi, H. A. Zebker, and J. Van Zyl. *Microwave radar and radiometric remote sensing*, volume 4. University of Michigan Press Ann Arbor, 2014.

F. Weng, Y. Han, P. Van Delst, Q. Liu, and B. Yan. JCSDA community radiative transfer model (CRTM). In *Proc. 14th Int. ATOVS Study Conf*, pages 217–222, 2005.

F. Wentz, T. Meissner, C. Gentemann, and M. Brewer. Remote sensing systems AQUA AMSR-E daily environmental suite on 0.25 deg grid, version 7.0, Remote Sensing Systems, Santa Rosa, CA, 2014.

F. J. Wentz and T. Meissner. AMSR ocean algorithm. Algorithm Theoretical Basis Document (ATBD). version 2, nov 2000.

F. J. Wentz and T. Meissner. Supplement 1 algorithm theoretical basis document for AMSR-E ocean algorithms. *NASA: Santa Rosa, CA, USA*, 2007.

A. Wiesmann and C. Mätzler. Microwave emission model of layered snowpacks. *Remote Sensing of Environment*, 70(3):307–316, 1999.

Acknowledgements

It would not have been possible to write this thesis without the help and support of the people around me, only some of whom it is possible to give particular mention here.

Above all I would like to thank my family for their support and unwavering confidence. I want to give a special thanks to my brother whose contagious enthusiasm means the world to me. For my friends that have supported me with advice, goodwill and comfort food, I hope I can repay you in kind.

This thesis would not have been possible without the help and patience of my principal supervisor, Dr. Georg Heygster. I am extremely grateful to Dr. Leif Pedersen for his interest in my work, for the good-natured criticism and the many great ideas he directed my way. My short stay with the Ocean and Ice group at the Danish Meteorological Institute has been both helpful and fun thanks to the efforts of Dr. Rasmus Tonboe and his colleagues to which I am also grateful. For support and advice in critical moments I want to acknowledge Dr. Gunnar Spreen. I also want to thank Prof. Dr. Justus Notholt for giving me the opportunity to work at the Institute für Umweltphysik (IUP). Many thanks to Dr. Marcus Huntemann and Dr. Christian Melsheimer for the life saving bug fixes, insightful discussions and patience. The support and assistance from my Polar Remote Sensing group colleagues at the IUP is greatly appreciated.

I would like to acknowledge the financial and academic support of the ArcTrain post-graduate programme with a special mention to ArcTrain speaker Michal Kucera, and ArcTrain secretary Gabriella Wehr. For the support and the nice time together I want to thank my fellow ArcTrain colleagues, you have given me many good memories.

This project was supported by the Deutsche Forschungsgemeinschaft (DFG) through the International Research Training Group "Processes and impacts of climate change in the North Atlantic Ocean and the Canadian Arctic" (IRTG 1904 ArcTrain).

The data provision from ECMWF and ASR is highly appreciated.